

Evolution of primordial magnetic fields in the early universe

Dissertation
von
Robi Banerjee

Max-Planck-Institut für Astrophysik
Ludwig-Maximilians-Universität München

Oktober 2002

1. Gutachter:
2. Gutachter:
Tag der mündlichen Prüfung:

Prof. Dr. Simon D. M. White
Prof. Dr. Harald Lesch
7. April 2003

Inhaltsverzeichnis

Zusammenfassung (Summary in German)	3
1. Introduction	7
2. Cosmic magnetic fields	11
2.1. Observations	11
2.2. Constraints on primordial magnetic fields	12
2.2.1. Constraints by the CMBR	12
2.2.2. Constraints from big bang nucleosynthesis	13
2.3. Models of magnetogenesis	14
2.3.1. Astrophysical models	15
2.3.2. Models of primordial magnetogenesis	15
3. Imperfect fluid dynamics and magnetic fields in the expanding universe	19
3.1. Imperfect fluid dynamics	19
3.2. Covariant description of electromagnetic fields	22
3.2.1. Medium with infinite conductivity	24
3.3. The MHD equations in the FRW universe	25
3.4. MHD equations in the radiation dominated universe	28
3.4.1. The incompressible limit	29
3.4.2. Dissipation in the free streaming regime	30
3.5. MHD equations in the matter dominated universe	32
3.5.1. The free streaming regime	34
4. Helicity	35
4.1. Implementation of stochastic fields with helicity	37
4.2. Magnetic fields with maximal helicity	39
4.3. Magnetic fields with fractional helicity	40
5. The linear regime	41
5.1. The diffusion regime	41
5.2. The free streaming regime	43
5.3. Numerical implementation	43

5.3.1. The diffusion regime	44
5.3.2. The free streaming regime	44
6. Nonlinear MHD	45
6.1. Dynamics of nonlinear MHD	45
6.2. Turbulence	47
6.3. Dynamics of helical magnetic fields	48
7. Damping of magnetic fields	51
7.1. Damping in the turbulent regime	51
7.2. Viscous damping	58
8. Evolution of primordial magnetic fields	63
8.1. Viscosities and conductivity in the early universe	66
8.2. The turbulent regime	69
8.2.1. Dissipation time scale in the turbulent regime	70
8.2.2. Damping in the turbulent regime	71
8.2.3. End of turbulence by diffusive viscosity	72
8.3. The viscous diffusion regime	74
8.4. The free streaming regime	75
8.4.1. Neutrino free streaming	76
8.4.2. Photon free streaming	78
8.5. Damping in the Viscous free streaming regime	79
8.5.1. Viscous neutrino free streaming	81
8.5.2. Viscous photon free streaming	81
8.6. Evolution after recombination	82
8.7. Damping scales	83
8.8. Examples	84
9. Summary and conclusions	87
A. Appendix	91
A.1. Notations for the FRW universe	91
A.2. Conventions for Fourier transformations	94
A.3. Numerical method	95
Bibliography	103

Zusammenfassung

In dieser Arbeit wird die zeitliche Entwicklung eventuell vorhandener primordialer Magnetfelder im Frühen Universum untersucht.

Magnetfelder werden in praktisch jedem astrophysikalischen Objekt, seien es Planeten, Sterne, Galaxien oder Galaxienhaufen, beobachtet. Der Ursprung der nachgewiesenen Magnetfelder in Galaxien und Galaxienhaufen ist nach wie vor nicht eindeutig geklärt. Bisherige Messungen schließen jedoch einen gänzlichen oder teilweisen primordialen Ursprung dieser galaktischen und extra-galaktischen Magnetfelder nicht aus. Die typischen Feldstärken, die man in Galaxien und Galaxienhaufen beobachtet, haben die Größenordnung von μG . Die entsprechenden Kohärenzlängen der Magnetfelder können von denselben Größenordnungen wie Galaxien bzw. Galaxienhaufen sein, d.h. galaktische Magnetfelder besitzen typische Kohärenzlängen von einigen kpc bis zu 100 kpc, während Magnetfelder in Galaxienhaufen auf Skalen von Mpc bis 10 Mpc kohärent sein können.

Der Schwerpunkt dieser Arbeit ist die Berechnung der Energiedichte und der Kohärenzlänge der primordialen Magnetfelder von der Epoche kurz nach ihrer möglichen Erzeugung, z.B. während des elektroschwachen-Phasenübergangs, bis zum Beginn der kosmischen Strukturformation. Die Evolution dieser Größen hängt von den Bedingungen zum Zeitpunkt der Magnetfeldgenerierung ab. Hierzu gehören unter anderem die Temperatur des Universums zum Zeitpunkt der Magnetfelderzeugung, das Spektrum des Magnetfeldes und der Anteil der magnetischen Helizität. Die Ergebnisse dieser Arbeit bieten die Möglichkeit für spezifische Modelle der Magnetfeldgenerierung im Frühen Universum, die Energie und die Kohärenzlänge dieser Magnetfelder zur gegenwärtigen Epoche zu berechnen.

Um die Evolution primordialer Magnetfelder zu verfolgen, wurden die nichtlinearen magnetohydrodynamischen (MHD) Differentialgleichungen mit Hilfe numerischer Methoden gelöst. Hierbei konnte ich auf das bereits bestehende Programm ZEUS3D zurückgreifen, das ich für die Untersuchung primordialer stochastischer Magnetfelder angepaßt und erweitert habe. Mit Hilfe dieser numerischen Lösungen konnten analytische Ausdrücke abgeleitet werden, die die Entwicklung der magnetischen Energiedichte sowie der Kohärenzlänge (integrale Skala) in Abhängigkeit der Temperatur des Universums beschreiben.

Im Rahmen dieser Arbeit konnte gezeigt werden, daß eventuell existente primordiale Magnetfelder nicht nur durch die adiabatische Expansion des Universums, sondern

auch durch dynamische Wechselwirkungen während der Evolution des Universums erheblich verringert werden. Obwohl der direkte Energieverlust der magnetischen Felder durch die endliche Leitfähigkeit der Materie im Frühen Universum vernachlässigbar klein ist, werden diese – indirekt über die Anregung von Fluktuationen – dissipiert. Die große magnetische Prandtl-Zahl ($P_m \gg 1$) im jungen Universum verdeutlicht diese Situation. Ist die magnetische Energie auf einer bestimmten Skala L konzentriert, dann entspricht die typische Zeitskala, während der die magnetische Energie dissipiert wird, in etwa der Zeit, die ein Flüssigkeitswirbel der Größe L benötigt eine Umdrehung zu vollziehen (eddy turnover time scale).

Üblicherweise durchlaufen primordiale Magnetfelder während der Expansion des Universums verschiedene Evolutionsbereiche. Während der turbulenten Phase, die durch eine große Reynolds-Zahl gekennzeichnet ist, erwartet man ein Gleichgewicht zwischen kinetischer und magnetischer Energie. Hierbei wird die Energie sukzessive zunächst von großen zu kleinen Skalen transferiert (*direkte Energiekaskade*) und schließlich auf der sehr kleinen Dissipationsskala durch die Viskosität in Wärme umgewandelt. Die Verlustrate der Gesamtenergie während der turbulenten Phase ist unabhängig von der der Viskosität zugrundeliegenden Mikrophysik. Die typische Zeitskala des Energieverlusts wird nur von den Eigenschaften des Magnetfeldes auf der integralen Skala L bestimmt.

Solange die mittlere freie Weglänge der Photonen bzw. Neutrinos kleiner ist als die Kohärenzlänge des Magnetfeldes, wird die Energie durch einen Diffusionsprozeß dissipiert. Während das Universum abkühlt nimmt die Stärke der kinetischen Viskosität zu und die Reynolds-Zahl kann kleiner als Eins werden. In dieser stark viskosen Phase ist die Bewegung der Flüssigkeitselemente stark eingeschränkt und vorhandene Fluktuationen werden schnell weggedämpft. Dann sind auch vorhandene Magnetfelder nicht mehr in der Lage weitere Fluktuationen anzuregen, was zur Folge hat, daß die Zeitskala der magnetischen Energiedissipation enorm lang wird. Tatsächlich übersteigt die typische Dissipationszeit während dieser viskosen Diffusionsphase die Hubblezeit, und wächst mit sinkender Temperatur an. Dies verhindert einen weiteren Energieverlust der Magnetfelder während der stark viskosen Diffusionsphase.

Im expandierenden Universum wächst die mittlere freie Weglänge von Neutrinos und Photonen schneller an als die Kohärenzlänge des Magnetfeldes. Wird die mittlere freie Weglänge größer als die Kohärenzlänge, überströmen (free stream) die Neutrinos bzw. Photonen die Fluktuationen. Im Gegensatz zur viskosen Diffusionsphase, während der die Dissipationszeit anwächst, nimmt die Dissipationszeit in der Überströmphase mit sinkender Temperatur des Universums ab. Dies kann zur Folge haben, daß Dissipation der magnetischen Energie beim Einsetzen der Überströmphase zunächst nicht stattfindet und erst später einsetzt. In der Überströmphase wird magnetische Energie auch dann effektiv dissipiert, wenn die Reynolds-Zahl wesentlich kleiner als Eins wird. Die Überströmphase dauert so lange an, bis die Photonen bzw. die Neutrinos vollständig von der Evolution des Universums entkoppelt sind. Anschließend sind die Wechselwirkungen des Fluids mit der Hintergrundstrahlung

äußerst schwach, so daß das Fluid wieder eine turbulente Phase entwickelt.

Nach der Entkoppelung der Photonen (etwa während der Epoche der kosmischen Rekombination) ist das Universum bereits materie-dominiert. Während des Übergangs vom strahlungs- zum materie-dominierten Universum ändert sich auch die Zustandsgleichung des Universums. Dies bedingt auch, daß im materie-dominierten Universum die Dissipationszeit (während der turbulenten Phase) und die Hubblezeit in gleicher Weise vom Skalenfaktor des Universums abhängen, was wiederum zur Folge hat, daß die Energie vorhandener Magnetfelder (abgesehen von logarithmischen Korrekturen) nicht weiter dissipiert wird.

Abgesehen von den verschiedenen Dissipations-Bereichen ist der Energieverlust primordialer magnetischer Felder auch von den spezifischen Magnetfeldeigenschaften abhängig. Die Steigung der Magnetfeldspektren, charakterisiert durch den spektralen Index n , bestimmt schließlich die Dissipationsrate der Magnetfeldenergie. Je steiler das Spektrum des Magnetfeldes ist, desto schneller wird magnetische Energie dissipiert. Wegen der Erhaltung der magnetischen Helizität in Fluiden mit großer Prandtl-Zahl, werden Magnetfelder mit nichtverschwindender Helizität langsamer dissipiert als solche ohne anfängliche Helizität. Magnetfelder mit Helizität haben zusätzlich die Eigenschaft, daß ihre Energie nicht nur zu kleinen Skalen transferiert, sondern die Magnetfeldenergie dynamisch auch auf große Skalen geschoben (*inverse Kaskade*) wird. Dies führt zu dem interessanten Effekt des dynamischen Anwachsens der Kohärenzlänge des Feldes.

Abgesehen von den allgemeinen Untersuchungen zur Evolution von Magnetfeldern in verschiedenen Dissipations-Bereichen, werden in dieser Arbeit zudem unterschiedliche Beispiele zur zeitlichen Entwicklung primordialer Magnetfelder gegeben. Diese Beispiele beziehen sich auf kausale Erzeugungsprozesse, z.B. während einer kosmischen Phasentransformation. Diese Berechnungen liefern für Magnetfelder, die während des elektroschwachen Phasenübergangs ($T \sim 100 \text{ GeV}$) mit einem spektralen Index von $n = 3$ (dieser taucht in Modellen mit stochastischen sphärischen "Magnetblasen" auf) generiert worden sind und deren Energiedichte ein Prozent der Gesamtenergiedichte betrug, eine Kohärenzlänge von $L \sim 5 \text{ pc}$ und eine Magnetfeldstärke von $B \sim 2 \times 10^{-14} \text{ G}$. Das gleiche Modell mit anfänglicher maximaler magnetischer Helizität liefert Kohärenzlängen von $L \sim 4 \text{ kpc}$ und Feldstärken von $B \sim 2.6 \times 10^{-11} \text{ G}$. Werden die Magnetfelder während des QCD Phasenübergangs ($T \sim 100 \text{ MeV}$) generiert, dann ergeben die Berechnungen Kohärenzlängen von $L \sim 0.5 \text{ kpc}$ ($L \sim 57 \text{ kpc}$) und Feldstärken von $B \sim 1.9 \times 10^{-12} \text{ G}$ ($B \sim 3.7 \times 10^{-10} \text{ G}$) für Felder ohne Helizität mit $n = 3$ (mit maximaler Helizität). Insbesondere bei Magnetfeldern mit maximaler Helizität sind die Feldstärken zum heutigen Zeitpunkt – trotz Dissipation – ausreichend, um die beobachteten Magnetfelder in Galaxienhaufen zu erklären. Hierzu werden Magnetfelder mit Feldstärken von $B \sim 10^{-11} \text{ G}$ benötigt, die durch adiabatische Kompression und Scherungsströmungen während des gravitativen Kollaps der Protogalaxie verstärkt werden.

1. Introduction

Magnetic fields exist in all astrophysical objects. They are observed in planets and stars, and in galaxies and galaxy clusters. The fields in galaxies have strength of a few $\times 10^{-6}$ G and are correlated up to kiloparsec scales [1]. In the intra-cluster medium (ICM) in clusters of galaxies magnetic fields have also a strength of μ G with a typical correlation length of 10 – 100 kpc [2]. The question of the origin of these quite strong galactic and intergalactic magnetic fields is still an outstanding problem in cosmology. There is an active ongoing debate whether these fields are of primordial origin and amplified due to adiabatic compression during the gravitational collapse of galaxies or whether they are due to amplification of a weak seed field by a galactic dynamo mechanism. In the first case a primordial field of the order of $B \sim 10^{-9}$ G is necessary to explain the observed galactic magnetic fields. In the second case initially only a weak seed field with strength $B \sim 10^{-20}$ (or even $B \sim 10^{-30}$ if the universe possess a positive cosmological constant[3]) is needed which gets exponentially amplified by a dynamo mechanism [4]. Such weak magnetic fields could be either be generated by pure astrophysical mechanisms in protogalaxies or high redshift quasars [5, 6], or could be remnants of primordial magnetic fields generated during an earlier stage of the universe [7].

A general argument to explain the large scale magnetic fields in galaxies is the *galactic dynamo* [4] (for an overview of galactic magnetic fields see [8]). By continuous transfer of kinetic energy of the turbulent motions of the conductive interstellar medium into magnetic energy, magnetic fields with coherence length of the order of the size of galaxies could be established and maintained. The main ingredients for the galactic dynamo to work are, turbulent motions, small but not vanishing conductivity of the interstellar medium, and differential rotation of the galactic system. Although, these ingredients are available in most of the galaxies, it was questioned by several authors (see e.g. [9]) whether the galactic dynamo can operate efficiently to establish the observed large scale magnetic fields. The main criticism is, that the dynamo amplification could be shut down before large scale magnetic fields are generated. This early termination can be due to the strong amplification of small scale magnetic fields which may come to equipartition with the turbulent motions resulting in the end of transfer of kinetic energy into magnetic energy. Furthermore, the origin of the seed fields which are needed by the dynamo amplification, are not explained by the dynamo theory itself, but must be assumed to preexist.

An even more challenging problem is to explain the origin of magnetic fields in galaxy clusters. Magnetic fields in clusters of galaxies have similar strengths and in some cases even larger coherence lengths than those observed in galaxies itself (see e.g. [10]). This is the case in spite of the lower matter density in the intra-cluster medium (ICM) compared to the density of interstellar medium in galaxies. It seems to be unlikely that the observed fields in the ICM originate from the ejection of magnetic fields from cluster galaxies. Two separate explanations, although feasible, are dissatisfying from the theoretical point of view. From the observed independence of the field strength from the local matter density, Kronberg [11] suggested that galactic systems should have evolved in a magnetic environment with $B \gtrsim 1 \mu\text{G}$. One possibility of such a scenario could be that outflows from high redshift quasars, whose fossil remnants fill a sizeable fraction of the intergalactic medium, leave behind large magnetized bubbles in the ICM [12, 13]. Here, the magnetic fields are believed to be generated within the accretion disk of the massive black hole in the center of the active galactic nuclei [14].

The authors of [15] addressed the general question which kind of high redshift magnetic fields are necessary to reproduce the observed properties, particularly the Faraday rotation measurements (RM), of magnetic fields in galaxy clusters. They find that, initial magnetic fields with field strength of order 10^{-9}G at $z = 15$ are required to reconstruct the Faraday rotation observed in this clusters. Their simulations showed that the initial magnetic fields are not only amplified by adiabatic compression during the gravitational collapse but are also due to shear flows. The internal structure of the primordial magnetic fields, i.e. whether the fields are homogeneous or chaotic, are washed out by the cluster collapse and shear flows.

Primordial magnetic fields, although not necessary to explain the origin of galactic or extra-galactic fields, may help to understand the origin of the observed magnetic fields in astronomical objects. Primordial magnetic fields, if they were existent, could in principle also have influenced particular stages of the evolution of the early universe. For instance, the influence of primordial magnetic fields on structure formation was investigated by Wasserman [16] and later by Kim et al., [17]. There exist a variety of models of magnetogenesis in the early universe (see e.g. [18, 19] and section 2.3). Whether the magnetic fields proposed by a particular model could contribute to the present large scale fields depends also on the evolution after the time of creation and during structure formation. As the early universe is an almost perfect conductor (see e.g. [20, 21]) one has commonly concluded that the evolution of cosmological magnetic fields is only determined by the expansion of the universe. One can argue, that due to flux freezing of magnetic field lines in an infinite conducting medium the energy density of magnetic fields would be only adiabatically diluted by the expansion of the universe in the same way as radiation. But, as was already shown in [22] and [23], magnetic field modes undergo also dynamical damping due to the interaction with the induced fluid motions in the plasma of the early universe. The first detailed studies of the damping of cosmic magnetic fields were

done by Jedamzik et al., [22], who determined the damping rates of fast and slow magnetosonic, and Alfvén waves. They found that, compressible fast magnetosonic waves are damped similarly to sound waves in a demagnetized plasma (*Silk damping* [24]), where all modes whose wavelength is smaller than the diffusion length of photons at cosmological recombination are dissipated. In contrast, slow magnetosonic and incompressible Alfvén waves get overdamped in the radiation diffusion regime inhibiting further dissipation of these modes. Therefore, the largest damping scale of slow magnetosonic and Alfvén modes is always smaller or equal to the damping scale of fast magnetosonic modes, and depends on the magnitude and orientation of the background magnetic field. This analysis was done by expanding the nonlinear magnetohydrodynamical (MHD) differential equations around a homogeneous magnetic background field and solving the resulting linear differential equations analytically for the individual modes.

A similar analysis was done by Subramanian and Barrow [23], coming to the same conclusion as Jedamzik et al. in [22]. For their analytic calculations they considered also a homogeneous background magnetic field but with tangled modes of arbitrary magnitude perpendicular to the uniform magnetic field. Furthermore, they assumed the velocity fluctuations to be also perpendicular to the background magnetic field, resulting in a linearized set of differential equations to describe the MHD system.

In this thesis, I extend the pioneering works done in [22] and [23] by studying the complete set of coupled nonlinear magnetohydrodynamical differential equation for the purpose to describe the evolution and damping of magnetic fields in the early universe. In this approach, one can study typical nonlinear features known from pure hydrodynamics (see e.g. [25]) and magnetohydrodynamics (see e.g. [26]) as, for example, energy cascade towards smaller scales in turbulence, and energy cascade towards larger scales for helical magnetic fields. The influence of such nonlinear effects on the evolution of primordial magnetic fields, in particular from magnetic helicity, has been estimated in [27, 28, 29, 30, 31] using simplified MHD models. In this work, I complete these investigations also with the help of numerical simulations. For this purpose, I used the already existing MHD solver ZEUS3D [32, 33, 34] developed at the National Center for Supercomputing Applications (NCSA) which I adapted and extended to analyze magnetic fields in particular damping regimes. Although this program solves the MHD equations including compressional modes, in this work I studied weak magnetic fields, where the Alfvén velocity is smaller than the speed of sound. Within this regime the magnetized fluid can be considered as incompressible, which allows one to find analytical expressions for the damping laws of the magnetic fields in the different damping regimes.

This work is organized as following. In chapter 2 a brief summary of basics about cosmic magnetic fields is given. In particular, it contains constraints on the field strengths from the consideration of different stages in the early universe and theoretical models of magnetogenesis. The general formalism which describes the evolution of large scale magnetic fields in an expanding universe is given in chapter 3. Therein,

special attention is directed to the possibility to rewrite these resulting MHD equations in the same form which they have on a static background. Magnetic helicity plays an important role for the evolution of magnetic fields. This quantity is introduced in chapter 4, where also its implementation for numerical methods is given. In chapter 6 the results found by the linear analysis of the MHD equations are briefly summarized to compare the analytic results with the results found by numerical simulations. The nonlinear properties of magnetohydrodynamics and the damping of magnetic fields on a static background are discussed in the chapters 6 and 7, respectively. These general findings are then applied to the conditions in the early universe in chapter 8. Therein are given also several examples of the evolution of primordial magnetic fields which were generated during the electroweak and QCD phase transitions. Finally, a summary and the conclusions of this work are given in chapter 9. In the appendices A.1 and A.2 my conventions when deriving the MHD equations in the Friedman-Robertson-Walker universe and for Fourier transformations can be found. Furthermore, the numerical method which is used for the simulations is described in appendix A.3. Herein, also the units of the numerical quantities, in particular the simulation time, are explained.

2. Cosmic magnetic fields

In this chapter, I briefly summarize the basic background knowledge of cosmic and primordial magnetic fields. A detailed compilation of this topic can be found in the review article [18] and the paper [35].

2.1. Observations

The primary observational methods to determine magnetic fields in galaxies and galaxy clusters are the measurements of Zeeman splitting of spectral lines, the measurements of the intensity and the polarization of synchrotron emission of free relativistic electrons, and Faraday rotation measurements (RM) of polarized background radiation passing through a magnetized plasma.

The measurement of the splitting of spectral lines by the Zeeman effect gives a direct indication of the magnetic field strength. Unfortunately, it is only feasible in our own Galaxy, because the effect becomes too small for more distant objects. The methods for measuring the synchrotron emission of relativistic electrons and Faraday rotation of polarized light can also be applied to very distant galaxies. These indirect measurements of the magnetic fields need an independent method to determine the electron density n_e in the galaxies or galaxy clusters. In some cases the electron density can be estimated by analyzing the observed X-ray spectra in clusters (see [10] and references herein). Another way to estimate the electron density is to assume equipartition of the magnetic and kinetic energy density. Calculations of the magnetic fields strength in clusters of galaxies using the latter method typically yield values of μG .

Electromagnetic waves from a background source propagating through a magnetized plasma experiences a phase shift of its two different circularly polarized components, resulting in a rotation of the polarization plane. The Faraday rotation measure (RM) gives the strength of the rotated polarization plane and is given by:

$$RM \equiv \frac{\Delta\chi}{\lambda^2} = 8.1 \times 10^5 \int_0^L n_e B_{\parallel} dl \frac{\text{rad}}{\text{m}^2} \quad , \quad (2.1)$$

where $\Delta\chi$ is the change of the rotation angle of polarization, λ is the wavelength of the light passing through the plasma, n_e is given in cm^{-3} , B_{\parallel} is the magnetic field

strength along the line of sight measured in μG , and dl is given in Mpc. Because the RM depends only on the magnetic field component in the direction of the line of sight, the assumed field topology (e.g. field reversal) enters the rotation measure. Typical values for the Faraday rotation measure in galaxy clusters are found to be of the order of 10 rad m^{-2} [10]. To produce these observed RM magnetic fields of the order of μG on Mpc scales are necessary.

2.2. Constraints on primordial magnetic fields

Primordial magnetic fields cannot be of arbitrary strength and size, but are constrained by several observational data. Some examples of constraints on primordial magnetic fields are summarized below.

2.2.1. Constraints by the CMBR

One of the most accurate observed “objects” in the early universe is the cosmic microwave background radiation (CMBR). Deviations of the CMBR from a perfect black body with the temperature $T_{\text{CMB}} = 2.726 \pm 0.01 \text{ K}$ [36] are only of the order $10 \mu\text{K}$ for the quadrupole anisotropy [37], which constrains any model releasing energy into the CMBR or giving rise to an anisotropic expansion of the universe.

It is well known that a homogeneous magnetic field gives an anisotropic contribution to the energy-momentum tensor and therefore induces an anisotropic expansion of the universe (see e.g. [38]). The latest analysis of the implication of a homogeneous cosmic magnetic field on the CMBR anisotropy was done by Barrow, Ferreira and Silk [39]. By using the normalization of the 4-year Cosmic Background Explorer (COBE) differential microwave radiometer (DMR) measurements [37], these authors obtained an upper limit for the magnetic field strength today*:

$$B_0 < 3.5 \times 10^{-9} f^{1/2} (\Omega_0 h_{50}^2)^{1/2} \text{ G} \quad , \quad (2.2)$$

where f is a shape factor of order unity, Ω_0 is the total energy density in terms of the critical density, and $h_{50} = H_0/(50 \text{ km/s/Mpc})$ with the Hubble constant H_0 today. Note, that magnetic fields of the order of $B_0 \sim 10^{-11} \text{ G}$ can be amplified by adiabatic compression and shear flows during the gravitational collapse of galaxies to the observed μG fields [15]. Hence, the COBE data cannot exclude a pure primordial origin of galactic magnetic fields.

Jedamzik, Katalinić and Olinto [40] developed a new method to constrain small scale magnetic fields using precise CMBR measurements. In a previous paper,

*Here, and hereafter, the magnetic field strengths refer to the values which they would have at present epoch, i.e. after cosmological expansion, unless otherwise stated

they had shown that spatially varying, stochastic magnetic fields undergo significant dissipation before recombination, due to excitations of velocity fluctuations by the non-force-free mode-components [22]. The induced kinetic energy, which will reach equipartition with the magnetic energy, is dissipated efficiently into heat due to photon viscosity. The released energy into the photon heat bath will result in an effective non-vanishing chemical potential μ , which depends on the strength and the spectrum of the magnetic field. The COBE/FIRAS data sets an upper limit for the chemical potential distortions to be $|\mu| < 9 \times 10^{-5}$ [41]. This limit constrains magnetic fields with comoving coherence length ≈ 400 pc to $B_0 \lesssim 3 \times 10^{-8}$ G. On slightly larger scales, dissipation of stochastic magnetic fields can distort the CMBR in a different way, which can be described by a superposition of blackbodies of different temperatures, which is characterized with the Compton- y -distortion. The observed CMBR does not show such a feature, which in turn does not allow magnetic fields of $\gtrsim 3 \times 10^{-8}$ G at ≈ 0.6 Mpc scale [40].

Recently, Subramanian and Barrow [42, 43] noted, that future experiments which probe the CMBR on smaller scales, or larger multipoles l , may be able to detect or limit tangled primordial magnetic fields. In [42] it was shown, that stochastic magnetic fields may produce vortical perturbations, which survive Silk damping [24] on much smaller scales than compressional modes. This could leave a specific imprint in the CMBR anisotropy spectrum at large l [43]. The absence or detection of such a feature in the CMBR spectrum put limits on the magnetic field strength. Additionally, potentially observational effects may originate from vector perturbations above the Silk damping scale [44], the depolarization of the cosmic microwave background by Faraday rotation [45, 46], and from the distortions of the acoustic peaks due to the change of the propagation velocity of sound waves at the epoch of recombination [47].

Further limits on the magnetic field strengths were derived by the considerations of possible CMBR distortions from magnetic field generated gravitational waves [48, 49].

2.2.2. Constraints from big bang nucleosynthesis

The detailed studies of the theory of primordial, or big bang nucleosynthesis (BBN) provide cosmologists with a number of constraints on particular theories of the early universe. In 1969 Matese and O'Connell [50, 51, 52, 53] and Greenstein [54] began to investigate the influence of cosmological magnetic fields on the standard BBN scenario. Several effects of cosmic magnetic fields potentially could have affected the synthesis of nuclei in the early universe. Strong magnetic fields with $B > B_c = m_e^2/4\pi\alpha \approx 4.4 \times 10^{13}$ G at the epoch of BBN significantly increase the β decay rate of neutrons [50]. This is due to the enlarged electron phase space in the background of a very strong magnetic field. In [51] it was shown that this effect should suppress the ${}^4\text{He}$ relic abundance with respect to the standard case. This is because a faster neutron decay after the freeze-out of weak proton-neutron interactions will leave less

neutrons to be bound in composite nuclei like ${}^4\text{He}$ and heavier elements. In [53] these authors also discuss qualitatively two other effects of magnetic fields on BBN. At first, they noted that strong magnetic fields would affect the energy density of the electron gas due to the increase of its phase space. And secondly, they discussed the influence of a uniform magnetic field on the geometry of the universe and its consequence on the BBN.

Greenstein [54] considered one other effect of primordial magnetic fields on BBN, namely the direct contribution of the magnetic field energy density to the total energy density, and therefore, to the expansion rate of the universe. By increasing the expansion rate of the universe due to an significant contribution to the total energy from magnetic fields, also the freeze-out temperature T_f of the proton-neutron conversion interaction increases. Since the neutron-to-proton ratio at freeze-out is approximately given by [55]:

$$\left(\frac{n}{p}\right)_{\text{freeze-out}} = \exp\left(-\frac{Q}{T_f}\right) \quad , \quad (2.3)$$

where $Q \equiv m_n - m_p$ (m_n and m_p is the neutron and proton mass, respectively), a small change in the freeze-out temperature T_f causes a large variation in the relative neutron abundance, and hence, in the abundances of the light elements. In [56] the same author analyzed this problem in detail. From the requirement that the relic ${}^4\text{He}$ mass fraction must not exceed 28%, the inferred upper limit for the magnetic field of $B \lesssim 10^{12}$ G at the time when $T = 5 \times 10^9$ K is a stronger constraint than obtained in [51]. Magnetic fields of such strength will have no effects on the geometry of the expanding universe if they are sufficiently tangled over distances small compared to the cosmological horizon [56].

More recently, Cheng et al. [57] reexamined in detail the effects of primordial magnetic fields on BBN [†]. These authors found also that the strongest constraints on magnetic fields during the epoch of nucleosynthesis in the early universe comes from the increase of the expansion rate due to the energy contribution of the magnetic fields. They concluded that the allowed magnetic field strength at the end of nucleosynthesis ($T = 0.01$ MeV) is about 2×10^9 G, corresponding to $\sim 10^{-6}$ G today. This field strength corresponds to an upper limit of the magnetic energy density ρ_{mag} of about 28% of the neutrino energy density ρ_ν ($\rho_{\text{mag}} \leq 0.28 \rho_\nu$).

2.3. Models of magnetogenesis

The theories and models of magnetogenesis in cosmology can be divided into pure astrophysical mechanisms of magnetic field generation and, maybe more speculative

[†]Other reinvestigations of the influence of cosmic magnetic fields on BBN was done by Grasso and Rubinstein [58], and by Kernan, Starkman and Vachaspati [59]

but not less important, models of magnetogenesis in the very early universe. In this section I will give a short review of the most common models of magnetogenesis.

2.3.1. Astrophysical models

Already in 1950 Biermann [60] recognized that stellar magnetic fields can be produced out of a zero magnetic field due to charge separation in a differential rotating system (so called *Biermann battery* mechanism). He also applied his analysis to the interstellar medium finding that magnetic fields with strength $B \sim 10^{-19}$ G can be generated in interstellar gas clouds [61].

Subramanian, Narasimha and Chitre [5] in 1994 worked out that weak magnetic fields could be generated in ionization fronts originated from quasars or young galaxies at redshift $z \gtrsim 5$. The proposed mechanism is that of a thermal battery in ionization fronts, similar to the Biermann battery. The field strength can have a field strength of $B \sim 3 \times 10^{-20}$ G on galactic scales which can serve as seed fields for further amplification by galactic dynamo.

A similar approach to astrophysical magnetogenesis is discussed by the authors of [6] who showed that weak magnetic seed fields of the order of $B \sim 10^{-21}$ G could be generated from zero initial fields during the pre-galactic era due to the Biermann battery mechanism. This is the first out of three phases of the development of galactic magnetic fields. In the second phase the weak magnetic fields will be amplified by Kolmogorov turbulence developing during the gravitational collapse of the proto-galaxy but they are coherent only on length scales comparable to the smallest eddy. During the third phase, the authors argue that the magnetic fields will reach equipartition with the turbulent energy and the coherence length will be of the size of the largest turbulent eddy, comparable to the size of the galaxy.

2.3.2. Models of primordial magnetogenesis

In contrast to the astrophysical models of magnetogenesis there exists a plethora of models which are able to generate magnetic fields in the very early universe (for reviews see e.g. [18, 62]). Some of these models are listed in what follows.

In [63] Turner and Widrow pointed out that large scale (\sim Mpc) magnetic fields of astrophysical interest could be produced during **inflation** only if the conformal invariance of the electromagnetic theory is broken. These authors proposed also three methods of breaking the conformal invariance: by coupling the photon to the gravitational field, by coupling the photon to a charged scalar field which is itself not conformally invariant, and by the anomalous coupling of the photons to axions. The resulting magnetic fields could be strong enough to seed for the galactic dynamo, but are very model dependent. However, in the recent past it was questioned whether large scale magnetic fields of sufficient strength for seeding the galactic fields could

be generated during cosmological inflation [64]. The authors of [64] argue that dissipation effects due to a finite conductivity during inflation must be taken into account to calculate the final magnetic fields strength after inflation. Further, they conclude that the net magnetic field commonly is much weaker than needed for the galactic dynamo to work. However, Dimopoulos et al. argued in [65] that the natural breaking of conformal invariance by the production of heavy Z bosons during inflation may generate magnetic fields which are sufficient to seed the galactic dynamo.

Other mechanism for magnetogenesis in the early universe are motivated from particle physics. The most promising scenarios to produce seed magnetic fields are first-order **phase transitions**. The first pioneering analysis in this direction was done in the work [66]. Due to the expansion of bubble walls of the nucleated bubbles of one phase, charge separation of positively and negatively charged particles could occur. Similar to the Biermann battery mechanism, this charge separation generates electric currents, resulting in the generation of magnetic fields. Such models of magnetogenesis were studied by several authors for the electroweak (see e.g. [67, 68, 69, 70]) and the QCD phase transition (see e.g. [71, 72, 70]). In general, all these models predict magnetic fields which may be sufficient to seed the galactic dynamo. But, as these fields are generated by a causal process, their comoving coherence length cannot be larger than the Hubble length at the epoch of generation, which is much smaller than the galactic scale. Dynamical enhancement of the coherence length in a MHD system is probable, but in the most cases not sufficient to lengthen the coherence length to cluster size scales (see [73, 31] and chapter 8 of this work). Furthermore, it is not yet clear, whether the mentioned phase transitions are of first or higher order. For instance, limits on the mass of the Higgs boson makes a strong first-order electroweak phase transition unlikely.

Recently, the authors of [74] proposed a scenario of magnetogenesis due to a putative **inhomogeneous distribution of lepton number** when the neutrinos entering the free streaming regime. The inhomogeneous distribution of neutrinos and anti-neutrinos and the different cross sections for νe^+ and νe^- scattering result in a local separation of e^+e^- . Again, magnetic fields are generated from the electrical currents induced by the spatially separated charge carrier. If this scenario occurs during the epoch of neutrino decoupling ($T \sim \text{MeV}$) the resulting coherence length of the magnetic field might be much larger than in scenarios of magnetogenesis during the electroweak (EW) or QCD phase transition. A very optimistic estimate for the magnetic fields strength of this scenario gives $B \sim 10^{-10} \text{ G}$ at 100 kpc scale.

Another proposed mechanism of primordial magnetic field generation is due to the possible excitation of plasma vorticities by **cosmic strings** [75]. The idea that vortical motions can produce magnetic fields is based on the work of Harrison [76]. The argument made in [76] is the following. Due to the much larger scattering cross sections for photons on electrons than on ions, the electrons are dragged with the photon gas. But, as the angular momentum for the photon gas and the nonrelativistic matter are separately conserved, the angular velocities for electrons and ions have

different scaling properties with respect to the scale factor of the universe before recombination. The resulting electromotive force induced by the differential motions of electrons and ions, respectively, produces a magnetic field. One main ingredient of this scenario is a primordial **vorticity** field. As the vorticity is decaying during the expansion of the universe, a rather strong vorticity field is needed if the produced magnetic fields should be strong enough to seed the galactic dynamo. Such strong vorticity requires that rotational, or vector perturbations must be dominant at the time of radiation-matter equality. This seems to be in conflict with the standard scenario for galaxy formation [77]. But, cosmic strings – one dimensional topological defects which could be remnants of a phase transition in the early universe – are able to produce plasma vorticity after the onset of structure formation. In the scenario of [75], fast moving cosmic strings excite vorticity in plasma. The vortical eddies are gravitationally bound to the cosmic strings and therefore, are not decaying with the expansion of the universe. The authors of [75] showed that magnetic fields of the order of $B \sim 10^{-18}$ G with a coherence length $\sim 10 - 100$ kpc, the typical size of the wiggles of the strings, could be generated at the time of recombination. This field strength should be sufficient to seed a galactic dynamo.

3. Imperfect fluid dynamics and magnetic fields in the expanding universe

In this chapter I summarize the equations which describe the evolution of a magnetized imperfect fluid in the expanding universe. As one knows that on large scales the universe is homogeneous and isotropic, I will also specify the evolution equations on a Friedman-Robertson-Walker (FRW) background. If one introduces a proper rescaling of the dynamical variables of the MHD system these equations can be reduced to the well known set of magnetohydrodynamical differential equations. This is due to the conformal invariance of the conservation equations of the energy-momentum tensor in the radiation dominated universe. If one further assumes incompressibility of the ionized gas, the MHD equations in the FRW universe can be written in the same form as the coupled set of nonrelativistic, Newtonian MHD equations. Therefore, one can use standard numerical tools which solve the latter nonrelativistic equations, e.g. ZEUS3D, to study a magnetized fluid in the early universe.

In the matter dominated regime, where the conservation equations are not conformally invariant, one can also find a proper rescaling of the MHD variables, which leads to the same form of evolution equations as for a nonrelativistic MHD system in Minkowski space.

3.1. Imperfect fluid dynamics

Following [78] one can define a *fundamental observer* in the universe moving with the averaged 4-velocity u^μ with the normalization $u_\mu u^\mu = 1$ *. Such observers are provided with the projection operator [79, 78]

$$P^{\mu\nu} \equiv g^{\mu\nu} - u^\mu u^\nu \quad . \quad (3.1)$$

*In this work, I use a metric with signs $(+1, -1, -1, -1)$. Except where otherwise stated, natural units are used, e.g. $c = k_B = \mu_0 = \hbar = 1$, where c , k_B , μ_0 , and \hbar are the speed of light, Boltzmann's constant, the vacuum permeability, and the reduced Planck constant, respectively.

This allows for a unique splitting of spacetime into the timelike vector field u^μ and the spacelike three dimensional hyperplane Σ orthogonal to u^μ at any instant of time. The projection operator $P^{\mu\nu}$ has the following properties [78]

$$P^\mu{}_\nu u^\nu = 0 \quad , \quad (3.2)$$

$$P^{\mu\nu} = P^\mu{}_\lambda P^{\lambda\nu} \quad , \quad (3.3)$$

$$P^\mu{}_\mu = 3 \quad . \quad (3.4)$$

With the projection tensor $P^{\mu\nu}$ and the 4-velocity u^μ one can decompose the energy-momentum tensor as well as the conservation equations of energy-momentum into its temporal and spatial part.

The stress-energy tensor of an ideal fluid can be split into a timelike and a spacelike component [78]

$$T_1^{\mu\nu} = \rho u^\mu u^\nu - p P^{\mu\nu} \quad , \quad (3.5)$$

where ρ and p are the proper energy density and the pressure, respectively.

The covariant derivative of the 4-velocity can be decomposed into the basic physical properties [78]

$$u^\mu{}_{;\nu} = \sigma^\mu{}_\nu + \omega^\mu{}_\nu + \frac{\Theta}{3} P^\mu{}_\nu + \dot{u}^\mu u_\nu \quad (3.6)$$

where

$$\sigma^{\mu\nu} \equiv P^{(\mu}{}_\lambda P^{\nu)}{}_\gamma u^{\lambda;\gamma} - \frac{\Theta}{3} P^{\mu\nu} \quad (3.7)$$

$$= \frac{1}{2} \left(P^\nu{}_\lambda u^{\mu;\lambda} + P^\mu{}_\lambda u^{\nu;\lambda} \right) - \frac{\Theta}{3} P^{\mu\nu} \quad ,$$

$$\omega^{\mu\nu} \equiv P^{[\mu}{}_\lambda P^{\nu]}{}_\gamma u^{\lambda;\gamma} \quad (3.8)$$

$$= \frac{1}{2} \left(P^\nu{}_\lambda u^{\mu;\lambda} - P^\mu{}_\lambda u^{\nu;\lambda} \right) \quad ,$$

$$\Theta \equiv u^\mu{}_{;\mu} \quad , \quad (3.9)$$

$$\dot{u}^\mu \equiv u^{\mu;\lambda} u_\lambda \quad , \quad (3.10)$$

are the shear tensor, the vorticity tensor, the expansion scalar and the 4-acceleration[†], respectively. As usual, $X^{(\mu\nu)} \equiv 1/2(X^{\mu\nu} + X^{\nu\mu})$ denotes the symmetric part of a tensor, whereas $X^{[\mu\nu]} \equiv 1/2(X^{\mu\nu} - X^{\nu\mu})$ is its antisymmetric part, and $X_{;\mu}$ is the covariant derivative of the tensor X , and $X_{,\mu}$ is its partial derivative with respect to the coordinate x^μ , respectively (cf. also appendix A.1). The expansion scalar is a measure of contraction or stretching of a fluid world line R , i.e. $\dot{R}/R = \Theta/3$, and coincides with the Hubble parameter H in the case of a perfect FRW universe.

[†]In this chapter a $\dot{}$ (over-dot) denotes always the projected timelike derivative $\dot{X} \equiv X_{;\lambda} u^\lambda$ of the tensor X , which is the generalized convective derivative and equal to $(\partial_t + \mathbf{v} \cdot \nabla) X$ in the Newtonian limit.

Together with the heat flow vector [79]

$$q^\mu \equiv P^\mu{}_\nu (T^{\nu} + T \dot{u}^\nu) \quad , \quad (3.11)$$

the most general stress-energy tensor for an imperfect fluid where u^μ is the velocity of particle transport is given by [79, 80]

$$T_{\text{NI}}^{\mu\nu} = 2\nu \sigma^{\mu\nu} + \xi \Theta P^{\mu\nu} + \chi (u^\mu q^\nu + q^\mu u^\nu) \quad , \quad (3.12)$$

where ν , ξ and χ can be identified by the shear viscosity, bulk viscosity and heat conduction, respectively.

In the relativistic approach of hydrodynamics one has to specify whether the velocity u^μ is connected with the transport of particles [79] or energy [25]. Of course, both approaches are totally equivalent and the choice of one of these is a matter of convenience. Here, I follow the approach used in [79], where u^μ is the velocity of particle transport. Then, the particle current 4-vector is given by:

$$n^\mu = n u^\mu \quad , \quad (3.13)$$

where n is the proper number density of the conserved particle species. The latter can be associated with the baryon number n_B which is conserved below temperatures of the electroweak phase transition.

The conservation of the particle number becomes [79]:

$$n^\mu{}_{;\mu} = 0 \quad . \quad (3.14)$$

The equations of motion of the imperfect fluid with the total energy tensor

$$T_{\text{fluid}}^{\mu\nu} = T_{\text{I}}^{\mu\nu} + T_{\text{NI}}^{\mu\nu} \quad (3.15)$$

are governed by the energy conservation equation [79]

$$(T_{\text{fluid}}^{\mu\nu})_{;\nu} = 0 \quad . \quad (3.16)$$

By projecting equation (3.16) to the timelike spacetime direction, i.e. $u_\mu T^{\mu\nu}{}_{;\nu} = 0$ one gets the scalar equation

$$\dot{\rho} + \Theta (\rho + p) = -2 u_\mu (\nu \sigma^{\mu\nu})_{;\nu} - u_\mu (\xi \Theta P^{\mu\nu})_{;\nu} - 2 u_\mu (\chi u^{(\mu} q^{\nu)})_{;\nu} \quad . \quad (3.17)$$

The vector equation of motion can be obtained by projecting equation (3.16) to the spacelike hypersurface, i.e. $P_{\mu\lambda} T^{\lambda\nu}{}_{;\nu} = 0$,

$$(\rho + p) \dot{u}_\mu - P^\mu{}_\lambda p^{;\lambda} = -P^\mu{}_\lambda \left[2 (\nu \sigma^{\lambda\nu})_{;\nu} + (\xi \Theta P^{\lambda\nu})_{;\nu} + 2 (\chi u^{(\lambda} q^{\nu)})_{;\nu} \right] \quad . \quad (3.18)$$

3.2. Covariant description of electromagnetic fields

This section gives a summary of the covariant description of the electromagnetic field embedded in a conducting fluid and seen by a fundamental observer. By inspecting the electromagnetic stress-energy tensor it can be seen that its structure is similar to a fluid with heat flow and shear [81].

The antisymmetric Maxwell tensor [82]

$$F^{\mu\nu} = A^{\mu;\nu} - A^{\nu;\mu} = A^{\mu,\nu} - A^{\nu,\mu} \quad (3.19)$$

obeys Maxwell's equations and the Bianchi identity, respectively [82]

$$F^{\mu\nu}{}_{;\nu} = 4\pi J^\mu \quad , \quad (3.20)$$

$$F^{[\mu\nu;\lambda]} = \frac{1}{3} (F^{\mu\nu;\lambda} + F^{\nu\lambda;\mu} + F^{\lambda\mu;\nu}) = 0 \quad , \quad (3.21)$$

where A^μ is the 4-vector potential of the electromagnetic field and J^μ is the 4-current density.

A fundamental observer can decompose the electromagnetic field tensor (3.19) into an electric and magnetic part by using the following relations [78]

$$E^\mu = u_\nu F^{\nu\mu} \quad , \quad (3.22)$$

$$B^\mu = \frac{1}{2} \epsilon^{\mu\nu\lambda\gamma} u_\nu F_{\lambda\gamma} \quad , \quad (3.23)$$

where E^μ and B^μ are the electric and magnetic 4-vectors and $\epsilon^{\mu\nu\lambda\gamma}$ is the total antisymmetric tensor with $\epsilon^{0123} = +1$, respectively. Due to the antisymmetry of (3.19), E^μ and B^μ possess only three independent components and therefore can be considered as 3-vectors \mathbf{E} and \mathbf{B} , respectively. This fact can also be seen by projecting (3.22) and (3.23) onto the observers instantaneous rest frame:

$$P^\mu{}_\nu E^\nu = E^\mu \iff u_\mu E^\mu = 0 \quad , \quad (3.24)$$

$$P^\mu{}_\nu B^\nu = B^\mu \iff u_\mu B^\mu = 0 \quad . \quad (3.25)$$

In what follows, I use therefore a frame where $E^\mu = (0, \mathbf{E})$ and $B^\mu = (0, \mathbf{B})$.

The definitions (3.22) and (3.23) together with the relations (3.24) and (3.25) can be used to rewrite Maxwell's tensor (3.19) in terms of the electric and magnetic field [78]

$$F^{\mu\nu} = u^\mu E^\nu - u^\nu E^\mu + \epsilon^{\mu\nu\lambda\gamma} u_\lambda B_\gamma \quad . \quad (3.26)$$

If one uses the dual transformation of the field tensor [82]

$$\mathcal{F}^{\mu\nu} \equiv \frac{1}{2} \epsilon^{\mu\nu\lambda\gamma} F_{\lambda\gamma} \quad , \quad (3.27)$$

which implies [82]

$$E^\mu \rightarrow B^\mu \quad , \quad (3.28)$$

$$B^\mu \rightarrow -E^\mu \quad , \quad (3.29)$$

the Bianchi identity can be written in the following form [82]:

$$\mathcal{F}^{\mu\nu}{}_{;\nu} = 0 \quad . \quad (3.30)$$

Together with the definitions (3.26), Maxwell's equations (3.20) and (3.30) become [78]

$$P^\mu{}_\nu E^\nu{}_{;\mu} + \epsilon^{\nu\lambda\gamma\sigma} u_\nu \omega_{\lambda\gamma} B_\sigma = 4\pi n_c \quad , \quad (3.31)$$

$$\begin{aligned} P^\mu{}_\nu \epsilon^{\nu\lambda\gamma\sigma} (u_\lambda B_{\gamma;\sigma} - B_\lambda u_{\gamma;\sigma}) - P^\mu{}_\nu \dot{E}^\nu \\ + \left(\sigma^\mu{}_\nu + \omega^\mu{}_\nu - \frac{2}{3} \Theta P^\mu{}_\nu \right) E^\nu = 4\pi P^\mu{}_\nu J^\nu \quad , \end{aligned} \quad (3.32)$$

$$P^\mu{}_\nu B^\nu{}_{;\mu} - \epsilon^{\nu\lambda\gamma\sigma} u_\nu \omega_{\lambda\gamma} E_\sigma = 0 \quad , \quad (3.33)$$

$$\begin{aligned} -P^\mu{}_\nu \epsilon^{\nu\lambda\gamma\sigma} (u_\lambda E_{\gamma;\sigma} - E_\lambda u_{\gamma;\sigma}) - P^\mu{}_\nu \dot{B}^\nu \\ + \left(\sigma^\mu{}_\nu + \omega^\mu{}_\nu - \frac{2}{3} \Theta P^\mu{}_\nu \right) B^\nu = 0 \quad , \end{aligned} \quad (3.34)$$

where $n_c = u_\mu J^\mu$ is the net number density of charged particles of the fluid.

The electromagnetic stress-energy tensor has the following general form [82, 79]

$$T_{\text{em}}^{\mu\nu} = \frac{1}{4\pi} \left(-F^{\mu\lambda} F^\nu{}_\lambda + \frac{1}{4} g^{\mu\nu} F^{\lambda\gamma} F_{\lambda\gamma} \right) \quad . \quad (3.35)$$

Using (3.26) the electromagnetic energy-momentum tensor (3.35) in terms of the electric and magnetic fields reads as follows [78, 81]:

$$\begin{aligned} 4\pi T_{\text{em}}^{\mu\nu} = & \left(\frac{\mathbf{E}^2 + \mathbf{B}^2}{2} \right) u^\mu u^\nu - \left(\frac{\mathbf{E}^2 + \mathbf{B}^2}{2} \right) P^{\mu\nu} - E^\mu E^\nu - B^\mu B^\nu \\ & + 2 u^{(\mu} \epsilon^{\nu)\alpha\lambda\beta} u_\alpha E_\lambda B_\beta \quad . \end{aligned} \quad (3.36)$$

The energy-momentum tensor of the electromagnetic field (3.36) can be associated with the energy tensor of the imperfect fluid (3.15) [81]

$$T_{\text{em}}^{\mu\nu} = \rho_{\text{em}} u^\mu u^\nu - p_{\text{em}} P^{\mu\nu} + 2 u^{(\mu} q_{\text{em}}^{\nu)} + 2 \pi^{\mu\nu} \quad . \quad (3.37)$$

The corresponding quantities which associate the electromagnetic field with an imperfect fluid are the electromagnetic energy density, the electromagnetic pressure, the momentum flow and the anisotropic pressure, respectively [81]

$$\rho_{\text{em}} \equiv \left(\frac{\mathbf{E}^2 + \mathbf{B}^2}{8\pi} \right) \equiv -\frac{1}{8\pi} P^\mu{}_\nu (B_\mu B^\nu + E_\mu E^\nu) \quad , \quad (3.38)$$

$$p_{\text{em}} \equiv \frac{1}{3} \left(\frac{\mathbf{E}^2 + \mathbf{B}^2}{8\pi} \right) = \frac{1}{3} \rho_{\text{em}} \quad , \quad (3.39)$$

$$q_{\text{em}}^\mu \equiv \frac{1}{4\pi} \epsilon^{\mu\nu\lambda\gamma} u_\nu E_\lambda B_\gamma \quad , \quad (3.40)$$

$$\pi^{\mu\nu} \equiv - \left(\frac{E^\mu E^\nu + B^\mu B^\nu}{8\pi} \right) - p_{\text{em}} P^{\mu\nu} \quad . \quad (3.41)$$

The equations of motion for the electromagnetic part can now be obtained by using (3.37), the definitions (3.41) – (3.38), and the results of (3.17). Then, one obtains the following equations for the energy conservation

$$\begin{aligned} \dot{\rho}_{\text{em}} + \Theta (\rho_{\text{em}} + p_{\text{em}}) &= -\frac{1}{4\pi} \epsilon^{\mu\nu\lambda\gamma} \left(u_{\nu;\mu} E_\lambda B_\gamma + u_\nu E_{\lambda;\mu} B_\gamma + u_\nu E_\lambda B_{\gamma;\mu} \right) \\ &\quad - \frac{1}{4\pi} \epsilon^{\mu\nu\lambda\gamma} u_\mu \dot{u}_\nu E_\lambda B_\gamma - \sigma_{\mu\nu} \left(\frac{E^\mu E^\nu + B^\mu B^\nu}{4\pi} \right) \quad , \end{aligned} \quad (3.42)$$

and for the vector part (3.18):

$$\begin{aligned} (\rho_{\text{em}} + p_{\text{em}}) \dot{u}^\mu - P^\mu{}_\lambda p_{\text{em}}^{;\lambda} &= -\frac{1}{4\pi} \epsilon^{\nu\lambda\gamma\sigma} \left(u^\mu{}_{;\nu} u_\lambda E_\gamma B_\sigma + u^\mu u_\nu \dot{u}_\lambda E_\gamma B_\sigma \right) \\ &\quad - \frac{1}{4\pi} \epsilon^{\nu\lambda\gamma\sigma} \left(\Theta u_\lambda E_\gamma B_\sigma - \dot{u}_\lambda E_\gamma B_\sigma \right) \\ &\quad - \frac{1}{4\pi} \epsilon^{\nu\lambda\gamma\sigma} \left(u_\lambda \dot{E}_\gamma B_\sigma + u_\lambda E_\gamma \dot{B}_\sigma \right) \\ &\quad + \frac{1}{4\pi} P^\mu{}_\lambda \left(E^\lambda{}_{;\nu} E^\nu + E^\lambda E^\nu{}_{;\nu} + B^\lambda{}_{;\nu} B^\nu + B^\lambda B^\nu{}_{;\nu} \right) \\ &\quad + 2 P^\mu{}_\lambda p_{\text{em}}^{;\lambda} - 2 p_{\text{em}} \dot{u}^\mu \quad . \end{aligned} \quad (3.43)$$

3.2.1. Medium with infinite conductivity

Ohm's law relates the current density with the electric field and is given in a neutral conducting medium by [82]

$$P^\mu{}_\nu J^\nu = \sigma P^\mu{}_\nu E^\nu = \sigma E^\mu \quad , \quad (3.44)$$

where σ is the conductivity of the medium. For an infinitely conducting fluid, i.e. $\sigma \rightarrow \infty$, the current J^μ remains finite and Ohm's law (3.44) is compatible with $E^\mu \rightarrow 0$. In this case Maxwell's equations (3.31) – (3.34) reduce to [81]

$$\epsilon^{\nu\lambda\gamma\sigma} u_\nu \omega_{\lambda\gamma} B_\sigma = 4\pi n_c = 0 \quad , \quad (3.45)$$

$$P^\mu{}_\nu \epsilon^{\nu\lambda\gamma\sigma} (u_\lambda B_{\gamma;\sigma} - B_\lambda u_{\gamma;\sigma}) = 4\pi P^\mu{}_\nu J^\nu \quad , \quad (3.46)$$

$$P^\mu{}_\nu B^\nu{}_{;\mu} = 0 \quad , \quad (3.47)$$

$$P^\mu{}_\lambda \dot{B}^\lambda - \left(\sigma^\mu{}_\lambda + \omega^\mu{}_\lambda - \frac{2}{3} \Theta P^\mu{}_\lambda \right) B^\lambda = 0 \quad . \quad (3.48)$$

Contracting Faraday's law (3.48) with B_μ one obtains again the energy equation for the magnetic field, i.e.

$$\dot{\rho}_{\text{mag}} + \Theta (\rho_{\text{mag}} + p_{\text{mag}}) + \frac{1}{4\pi} \sigma^\mu{}_\nu B_\mu B^\nu = 0 \quad , \quad (3.49)$$

where $\rho_{\text{mag}} = \mathbf{B}^2/(8\pi) = -P^\mu{}_\nu B_\mu B^\nu/(8\pi) = 3p_{\text{mag}}$. Note, this is not a trivial result because it states that the magnetic “energy” is conserved on its own (i.e. this conservation law is already contained in Maxwell's equations) even when combined with an imperfect fluid such as (3.15).

The vector part of the equations of motions (3.43) with a vanishing electrical field becomes:

$$2\rho_{\text{mag}} \dot{u}^\mu - P^\mu{}_\nu \rho_{\text{mag}}^{\nu} - \frac{1}{4\pi} P^\mu{}_\lambda B^\lambda{}_{;\nu} B^\nu - \frac{1}{4\pi} B^\mu B^\nu{}_{;\nu} = 0 \quad . \quad (3.50)$$

3.3. The MHD equations in the FRW universe

In General Relativity the local energy distribution induces the metric of the spacetime which is described by Einstein's equation [79]

$$G^{\mu\nu} = \kappa T^{\mu\nu} \quad , \quad (3.51)$$

where $G^{\mu\nu}$ is the Einstein tensor and $\kappa = 8\pi G$ with G being Newton's gravitational constant. Here, the total energy-momentum tensor for a nonideal magnetized fluid is

$$T^{\mu\nu} = T_{\text{fluid}}^{\mu\nu} + T_{\text{em}}^{\mu\nu} \quad , \quad (3.52)$$

where $T_{\text{fluid}}^{\mu\nu}$ and $T_{\text{em}}^{\mu\nu}$ are given by the equations (3.15) and (3.37), respectively.

One knows from various kinds of observations (e.g. observations of the CMBR or large scale structures of the universe) that the large scale universe is homogeneous and isotropic. Furthermore, I assume that the spacetime is described by the Friedman-Robertson-Walker (FRW) metric

$$g_{\mu\nu} = \text{diag}(1, -a^2, -a^2, -a^2) \quad (3.53)$$

with the scale factor $a = a(t)$. In this case the anisotropic stresses of (3.15) and (3.35) must be small compared to the diagonal parts of the total energy-momentum tensor[‡]. This condition has the following implications. First of all the local fluid 3-velocity \mathbf{v} must be small compared to the speed of light, e.g. $|\mathbf{v}| \ll 1$. Therefore, the 4-velocity in Minkowski space[§] can be written as

$$u'^{\mu} = (1, \mathbf{v}) \quad . \quad (3.54)$$

[‡]The Einstein tensor of the metric (3.53) contains only diagonal elements.

[§]In this section, primed quantities are given in Minkowski space

Furthermore, the electromagnetic field components have to be small compared to the energy density of the universe if one does not take into account back reactions to the metric $g_{\mu\nu}$. Limits on the magnetic field strength due to gravitational wave production are computed by the authors of [83]. The observed isotropy of the universe also does not allow the existence of a strong, homogeneous, large-scale magnetic or electric field. The best current constraint on the field strength of such a homogeneous magnetic field is $B_0 < 3.4 \times 10^{-9}$ G today [39]. This limit was derived from statistical analysis of the 4-year Cosmic Background Explorer (COBE) data for anisotropy patterns [37].

For vanishing velocity fluctuations, i.e. $\mathbf{v} = 0$ the energy conservation equation for the electromagnetic field (3.42) reduces to

$$\left(\frac{\partial}{\partial t} + 4H \right) \rho_{\text{em}} = 0 \quad , \quad (3.55)$$

which has the solution $a^4 \rho_{\text{em}} = \text{const.}$ Therefore, the energy density of magnetic fields is diluted by the expansion of the universe in the same way as the energy density of radiation.

The equivalence principle of General Relativity allows the transformation of any tensor X' which is properly defined in gravity-free Minkowski space, with the coordinates x'^{μ} into the expanding FRW universe with coordinates x^{μ} . Contravariant tensors transform according to [79]

$$X^{\alpha_1 \alpha_2 \dots \alpha_n} = \Lambda^{\alpha_1}_{\beta_1} \Lambda^{\alpha_2}_{\beta_2} \dots \Lambda^{\alpha_n}_{\beta_n} X'^{\alpha_1 \alpha_2 \dots \alpha_n} \quad , \quad (3.56)$$

with the transformation matrix $\Lambda^{\mu}_{\nu} \equiv \frac{\partial x^{\mu}}{\partial x'^{\nu}}$. Covariant tensors transform with the inverse of Λ^{μ}_{ν} .

By transforming the 4-velocity (3.54) and the electromagnetic field tensor (3.26) from Minkowski to FRW space using the above transformation law one gets the following coupled set of equations for a magnetized plasma,

$$T^{\mu\nu}_{;\nu} = (T^{\mu\nu}_{\text{fluid}})_{;\nu} + (T^{\mu\nu}_{\text{em}})_{;\nu} = 0 \quad (3.57)$$

with infinite conductivity

$$\frac{\partial \rho}{\partial t} + \frac{1}{a} \nabla \cdot ((\rho + p) \mathbf{v}) + 3H (\rho + p) = \frac{6}{a} H \xi (\nabla \cdot \mathbf{v}) - \chi \nabla \cdot \mathbf{q} \quad , \quad (3.58)$$

$$\begin{aligned} & \frac{1}{a} \left(\frac{\partial}{\partial t} + \frac{1}{a} (\mathbf{v} \cdot \nabla) + H \right) \mathbf{v} + \frac{1}{a} \frac{\mathbf{v}}{\rho + p} \frac{\partial p}{\partial t} + \frac{1}{a^2} \frac{\nabla p}{\rho + p} + \frac{1}{a^2} \left(\frac{\mathbf{B} \times (\nabla \times \mathbf{B})}{4\pi (\rho + p)} \right) = \\ & \frac{1}{a^3} \frac{\nu}{\rho + p} \left(\nabla^2 \mathbf{v} + \frac{1}{3} \nabla (\nabla \cdot \mathbf{v}) \right) + \frac{1}{a^3} \frac{\xi}{\rho + p} \nabla (\nabla \cdot \mathbf{v}) - \frac{1}{\rho + p} \left(\frac{\partial}{\partial t} + 5H \right) \chi \mathbf{q} \quad , \end{aligned} \quad (3.59)$$

$$\frac{1}{a} \left(\frac{\partial}{\partial t} + 2H \right) \mathbf{B} = \frac{1}{a^2} \nabla \times (\mathbf{v} \times \mathbf{B}) , \quad (3.60)$$

where it was assumed that $\rho_{\text{em}} \ll \rho = \rho_{\text{fluid}}$ and only terms of the lowest order in v/c were kept. In the small velocity approximation the three dimensional heat flow vector

$$\begin{aligned} \mathbf{q} &= -\frac{1}{a^2} \nabla T + \frac{1}{a} \mathbf{v} \frac{\partial T}{\partial t} + \frac{1}{a} T \left(\frac{\partial}{\partial t} + \frac{1}{a} (\mathbf{v} \cdot \nabla) + H \right) \mathbf{v} \\ &= -\frac{1}{a^2} \left(\nabla T - \frac{\partial}{\partial t} (a T \mathbf{v}) - T (\mathbf{v} \cdot \nabla) \mathbf{v} \right) \end{aligned} \quad (3.61)$$

becomes $\mathbf{q} \approx -a^{-2} \nabla T$. The last terms in (3.61) can be neglected because the derivatives are of $\mathcal{O}((v/c)^2)$ and $a^{-1} \nabla T \approx T/l_{\text{phys}} \gg HT \approx T/l_H$ as $l_H \gg l_{\text{phys}}$ for causally connected regions.

The shear viscosity ν , the bulk viscosity ξ , and the heat conductivity χ , are given by [84, 79]:

$$\nu = \frac{4}{15} \frac{\pi^2}{30} g_* T^4 l_{\text{mfp}} , \quad (3.62)$$

$$\xi = 4 \frac{\pi^2}{30} g_* T^4 l_{\text{mfp}} \left[\frac{1}{3} - \left(\frac{\partial p}{\partial \rho} \right)_n \right]^2 , \quad (3.63)$$

$$\chi = \frac{4}{3} \frac{\pi^2}{30} g_* T^3 l_{\text{mfp}} , \quad (3.64)$$

where g_* is the number of relativistic degrees of freedom, i.e. [55],

$$g_* = \sum_{i=\text{bosons}} g_i + \frac{7}{8} \sum_{i=\text{fermions}} g_i , \quad (3.65)$$

and l_{mfp} is the mean free path of the relativistic particles (photons or neutrinos) as specified in chapter 8.

The trace of (3.52) is in general non-vanishing and is given by:

$$T^\mu{}_\mu = \rho - 3p + 3\Theta\xi . \quad (3.66)$$

For relativistic particles, where $p = \rho/3$ and $\xi = 0$, the trace of the total energy-momentum tensor vanishes. In this case, the equations of motion (3.57) become *conformally invariant* in the FRW universe. This implies that the MHD variables can be transformed such that the equations of motion have exactly the same form as in Minkowski space [85]. Such a transformation may not be found if the r.h.s of equation (3.66) is not zero.

3.4. MHD equations in the radiation dominated universe

By introducing the conformal time variable

$$d\tilde{t} = dt a^{-1} \quad , \quad (3.67)$$

the line element becomes

$$ds^2 = a^2 \left(d\tilde{t}^2 - \sum_{i=1}^3 dx^i dx^i \right) \quad , \quad (3.68)$$

where x^i are the comoving coordinates.

From (3.68) it can be seen that the metric of the FRW universe (3.53) is *conformally equivalent* to the metric of the flat Minkowski space (cf. e.g. [85]), i.e.

$$g_{\mu\nu} = \Omega^2(x'^{\mu}) g'_{\mu\nu} \quad , \quad (3.69)$$

where $\Omega = a(t)$ and $g'_{\mu\nu} = \text{diag}(1, -1, -1, -1)$ is the metric in Minkowski space.

If the fluid consists of relativistic particles in the radiation dominated universe the total pressure is the radiation pressure

$$p = \frac{1}{3} \rho \quad . \quad (3.70)$$

This implies that the trace $T = T^{\mu}_{\mu}$ of the total stress-energy tensor of the magnetized fluid (3.52) vanishes (cf. equation (3.66)) which in turn means that the equations of motion are invariant under the conformal transformation [85]:

$$T'^{\mu\nu}{}_{;\nu} = 0 \iff T^{\mu\nu}{}_{;\nu} = 0 \quad \text{for} \quad T^{\mu\nu} = \Omega^{-6} T'^{\mu\nu} \quad , \quad (3.71)$$

where the covariant derivative of the primed (unprimed) tensor is given with respect to the primed (unprimed) metric.

With the following rescaled variables (see e.g. [28]):

$$\begin{aligned} \tilde{\rho} &\equiv \rho a^4 & \tilde{p} &\equiv p a^4 & \tilde{\mathbf{B}} &\equiv \mathbf{B} a^2 \\ \tilde{\mathbf{v}} &\equiv \mathbf{v} & \tilde{T} &\equiv T a & \tilde{\chi} &\equiv \chi a^2 \\ \tilde{\nu} &\equiv \nu a^3 \end{aligned} \quad (3.72)$$

one obtains the MHD equations which have the same form as in Minkowski space:

$$\frac{\partial \tilde{\rho}}{\partial \tilde{t}} + \nabla \cdot \left((\tilde{\rho} + \tilde{p}) \tilde{\mathbf{v}} \right) = \tilde{\chi} \nabla^2 \tilde{T} \quad , \quad (3.73)$$

$$\begin{aligned} \left(\frac{\partial}{\partial \tilde{t}} + (\tilde{\mathbf{v}} \cdot \nabla) \right) \tilde{\mathbf{v}} + \frac{\tilde{\mathbf{v}}}{\tilde{\rho} + \tilde{p}} \frac{\partial \tilde{p}}{\partial \tilde{t}} + \frac{\nabla \tilde{p}}{\tilde{\rho} + \tilde{p}} + \frac{\tilde{\mathbf{B}} \times (\nabla \times \tilde{\mathbf{B}})}{4\pi (\tilde{\rho} + \tilde{p})} = \\ \frac{\tilde{\nu}}{\tilde{\rho} + \tilde{p}} \left(\nabla^2 \tilde{\mathbf{v}} + \frac{1}{3} \nabla (\nabla \cdot \tilde{\mathbf{v}}) \right) + \frac{1}{\tilde{\rho} + \tilde{p}} \frac{\partial}{\partial \tilde{t}} (\tilde{\chi} \nabla \tilde{T}) , \end{aligned} \quad (3.74)$$

$$\frac{\partial \tilde{\mathbf{B}}}{\partial \tilde{t}} = \nabla \times (\tilde{\mathbf{v}} \times \tilde{\mathbf{B}}) \quad , \quad (3.75)$$

Note, that the scaling laws (3.72) are unique if one wants to omit any terms which include the Hubble rate H in the MHD equations. Hence, all tilded variables have the physical meaning of *comoving* quantities.

3.4.1. The incompressible limit

As already mentioned, observations limit the relative density fluctuations to be smaller than 10^{-5} in the radiation dominated epoch of the universe. This fact and the restriction to small velocity fluctuations which are in fact much smaller than the sound velocity $c_s = 1/\sqrt{3}$ for relativistic particles, allows one to consider the MHD system in the incompressible approximation. It is clear, that one can not study density perturbations excited by magnetic fields within the incompressible limit because all compressional magnetosonic modes are suppressed with respect to Alfvénic modes. For weak magnetic fields, i.e. $\rho_{\text{mag}}/\rho \ll 1$, the incompressible limit is a reasonable approximation to study the damping of magnetic fields.

In this incompressible limit the divergence of the fluid velocity, which induces density perturbations, vanishes

$$\nabla \cdot \mathbf{v} = 0 \quad . \quad (3.76)$$

By splitting the energy density and the radiation pressure into dominant, homogeneous, parts (ρ_0 and p_0) and into small fluctuating parts (ρ_1 and p_1), i.e.

$$\tilde{\rho} = \tilde{\rho}_0 \left(1 + \Delta_\rho^{\text{matter}} + \Delta_\rho^{\text{thermal}} \right) \quad \text{and} \quad (3.77)$$

$$\tilde{p} = \tilde{p}_0 (1 + \Delta_p) \quad (3.78)$$

with $\Delta_\rho^{\text{matter}}, \Delta_\rho^{\text{thermal}} \ll 1$ and $\Delta_p \ll 1$, the MHD equations in the incompressible limit become:

$$\left(\frac{\partial}{\partial \tilde{t}} + \tilde{\mathbf{v}} \cdot \nabla \right) \tilde{\mathbf{v}} + \frac{\tilde{\mathbf{B}} \times (\nabla \times \tilde{\mathbf{B}})}{4\pi (\tilde{\rho}_0 + \tilde{p}_0)} = \tilde{\nu}_{\text{eff}} \nabla^2 \tilde{\mathbf{v}} + \tilde{\chi}_{\text{eff}} \frac{\partial}{\partial \tilde{t}} (\nabla \tilde{T}) \quad , \quad (3.79)$$

$$\frac{\partial \tilde{\mathbf{B}}}{\partial \tilde{t}} = \nabla \times (\tilde{\mathbf{v}} \times \tilde{\mathbf{B}}) \quad . \quad (3.80)$$

The above equations are identical to the incompressible MHD equations in the Newtonian case. This allows one to use already existing numerical methods which

are designed for the investigation of strictly Newtonian MHD problems on a static background to solve the equations (3.79)–(3.80). As already mentioned at the beginning of this chapter, to find numerical solutions of the above equations for stochastic initial magnetic fields, I used the code ZEUS3D [34].

Here, I introduced also the effective shear viscosity and effective heat conduction

$$\tilde{\nu}_{\text{eff}} = \frac{\tilde{\nu}}{\tilde{\rho}_0 + \tilde{p}_0} \quad , \quad (3.81)$$

$$\tilde{\chi}_{\text{eff}} = \frac{\tilde{\chi}}{\tilde{\rho}_0 + \tilde{p}_0} \quad . \quad (3.82)$$

In the radiation dominated universe the energy density and the pressure of relativistic particles are respectively, $\rho = \pi^2/30 g_* T^4$ and $p = \rho/3 = \pi^2/90 g_* T^4$. Therefore, the effective dissipation parameters are

$$\tilde{\nu}_{\text{eff}} = \frac{1}{5} \tilde{l}_{\text{mfp}} \quad , \quad (3.83)$$

$$\tilde{\chi}_{\text{eff}} = \tilde{T} \tilde{l}_{\text{mfp}} \quad , \quad (3.84)$$

where \tilde{l}_{mfp} is the comoving mean free path, $\tilde{l}_{\text{mfp}} = l_{\text{mfp}}/a$. Note, that the comoving mean free path of neutrinos is increasing already at temperatures of the universe below 100 GeV and the comoving photon mean free path is increasing after electrons and positrons become nonrelativistic. This fact has an important influence on the dynamics of the magnetized fluid which will be discussed in the next paragraph.

3.4.2. Dissipation in the free streaming regime

Dissipation of MHD modes occurs through interaction of the conducting fluid particles with the radiation background. This process becomes important whenever the interaction rate of the background particle (e.g. neutrinos or photons) $1/l_{\text{mfp}}$ gets smaller than the interaction rate of the fluid particles (e.g. protons or e^\pm) with themselves. Then the background radiation no longer participates in local fluid flows and therefore is decoupled from the fluid. In the expanding universe the comoving mean free path of the background radiation particles l_{mfp}/a starts to increase after the radiation decouples from the fluid while the comoving wavelength λ of a certain mode stays constant. Now consider modes with wavelength λ much larger than the mean free path of the fluid particles l_{fluid} . Then, when the mean free path l_{mfp} gets larger than the wavelength λ , the decoupled background particles start to *free stream* over that mode. For such modes the decoupled particles act as a uniform heat bath and dissipation occurs through occasional scatter of the fluid particles with the radiation background. The dissipation process in this free streaming regime is different from the dissipation of velocity fluctuations in the diffusion regime where the mean free path is much shorter than the wavelength of the mode.

In the free streaming regime, or “optical thin” medium, one can define a drag coefficient α and a heat exchange coefficient β which account in a statistical manner for the incidental interactions of the fluid particles with the background particles [86, 22]. Then the drag force per unit volume is given by [22]

$$\mathbf{f} \equiv -\alpha \mathbf{v} \rho_{\text{fluid}} \quad (3.85)$$

and heat exchange is [22]:

$$\frac{\partial \rho_{\text{thermal}}}{\partial t} = -\beta \rho_{\text{thermal}} \quad . \quad (3.86)$$

The coefficients α and β can be computed by calculating the momentum and heat transfer in each interaction process and averaging it over the distribution of background and fluid particles. The exact form of these coefficients can be found in chapter 8, where the evolution of subhorizon magnetic fields in the neutrino and photon free streaming regime are discussed.

With the definitions (3.85) and (3.86) one obtains the energy conservation (3.73) and the Euler equation (3.74) in the free streaming regime

$$\frac{\partial \tilde{\rho}}{\partial \tilde{t}} + \nabla \cdot \left((\tilde{\rho} + \tilde{p}) \tilde{\mathbf{v}} \right) = -\tilde{\beta} \tilde{\rho}_{\text{thermal}} \quad , \quad (3.87)$$

$$\left(\frac{\partial}{\partial \tilde{t}} + (\tilde{\mathbf{v}} \cdot \nabla) \right) \tilde{\mathbf{v}} + \frac{\tilde{\mathbf{v}}}{\tilde{\rho} + \tilde{p}} \frac{\partial \tilde{p}}{\partial \tilde{t}} + \frac{\nabla \tilde{p}}{\tilde{\rho} + \tilde{p}} + \frac{\tilde{\mathbf{B}} \times (\nabla \times \tilde{\mathbf{B}})}{4\pi (\tilde{\rho} + \tilde{p})} = -\frac{\tilde{\rho}}{\tilde{\rho} + \tilde{p}} \tilde{\alpha} \tilde{\mathbf{v}} \quad , \quad (3.88)$$

where ρ is the energy density of the fluid and ρ_{thermal} is the thermal energy density which can be the same in the high temperature regime where the fluid particles are relativistic. The drag and heat exchange coefficients have the following rescaled properties in the radiation dominated universe:

$$\tilde{\alpha} \equiv a \alpha \quad , \quad (3.89)$$

$$\tilde{\beta} \equiv a \beta \quad . \quad (3.90)$$

In the incompressible limit the pressure derivative can be neglected and the Euler equation (3.88) becomes:

$$\left(\frac{\partial}{\partial \tilde{t}} + \tilde{\mathbf{v}} \cdot \nabla \right) \tilde{\mathbf{v}} + \frac{\tilde{\mathbf{B}} \times (\nabla \times \tilde{\mathbf{B}})}{4\pi (\tilde{\rho}_0 + \tilde{p}_0)} = -\tilde{\alpha}_{\text{eff}} \tilde{\mathbf{v}} \quad , \quad (3.91)$$

where

$$\tilde{\alpha}_{\text{eff}} = \frac{\tilde{\rho}_0}{\tilde{\rho}_0 + \tilde{p}_0} \tilde{\alpha} \quad (3.92)$$

3.5. MHD equations in the matter dominated universe

In the matter dominated universe the energy density of nonrelativistic particles ρ_{mat} is much larger than the energy density of radiation ρ_{rad} and the thermal pressure p is only a fraction $\mathcal{O}(T/M)$ (M is the mass of the dominating nonrelativistic particles) of the energy density. The onset of matter domination happened when the temperature of the universe was around $T \sim 5.5 \Omega_0 h^2 \text{ eV}$, where Ω_0 is the total density in terms of the critical density and h is the dimensionless present day Hubble constant given in units of $100 \text{ km s}^{-1} \text{ Mpc}^{-1}$. At this temperature protons and neutrons are nonrelativistic and the contribution from radiation to the thermal pressure can be neglected.

For completeness, I will first show the MHD equations in the diffusion regime, though it not very likely that primordial magnetic fields will suffer damping during this regime while the universe is matter dominated. The dissipation terms for the free streaming regime are given in the next paragraph, and the evolution of magnetic fields in the different damping regimes is discussed in chapter 8.

Although, the equation (3.57) is not conformally invariant in the nonrelativistic limit (the trace of the total energy-momentum tensor is not zero), it was shown in [87] that a very useful set of rescaled variables can be found:

$$\begin{aligned}
 \tilde{\rho} &\equiv \rho a^3 & \tilde{p} &\equiv p a^4 & \tilde{\mathbf{B}} &\equiv \mathbf{B} a^2 \\
 \tilde{\mathbf{v}} &\equiv \mathbf{v} a^{1/2} & \tilde{\epsilon} &\equiv \epsilon a^4 & \tilde{T} &\equiv T a^2 \\
 \tilde{\chi} &\equiv \chi a^{3/2} & \tilde{\nu} &\equiv \nu a^{5/2} & d\tilde{t} &\equiv dt a^{-3/2} \\
 \tilde{\xi} &\equiv \xi a^{5/2} & \tilde{H} &\equiv a^{3/2} H
 \end{aligned} \tag{3.93}$$

The nonrelativistic MHD equations with the new *super comoving* variables are [87]:

$$\frac{\partial \tilde{\rho}}{\partial \tilde{t}} + \nabla \cdot (\tilde{\rho} \tilde{\mathbf{v}}) = 0 \quad , \tag{3.94}$$

$$\frac{\partial \tilde{\mathbf{v}}}{\partial \tilde{t}} + (\tilde{\mathbf{v}} \cdot \nabla) \tilde{\mathbf{v}} + \frac{1}{\tilde{\rho}} \nabla \tilde{p} + \frac{1}{4\pi \tilde{\rho}} \tilde{\mathbf{B}} \times (\nabla \times \tilde{\mathbf{B}}) = -\tilde{\mathbf{s}} \quad , \tag{3.95}$$

$$\frac{\partial \tilde{\epsilon}}{\partial \tilde{t}} + \nabla \cdot (\tilde{\epsilon} \tilde{\mathbf{v}}) + \tilde{p} (\nabla \cdot \tilde{\mathbf{v}}) = -\tilde{\Gamma} \quad , \tag{3.96}$$

$$\frac{\partial \tilde{\mathbf{B}}}{\partial \tilde{t}} - \nabla \times (\tilde{\mathbf{v}} \times \tilde{\mathbf{B}}) = 0 \quad . \tag{3.97}$$

Here, $\tilde{\rho}$ is the rescaled matter density and $\tilde{\epsilon}$ is the internal rescaled energy density.

The dissipation terms are

$$\tilde{\mathbf{s}} = \frac{1}{2} \tilde{H} \tilde{\mathbf{v}} - \frac{\tilde{\nu}}{\tilde{\rho}} \left(\nabla^2 \tilde{\mathbf{v}} + \frac{1}{3} \nabla (\nabla \cdot \tilde{\mathbf{v}}) \right) + \frac{\tilde{\xi}}{\tilde{\rho}} \nabla (\nabla \cdot \tilde{\mathbf{v}})$$

$$-\frac{1}{a} \frac{\tilde{\chi}}{\tilde{\rho}} \left(\frac{\partial}{\partial \tilde{t}} - \frac{1}{2} \tilde{H} \right) \nabla \tilde{T} \quad , \quad (3.98)$$

$$\tilde{\Gamma} = (3\gamma - 4) \tilde{H} \tilde{\epsilon} - 6 \tilde{H} \tilde{\xi} (\nabla \cdot \tilde{\mathbf{v}}) - \tilde{\chi} \nabla^2 \tilde{T} \quad . \quad (3.99)$$

The choice of the transformation law (3.93) is not unique (cf. e.g. [88]). Here, I choose a set of transformations which corresponds to comoving quantities for the matter density ρ and energy density of the magnetic field ρ_{mag} in the matter dominated universe.

To close the set of equations (3.94) to (3.97) one has to know also the equation of state for the thermal pressure p . In the case of an ideal gas the pressure is only a function of the energy ϵ which can be expressed by the equation of state, i.e. $p = p(\epsilon)$. For an adiabatic equation of state one obtains $p \rho^{-\gamma} = \text{const.}$, where γ is the adiabatic index and equal to $4/3$ for relativistic particles and equal to $5/3$ for nonrelativistic particles. In the case of an adiabatic equation of state the pressure and internal energy are related by

$$\epsilon = \frac{1}{\gamma - 1} p \quad . \quad (3.100)$$

For the purpose of this work I use an isothermal equation of state with the sound velocity c_s

$$c_s^2 = \left(\frac{\partial p}{\partial \rho} \right)_S \quad . \quad (3.101)$$

In the matter dominated universe the scale factor a varies with the cosmic time t as $a \propto t^{2/3}$. Therefore, the rescaled Hubble parameter $\tilde{H} = a^{3/2} H$ is constant because $H \propto t^{-1}$. Hence, the expansion of the universe acts as a constant friction to the fluid motions and a constant dissipation rate of the internal energy.

Here, the ‘‘conformal’’ time \tilde{t} depends only weakly on the scale factor a (and cosmic time t), namely

$$\tilde{t} = H_0^{-1} \ln \left(\frac{a}{a_0} \right) \quad , \quad (3.102)$$

where, H_0 and a_0 are the Hubble constant and scale factor today, respectively. The relation (3.102) is not only a mathematical notation but is of physical relevance. Comparing the typical time scale of the system, L/V , with the cosmic time $t \sim H^{-1}$ one gets:

$$\frac{L/V}{H^{-1}} = \frac{a \tilde{L}/(a^{-1/2} \tilde{V})}{a^{3/2} H_0^{-1}} \approx \frac{\tau_{\text{dyn}}}{H_0^{-1}} \quad , \quad (3.103)$$

where $\tau_{\text{dyn}} = \tilde{L}/\tilde{V}$ is the dynamical (or intrinsic) time scale of the system. In contrast to the radiation dominated era, the ratio (3.103) has no further dependence on the scale factor a . This implies that those MHD modes (resp. eddies) whose comoving length scales are larger than $\tilde{L} \sim \tilde{V} H_0^{-1}$ will never contribute to the dynamical

evolution of the system. This is different from the radiation dominated universe, where the equation (3.103) can be written as $\tilde{L} = a \tilde{V} H_0^{-1}$. This allows a further growing of the comoving length \tilde{L} and larger eddies can contribute to the dynamical evolution of the system.

In this context I want also to note, that the rescaling of the fluid velocity, i.e. $V = a^{-1/2} \tilde{V}$, is a physical behavior in the expanding universe during matter domination. This can be seen by inspecting the Alfvén velocity

$$\mathbf{v}_A = \frac{\mathbf{B}}{\sqrt{4\pi\rho}} = \frac{a^{-2}\tilde{\mathbf{B}}}{\sqrt{4\pi a^{-3}\tilde{\rho}}} = a^{-1/2}\tilde{\mathbf{v}}_A \quad , \quad (3.104)$$

which has the same scaling properties as the fluid velocity V (the same argument holds of course for the speed of sound in the matter dominated universe $c_s = \sqrt{\partial p/\partial\rho} \propto a^{-1/2}$).

3.5.1. The free streaming regime

In the matter dominated universe the only relativistic particle with sufficiently large interaction rate, e.g. $l_{\text{mfp}} < H^{-1}$, is the photon. Its comoving mean free path l_γ/a starts to increase at temperature $T \sim m_e$, when the electrons become nonrelativistic. Most likely all subhorizon modes will suffer damping in the photon free streaming regime, which can be described with the following method.

The dissipation terms in the Euler equation (3.95) and for the internal energy (3.96) in the free streaming regime are:

$$\tilde{\mathbf{s}} = \left(\frac{1}{2} \tilde{H} + \tilde{\alpha} \right) \tilde{\mathbf{v}} \quad , \quad (3.105)$$

$$\tilde{\Gamma} = \left((3\gamma - 4) \tilde{H} + \tilde{\beta} \right) \tilde{\epsilon} \quad , \quad (3.106)$$

where rescaled drag and heat exchange coefficients in the matter dominated universe are respectively,

$$\tilde{\alpha} \equiv a^{3/2} \alpha \quad , \quad (3.107)$$

$$\tilde{\beta} \equiv a^{3/2} \beta \quad . \quad (3.108)$$

The exact form of the coefficients for the photon free streaming regime are can be found in chapter 8.

4. Helicity

The complex structures of magnetic fields possess some interesting properties. Depending on the characteristics of magnetic fields these structures have a strong influence on the evolution of a magnetized plasma. One important quantity which accounts for the complexity of magnetic field line structure is the *magnetic helicity* (cf. e.g. [26]):

$$\mathcal{H} \equiv \int_V d^3x \mathbf{A}(\mathbf{x}) \cdot \mathbf{B}(\mathbf{x}) \quad , \quad (4.1)$$

where \mathbf{A} is the vector potential of the magnetic field \mathbf{B} . Here, the considered volume V should be large enough to contain the main fluctuations of the magnetic field, i.e. $V \gg L^3$, where L is the coherence length of the magnetic field.

The magnetic helicity \mathcal{H} is a topological quantity, which counts the kinks and twists of the magnetic field lines [26]. Generally, it has two contributions. One is the internal helicity which is connected with kinks and twists of the individual tubes. The external helicity is connected to the inter-linkage of field lines.

The magnetic helicity \mathcal{H} has an analogy in field theory where it is called the topological Chern-Simon number. A non-vanishing net Chern-Simon number is an indication for the violation of P and CP symmetry. In the last years, several suggestions have been made on the production of magnetic helicity due particle physics processes in the early universe. One main idea is that during an electroweak phase transition the non Abelian Chern-Simon number is projected onto the $U(1)$ electromagnetic gauge group resulting in a non-vanishing magnetic helicity [27, 89, 73].

As the definition of the magnetic helicity (4.1) includes also the vector potential of the magnetic field it is not manifestly gauge invariant. The behavior of (4.1) under a gauge transformation

$$\mathbf{A} \rightarrow \mathbf{A}' = \mathbf{A} + \nabla \chi \quad (4.2)$$

is

$$\begin{aligned} \mathcal{H}' &= \int_V d^3x \mathbf{A}' \cdot \mathbf{B} \\ &= \mathcal{H} + \oint_{\partial V} ds \cdot (\chi \mathbf{B}) \quad , \end{aligned} \quad (4.3)$$

where ∂V is the surface boundary of the volume V . For the considered physical configurations the surface integral of (4.3) gives only a minor contribution because the

magnetic field B should die off sufficiently fast at scales $\gg L$. Hence, the definition (4.1) can be regarded as a “physically” gauge invariant. In the performed simulations, I used periodic boundary conditions, where the surface terms vanish identically. This choice of boundary conditions mimic also an infinite volume.

Why is the magnetic helicity so interesting? As I will show below, the helicity is a conserved number in an infinite conducting medium and has therefore strong influence on the evolution of the magnetic field. The phenomenon which is associated with a non-vanishing magnetic helicity is called an *inverse cascade*. Then, on dimensional grounds, any loss of magnetic energy (e.g. by turbulent fluid motions) leads to the transfer of magnetic energy from smaller to larger scales. This phenomenon is very well confirmed by numerical simulations (e.g. [90, 91] and the results of this work).

Using the induction equation in a neutral medium with finite resistivity $\eta = 1/(4\pi\sigma)$, where σ is the conductivity [82]

$$\frac{\partial \mathbf{B}}{\partial t} = \nabla \times (\mathbf{v} \times \mathbf{B}) + \eta \nabla^2 \mathbf{B} \quad (4.4)$$

and the three-dimensional relation of the magnetic field \mathbf{B} and the vector potential \mathbf{A}

$$\mathbf{B} = \nabla \times \mathbf{A} \quad (4.5)$$

one obtains for the time evolution of the magnetic helicity:

$$\begin{aligned} \frac{d\mathcal{H}}{dt} = & -2\eta \int d^3x \mathbf{B} \cdot (\nabla \times \mathbf{B}) \\ & + \oint_{\partial V} d\mathbf{s} \cdot [\mathbf{B}(\mathbf{A} \cdot \mathbf{v}) - \mathbf{v}(\mathbf{A} \cdot \mathbf{B}) - \eta(\nabla \times \mathbf{B}) \times \mathbf{A}] \quad . \end{aligned} \quad (4.6)$$

The surface integral in (4.6) does not contribute to the helicity dissipation if the magnetic field B vanishes at the surface boundaries of the volume V . As already mentioned at the beginning of this chapter, the chosen volume V should be large enough to contain the global properties of the considered magnetic field. In this case, the surface integral of equation (4.6) give also a negligible contribution.

From (4.6) it is clear that the magnetic helicity is a conserved quantity in an ideal MHD system, i.e. a system with vanishing resistivity η . Using the nonideal Euler equation for an incompressible fluid, i.e. (cf. equation (3.79))

$$\frac{\partial \mathbf{v}}{\partial t} + (\mathbf{v} \cdot \nabla) \mathbf{v} + \frac{\mathbf{B} \times (\nabla \times \mathbf{B})}{4\pi \rho} = \nu \nabla^2 \mathbf{v} \quad (4.7)$$

together with the induction equation (4.4) one obtains for the total energy dissipation

$$\frac{\partial E}{\partial t} = -\nu \rho \int d^3x |\nabla \times \mathbf{v}|^2 - \eta \int d^3x \frac{|\nabla \times \mathbf{B}|^2}{4\pi} \quad , \quad (4.8)$$

where $E = \rho/2 \int d^3x \mathbf{v} \cdot \mathbf{v} + (8\pi)^{-1} \int d^3x \mathbf{B} \cdot \mathbf{B}$. In the early universe the kinetic viscosity ν is much larger than the resistivity η (cf. section 8.1) , which is expressed by a large

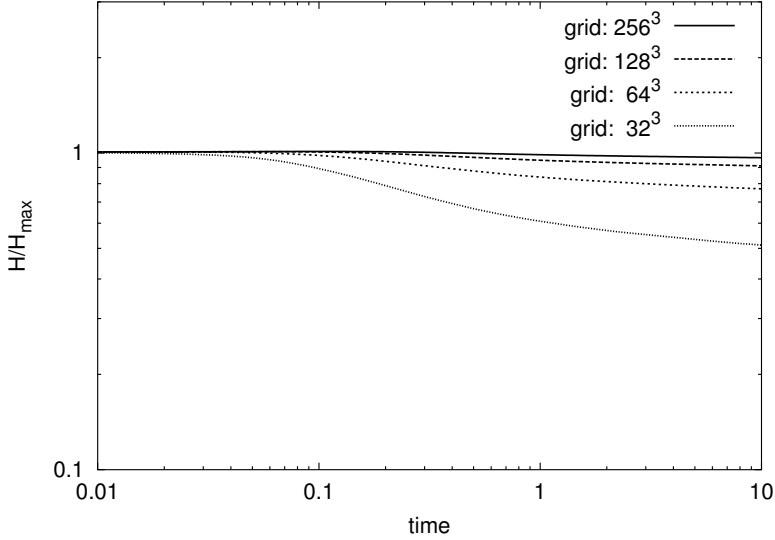


Figure 4.1.: Time evolution of the magnetic helicity \mathcal{H} in terms of the initial helicity for maximal helical magnetic fields. The loss of helicity is due to magnetic diffusion, which is solely due to numerical diffusion which can be seen by the resolution study. For these simulations the wavenumber cut-off was set to $k_c \approx 8$.

magnetic Prandtl number, i.e. $P_m = \nu/\eta \gg 1$. Assuming equipartition of kinetic and magnetic energy (see chapter 6 for the discussion on MHD equipartition) the energy dissipates much faster than the helicity because, $(\dot{E}/E)/(\dot{\mathcal{H}}/\mathcal{H}) \sim P_m \gg 1$. Therefore, the helicity is an almost conserved quantity in the early universe.

Figure 4.1 shows the results of the numerical simulations, which I performed to study the “goodness” of helicity conservation with ZEUS3D. Because the MHD equations were solved without including physical resistivity in the code, the loss of helicity is due to numerical diffusion. These studies show that the helicity is well conserved in simulation boxes with $\geq 128^3$ grid points.

4.1. Implementation of stochastic fields with helicity

To excite a stochastic magnetic field with or without initial helicity I choose a coordinate system in k -space useful for helical systems with the orthogonal unit vectors $\{\mathbf{e}_+, \mathbf{e}_-, \hat{\mathbf{k}}\}$. They are defined by [82]:

$$\begin{aligned} \mathbf{e}_+ &= \frac{1}{\sqrt{2}} (\mathbf{e}_1 + i \mathbf{e}_2) \quad , \\ \mathbf{e}_- &= \frac{1}{\sqrt{2}} (\mathbf{e}_1 - i \mathbf{e}_2) \quad , \end{aligned} \tag{4.9}$$

$$\hat{\mathbf{k}} = \frac{\mathbf{k}}{|\mathbf{k}|} ,$$

and

$$\mathbf{e}_1 = \frac{\mathbf{k} \times \hat{\mathbf{z}}}{|\mathbf{k} \times \hat{\mathbf{z}}|} , \quad (4.10)$$

$$\mathbf{e}_2 = \frac{\mathbf{k} \times \mathbf{e}_1}{|\mathbf{k} \times \mathbf{e}_1|} = \frac{\mathbf{k} \times (\mathbf{k} \times \hat{\mathbf{z}})}{|\mathbf{k} \times (\mathbf{k} \times \hat{\mathbf{z}})|} , \quad (4.11)$$

with the reference frame

$$\hat{\mathbf{z}} = \frac{1}{\sqrt{3}} \begin{pmatrix} 1 \\ 1 \\ 1 \end{pmatrix} . \quad (4.12)$$

The unit vectors (4.9) have the properties (cf. [82])

$$\begin{aligned} \mathbf{e}_\pm^* \cdot \mathbf{e}_\mp &= 0 , \\ \mathbf{e}_\pm^* \cdot \hat{\mathbf{k}} &= 0 , \\ \mathbf{e}_\pm^* \cdot \mathbf{e}_\pm &= 1 , \\ \mathbf{e}_\pm^* &= \mathbf{e}_\mp , \\ \mathbf{e}_{-\mathbf{k}}^\pm &= -\mathbf{e}_\pm^* , \\ i \mathbf{k} \times \mathbf{e}_\pm &= \pm k \mathbf{e}_\pm . \end{aligned} \quad (4.13)$$

By expanding the Fourier transformed vector potential $\hat{\mathbf{A}}$ in this basis, i.e.

$$\hat{\mathbf{A}}_{\mathbf{k}} = A_{\mathbf{k}}^+ \mathbf{e}_+ + A_{\mathbf{k}}^- \mathbf{e}_- + A_{\mathbf{k}}^k \hat{\mathbf{k}} \quad (4.14)$$

and using the relations (4.13) one obtains the magnetic field in the new basis

$$\hat{\mathbf{B}}_{\mathbf{k}} = -i \mathbf{k} \times \hat{\mathbf{A}}_{\mathbf{k}} = -k \left(A_{\mathbf{k}}^+ \mathbf{e}_+ - A_{\mathbf{k}}^- \mathbf{e}_- \right) . \quad (4.15)$$

With this set of basis vectors the magnetic field spectra are the given by (cf. also [90])

$$|\hat{\mathbf{B}}_{\mathbf{k}}|^2 = k^2 \left(|A_{\mathbf{k}}^+|^2 + |A_{\mathbf{k}}^-|^2 \right) , \quad (4.16)$$

whereas the magnetic helicity becomes

$$\mathcal{H} = \frac{1}{(2\pi)^3} \int d^3k \hat{\mathbf{A}}_{\mathbf{k}}^* \cdot \hat{\mathbf{B}}_{\mathbf{k}} = \frac{1}{(2\pi)^3} \int d^3k H_{\mathbf{k}} \quad (4.17)$$

with

$$H_{\mathbf{k}} \equiv \hat{\mathbf{A}}_{\mathbf{k}}^* \cdot \hat{\mathbf{B}}_{\mathbf{k}} = -k \left(|A_{\mathbf{k}}^+|^2 - |A_{\mathbf{k}}^-|^2 \right) . \quad (4.18)$$

Note, that the choice of coordinate system (4.9) reflects also that the helicity (4.17) is a well defined physical quantity as it is gauge independent, i.e. independent of $A_{\mathbf{k}}^k$.

To ensure a real vector potential $\mathbf{A}(\mathbf{x})$ and from that a real magnetic field $\mathbf{B}(\mathbf{x})$ the $A_{\mathbf{k}}^{\pm}$ have to fulfill the relation

$$(A_{\mathbf{k}}^{\pm})^* = -A_{-\mathbf{k}}^{\pm} \quad . \quad (4.19)$$

The magnetic helicity can be of either sign but the magnitude $|H_{\mathbf{k}}|$ is limited by the relation

$$|H_{\mathbf{k}}| \leq k^{-1} |\hat{\mathbf{B}}_{\mathbf{k}}|^2 \quad . \quad (4.20)$$

A magnetic field is said to be maximally helical if the equals sign in the above equation is valid.

From the relations (4.16) and (4.18) it can be seen that the strength of the magnetic field can be chosen independently of the magnetic helicity (in this approach one can consider either $(A_{\mathbf{k}}^+, A_{\mathbf{k}}^-)$ or $(B_{\mathbf{k}}, H_{\mathbf{k}})$ as independent variables). This allows to excite stochastic magnetic fields with arbitrary helicity.

4.2. Magnetic fields with maximal helicity

For a given magnetic field $\hat{\mathbf{B}}_{\mathbf{k}}$ the amplitude of the maximal helicity is always given by

$$|H_{\mathbf{k}}^{\max}| = k^{-1} |\hat{\mathbf{B}}_{\mathbf{k}}|^2 \quad , \quad (4.21)$$

independent of the choice of the coordinate system. This can be seen by using the fact that (from equation (4.15))

$$\hat{\mathbf{A}}_{\mathbf{k}}^* = \frac{i}{k^2} \left[\mathbf{k} \times \hat{\mathbf{B}}_{\mathbf{k}}^* - i \mathbf{k} (\mathbf{k} \cdot \hat{\mathbf{A}}_{\mathbf{k}}^*) \right] \quad (4.22)$$

and

$$|H_{\mathbf{k}}| = |\hat{\mathbf{A}}_{\mathbf{k}}^* \cdot \hat{\mathbf{B}}_{\mathbf{k}}| = k^{-2} \left| (\hat{\mathbf{B}}_{\mathbf{k}}^* \times \hat{\mathbf{B}}_{\mathbf{k}}) \cdot \mathbf{k} \right| \quad . \quad (4.23)$$

The maximal volume of the parallelepiped $|(\hat{\mathbf{B}}_{\mathbf{k}}^* \times \hat{\mathbf{B}}_{\mathbf{k}}) \cdot \mathbf{k}|$ is given by $|\hat{\mathbf{B}}_{\mathbf{k}}|^2 k$, leading to the expression (4.21) for a maximal helical magnetic field.

This has important consequences for the dynamics of magnetic fields in an ideal conducting medium where the helicity is conserved. For an isotropic magnetic energy spectrum

$$E_k \equiv \frac{k^3 \langle |\hat{\mathbf{B}}_k|^2 \rangle}{8\pi} \propto k^n \quad (4.24)$$

which is not too shallow (e.g. $n \gtrsim 1$) the helicity can be approximated by

$$H_{\max} \approx 8\pi k_c^{-1} E_{k_c} \sim L_c E_{\text{mag}} \quad , \quad (4.25)$$

where k_c is the cut-off of the spectra corresponding to the coherence length $L_c \sim k_c^{-1}$ of the magnetic field. Already, from the relation (4.25) it can be seen that the

coherence length L_c of the system has to *grow* while the magnetic energy E_{mag} is dissipating due to the conservation of the magnetic helicity. This phenomenon is called an *inverse cascade* as energy is transferred from smaller to larger scales. This dynamical process is very different from the “increase” of the coherence length due to the dissipation of energy at small scales in the case of a non-helical magnetic field (cf. figure 7.3) and 7.6). The energy spectra of a maximal helical field evolve *self-similarly*, i.e. at each time the spectra have the shape just “shifted” towards larger scales and the amplitude only slightly reduced (see also [90]).

At the end of this section, I want to note that the helicity (4.1) is a dimensionless quantity, because

$$[\mathcal{H}] = [V L B^2] = L E = E^0 \quad , \quad (4.26)$$

indicating that it transforms as a scalar which does not suffer adiabatic damping due to the expansion of the universe.

4.3. Magnetic fields with fractional helicity

In the coordinate system introduced in section 4.1 one can also excite stochastic magnetic fields with a fractional helicity by choosing $A_{\mathbf{k}}^-$ in terms of $A_{\mathbf{k}}^+$, i.e.

$$A_{\mathbf{k}}^- \equiv \sqrt{f} A_{\mathbf{k}}^+ \quad , \quad (4.27)$$

where $f \in [0, 1]$. Using this convention the magnitude of the magnetic field spectra become

$$|\hat{\mathbf{B}}_{\mathbf{k}}|^2 = k^2 (1 + f) |A_{\mathbf{k}}^+|^2 \quad , \quad (4.28)$$

and the helicity amplitude is

$$H_{\mathbf{k}} = -k (1 - f) |A_{\mathbf{k}}^+|^2 \quad . \quad (4.29)$$

One obtains for the magnitude of the helicity in terms of the magnetic field

$$|H_{\mathbf{k}}| = \frac{1}{k} |\hat{\mathbf{B}}_{\mathbf{k}}|^2 \frac{1 - f}{1 + f} \quad . \quad (4.30)$$

From equation (4.30) it can be seen that $(1 - f)/(1 + f)$ is the fraction of the maximal helicity magnitude $H_{\text{max}} = k^{-1} |\hat{\mathbf{B}}_{\mathbf{k}}|^2$. This can be used to adjust the magnetic helicity to an arbitrary magnitude.

Note, that the choice of exciting magnetic fields with a fractional helicity (4.30) is not unique. This particular choice just reduces the amplitude of the helicity spectra (compared to that of the maximal helicity spectra) by a factor of $(1 - f)/(1 + f)$. For non-maximal helicity it is also possible that the helicity spectra $H_{\mathbf{k}}$ do not follow the spectra of the magnetic field $|\hat{\mathbf{B}}_{\mathbf{k}}|^2$, but are rather independently distributed in k -space. The particular choice of the implementation of a fractional helicity may influence the evolution of magnetic fields. For simplicity, I restrict myself to the option (4.30) to excite fractional helical magnetic fields.

5. The linear regime

In this chapter I give a summary of the results obtained from the analysis of the evolution of cosmic magnetic fields in the linear regime [22] where the magnetic field is dominated by the homogeneous background field B_0 and perturbed by fluctuations \mathbf{b}_k . I verified these results with numerical simulations, which I performed, to check the capability of the program ZEUS3D for the purpose of this work.

5.1. The diffusion regime

One can derive a set of linearized MHD equations by expanding the variables on constant homogeneous background values* [82]

$$\rho(t, \mathbf{x}) = \rho_0 + \rho_1(t, \mathbf{x}) \quad (5.1)$$

$$p(t, \mathbf{x}) = p_0 + p_1(t, \mathbf{x}) \quad (5.2)$$

$$\mathbf{B}(t, \mathbf{x}) = \mathbf{B}_0 + \mathbf{b}(t, \mathbf{x}) \quad (5.3)$$

with $|\rho_1| \ll \rho_0$ and $|\mathbf{b}| \ll |\mathbf{B}_0|$. The velocity fluctuation \mathbf{v} is already a small quantity compared to the speed of light, i.e. $|\mathbf{v}| \ll 1$.

Keeping only terms linear in the small quantities the MHD equations in the diffusion regime are:

$$\frac{\partial \rho_1}{\partial t} + (\rho_0 + p_0) \nabla \cdot \mathbf{v} = 0 \quad , \quad (5.4)$$

$$(\rho_0 + p_0) \frac{\partial \mathbf{v}}{\partial t} + \nabla p_1 + \frac{\mathbf{B}_0 \times (\nabla \times \mathbf{b})}{4\pi} = \nu \nabla^2 \mathbf{v} \quad , \quad (5.5)$$

$$\frac{\partial \mathbf{b}}{\partial t} = \nabla \times (\mathbf{v} \times \mathbf{B}_0) \quad . \quad (5.6)$$

These equations can be combined to a single second order equation for the fluid velocity \mathbf{v} :

$$\ddot{\mathbf{v}} - c_s^2 \nabla (\nabla \cdot \mathbf{v}) + \mathbf{v}_A \times (\mathbf{v}_A \cdot \nabla) (\nabla \times \mathbf{v}) + \left(\mathbf{v}_A (\mathbf{v}_A \cdot \nabla) - v_A^2 \nabla \right) (\nabla \cdot \mathbf{v}) = \nu_{\text{eff}} \nabla^2 \dot{\mathbf{v}} \quad (5.7)$$

*For simplicity, I neglect all effects coming from the expansion of the universe and keep all diffusion parameters constant.

where $\mathbf{v}_A = \mathbf{B}_0/\sqrt{4\pi(\rho_0 + p_0)}$ is the Alfvén velocity, $\nu_{\text{eff}} = \nu/(\rho_0 + p_0)$, and overdots denote derivations with respect to time t . Solutions of the linearized MHD equation (5.7) can be found by expanding the fluid velocity in Fourier modes,

$$\mathbf{v}(\mathbf{x}, t) = \frac{1}{(2\pi)^3} \int d^3k \mathbf{v}_{\mathbf{k}}(t) e^{-i\mathbf{k}\cdot\mathbf{x}} \quad (5.8)$$

with

$$\mathbf{v}_{\mathbf{k}}(t) = \mathbf{v}_{\mathbf{k}}(0) e^{i\omega t} \quad . \quad (5.9)$$

By expanding also the magnetic field fluctuations in Fourier space the induction equation (5.6) relates the magnetic field modes and the velocity fluctuations,

$$\mathbf{b}_{\mathbf{k}}(t) = -\frac{\mathbf{k} \times (\mathbf{v}_{\mathbf{k}}(0) \times \mathbf{v}_A)}{\omega} \exp(i\omega t) \quad . \quad (5.10)$$

Using the solution (5.8) for the equation (5.7) one obtains the dispersion relation

$$\begin{aligned} & -\omega^2 \mathbf{v}_{\mathbf{k}} + \mathbf{k} (c_s^2 + v_A^2) (\mathbf{v}_{\mathbf{k}} \cdot \mathbf{k}) \\ & - (\mathbf{k} (\mathbf{v}_A \cdot \mathbf{v}_{\mathbf{k}}) - \mathbf{v}_{\mathbf{k}} (\mathbf{v}_A \cdot \mathbf{k}) + \mathbf{v}_A (\mathbf{v}_{\mathbf{k}} \cdot \mathbf{k})) (\mathbf{v}_A \cdot \mathbf{k}) \\ & + i\omega \nu_{\text{eff}} k^2 \mathbf{v}_{\mathbf{k}} = 0 \quad . \end{aligned} \quad (5.11)$$

For transverse Alfvén waves (cf. [82]), where the fluid velocity \mathbf{v} is perpendicular to the background magnetic field, i.e. $\mathbf{v} \perp \mathbf{v}_A$, the dispersion relation (5.11) reduces to

$$-\omega^2 + (\mathbf{v}_A \cdot \mathbf{k})^2 + i\omega \nu_{\text{eff}} k^2 = 0 \quad . \quad (5.12)$$

The solutions of this equation are:

$$\omega_{\pm} = \frac{i}{2} \nu_{\text{eff}} k^2 \pm \sqrt{(\mathbf{v}_A \cdot \mathbf{k})^2 - \left(\frac{\nu_{\text{eff}} k^2}{2}\right)^2} \quad . \quad (5.13)$$

In the oscillatory regime, i.e. $\mathbf{v}_A \cdot \mathbf{k} \gg \nu_{\text{eff}} k^2/2$ the solutions are those for damped oscillators [22],

$$\omega_{\text{osc}} = \pm (\mathbf{v}_A \cdot \mathbf{k}) + \frac{i}{2} \nu_{\text{eff}} k^2 \quad . \quad (5.14)$$

whereas, in the viscous regime, i.e. $\nu_{\text{eff}} k^2/2 \gg \mathbf{v}_A \cdot \mathbf{k}$, the overdamped solution is [22]

$$\omega_{\text{od}} = i \frac{(\mathbf{v}_A \cdot \mathbf{k})^2}{\nu_{\text{eff}} k^2} = i \frac{v_A^2 \cos^2(\theta)}{\nu_{\text{eff}}} \quad , \quad (5.15)$$

where θ is the angle between the background magnetic field and the wave vector.

Note, that the damping time scale in the viscous diffusion regime $\tau = \nu_{\text{eff}} / (v_A^2 \cos^2(\theta))$ is independent on the scale $l \sim 1/k$. Hence, all modes suffer the same amount of dissipation during the same time.

5.2. The free streaming regime

In the free streaming regime, when the mean free path of the background radiation particles is much larger than the wave length of the particular mode, the interaction of the fluid with the decoupled background radiation can be described by a drag force with the drag coefficient α (cf. chapter 3). Then the dispersion relation becomes,

$$\begin{aligned} & -\omega^2 \mathbf{v}_{\mathbf{k}} + \mathbf{k} (c_s^2 + v_A^2) (\mathbf{v}_{\mathbf{k}} \cdot \mathbf{k}) \\ & - (\mathbf{k} (\mathbf{v}_A \cdot \mathbf{v}_{\mathbf{k}}) - \mathbf{v}_{\mathbf{k}} (\mathbf{v}_A \cdot \mathbf{k}) + \mathbf{v}_A (\mathbf{v}_{\mathbf{k}} \cdot \mathbf{k})) (\mathbf{v}_A \cdot \mathbf{k}) \\ & + i \omega \alpha \mathbf{v}_{\mathbf{k}} = 0 \quad . \end{aligned} \quad (5.16)$$

For Alfvén waves the dispersion relation reduces to [22]

$$-\omega^2 + (\mathbf{v}_A \cdot \mathbf{k})^2 + i \omega \alpha = 0 \quad , \quad (5.17)$$

which has the solutions

$$\omega_{\pm} = \frac{i}{2} \alpha \pm \sqrt{(\mathbf{v}_A \cdot \mathbf{k})^2 - \left(\frac{\alpha}{2}\right)^2} \quad . \quad (5.18)$$

For oscillating modes ($\mathbf{v}_A \cdot \mathbf{k} \gg \alpha/2$) these solutions are

$$\omega_{\text{osc}} = \pm (\mathbf{v}_A \cdot \mathbf{k}) + \frac{i}{2} \alpha \quad , \quad (5.19)$$

and in the viscous free streaming regime ($\alpha/2 \gg \mathbf{v}_A \cdot \mathbf{k}$) the overdamped solution is

$$\omega_{\text{od}} = i \frac{v_A^2 k^2 \cos^2(\theta)}{\alpha} \quad . \quad (5.20)$$

5.3. Numerical implementation

To verify the above results with the ZEUS3D code I choose the following initial configuration for the magnetic field

$$\mathbf{B}(\mathbf{x}) = \mathbf{B}_0 + \mathbf{b} \sum_{n=1}^m \sin(2\pi n z) \quad , \quad (5.21)$$

where $\mathbf{B}_0 = B_0 (1, 1, 1)$ and $\mathbf{b} = b \mathbf{e}_x$ with $b \ll B_0$. The number of excited modes is indicated by the integer m . A full sine wave should be resolved with at least 16 grid points. Depending on the used resolution N^3 the number of excited modes should not exceed $N/16$.

The Fourier components of the initial magnetic field are

$$\mathbf{b}_{\mathbf{k}}(0) = \mathbf{b} \delta(k_x) \delta(k_y) \sum_{n=1}^m \frac{\delta(k_z - 2\pi n) - \delta(k_z + 2\pi n)}{2i} \quad . \quad (5.22)$$

5. The linear regime

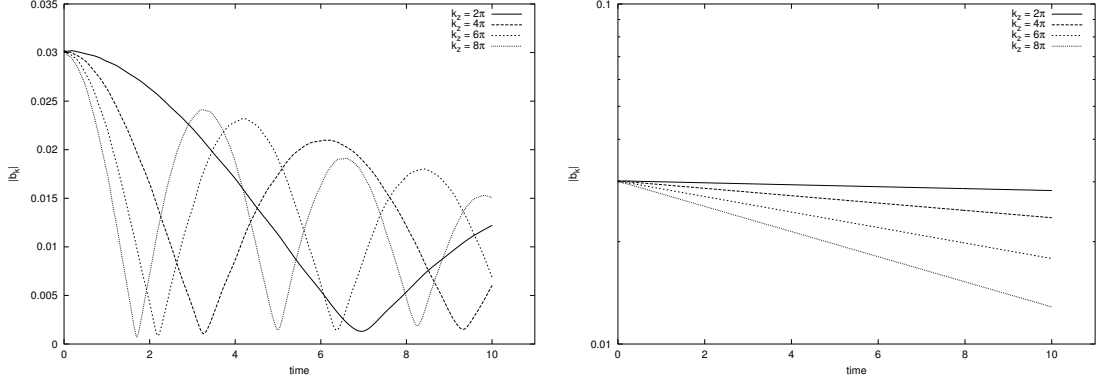


Figure 5.1.: Time evolution of the B-field Fourier components $\mathbf{b}_{\mathbf{k}}$ on a mesh with 32^3 grid points in the linear regime. The *left panel* shows the oscillatory regime with $\alpha = 0.116$ and the *right panel* shows the overdamped regime with $\alpha = 11.6$. The Alfvén velocity in both cases is $v_z^A = 4.2 \times 10^{-2}$.

5.3.1. The diffusion regime

Using the results of the previous sections the time evolution of magnetic fluctuations in the diffusive oscillatory regime are

$$\mathbf{b}_{k_z}(t) = \mathbf{b} \cos(v_z^A k_z t) \exp\left(-\frac{\nu_{\text{eff}}}{2} k_z^2 t\right); \quad k_z = 2\pi n; \quad n = 1 \dots m, \quad (5.23)$$

where $v_z^A = B_0 = |\mathbf{B}_0|/\sqrt{3}$. The solutions in the viscous (i.e. overdamped) diffusion regime are

$$\mathbf{b}_{k_z}(t) = \mathbf{b} \exp\left(-\frac{(v_z^A)^2}{\nu_{\text{eff}}} t\right) \quad (5.24)$$

5.3.2. The free streaming regime

In the free streaming regime the solutions for the oscillatory and overdamped modes are, respectively,

$$\mathbf{b}_{k_z}(t) = \mathbf{b} \cos(v_z^A k_z t) \exp\left(-\frac{\alpha}{2} t\right) \quad (5.25)$$

and

$$\mathbf{b}_{k_z}(t) = \mathbf{b} \exp\left(-\frac{v_z^A k_z}{\alpha} t\right), \quad (5.26)$$

The results given by the numerical simulations are summarized in the figure 5.1. Comparisons of those numerical results with the theoretical expectations give a good agreement.

6. Nonlinear MHD

In this chapter I will focus on the behavior of a strongly nonlinear magnetized plasma. An overview of nonlinear magnetohydrodynamics can be found in [26]. Here, I consider a simplified version of the MHD equations on a static background*. Furthermore, I focus on weak magnetic fields, whose Alfvén velocity is small compared to the sound velocity, which will not produce large density perturbations. Therefore, it is sufficient to study the evolution of such magnetic fields in the limit of an incompressible fluid. This is different to investigations of density perturbations caused by magnetic fields. The assumption of an incompressible fluid is very well satisfied in the early universe as the density fluctuations are less than 10^{-5} and the velocity fluctuations and the Alfvén velocity are much smaller than the sound velocity. By neglecting the density perturbations the homogeneous energy density ρ can be normalized, without loss of generality, such that $\rho = 1$ in a box with unit volume†. Using this convention the kinetic and magnetic energy density are $v^2/2$, and $v_A^2/2$, respectively, where $\mathbf{v}_A = \mathbf{B}/\sqrt{4\pi(\rho + p)}$ ‡.

6.1. Dynamics of nonlinear MHD

Using the conventions introduced in the beginning of this chapter one may derive a simplified set of MHD equations which I use to study the main features of a magnetized fluid in the nonlinear regime. The simplified equations are:

$$\frac{\partial \mathbf{v}}{\partial t} + (\mathbf{v} \cdot \nabla) \mathbf{v} + \mathbf{v}_A \times (\nabla \times \mathbf{v}_A) = -\mathbf{f} \quad , \quad (6.1)$$

$$\frac{\partial \mathbf{v}_A}{\partial t} - \nabla \times (\mathbf{v} \times \mathbf{v}_A) = \eta \nabla^2 \mathbf{v}_A \quad , \quad (6.2)$$

where \mathbf{f} is an additional force acting on the fluid. The latter can be a diffusion term $-\mathbf{f} = \nu \nabla^2 \mathbf{v}$ or a drag force, i.e. $\mathbf{f} = \alpha \mathbf{v}$ with the drag coefficient α .

*The effects coming from the expansion of the universe can be hidden by using comoving variables, cf. chapter 3.

†Such a system has only two fundamental dimensional quantities. For the purpose of this chapter, I choose the dimensional quantities: velocity V and length L , respectively.

‡Here, the Alfvén velocity \mathbf{v}_A is *not* the Alfvén velocity knowing from linear theory associated with the homogeneous background magnetic field but is introduced as a local quantity having the same dimension as the velocity fluctuations \mathbf{v} .

The relative strength of the nonlinear interaction in the Euler equation (6.1) and the external force is expressed by the kinetic Reynolds number

$$R_e = \frac{V^2/L}{f} = \begin{cases} \frac{VL}{\nu} & : & -\mathbf{f} = \nu \nabla^2 \mathbf{v} \\ \frac{V}{\alpha L} & : & -\mathbf{f} = -\alpha \mathbf{v} \end{cases}, \quad (6.3)$$

where f and V are typical magnitudes of the force and velocity, respectively. The length scale L in the definition of the global Reynolds number (6.3) is the *integral scale* at which most of the kinetic energy is concentrated. If the Reynolds number becomes very large, i.e. $R_e \gg 1$, the fluid motions become turbulent. A strong dissipation force, indicated by a small Reynolds number, inhibits fluid motions and the fluid becomes viscous.

One can also define a local Reynolds number as measure of the relative importance of the nonlinear fluid interaction and the dissipation force at a certain length scale l (or mode $k \sim 1/l$)

$$R_{el} = \frac{v_l l}{\nu}, \quad (6.4)$$

where v_l is the averaged velocity at the length scale l (cf. appendix A.2). Then, the dissipation becomes important at the scale l_{diss} where the local Reynolds number is of order unity:

$$l_{\text{diss}} = \frac{\nu}{v_l}. \quad (6.5)$$

The Reynolds number has also the interpretation of comparing two dynamical time scales. Namely, the time of an *eddy turnover* which is the time needed by a fluid element to cover the distance l

$$\tau_{\text{eddy}} = \frac{l}{v} = \tau_l \quad (6.6)$$

and the diffusion time scale

$$\tau_{\text{diff}} = \frac{l^2}{\nu}. \quad (6.7)$$

As long as the (local) eddy turnover time is much smaller than the diffusion time, i.e. $R_e \gg 1$, hydrodynamic system will transfer the energy located at the scale l to the next neighboring scale $l - \Delta l$ due to the nonlinear interactions of the fluid motions (this argument assumes locality in k -space see e.g. [26]). This shift of energy from large scales to small scales is called *direct cascade*. A large Reynolds number also indicates that the integral scale L and the dissipation scale l_{diss} are separated by a large range, i.e. $L/l_{\text{diss}} \gg 1$, where this range in k -space is the so called *inertial range*. The transfer time from the scale l to $l - \Delta l$ within the inertial range is again the local eddy turnover time τ_l and the time scale for the total energy dissipation is the eddy turnover time at the integral scale L , i.e. $\dot{E}/E = V/L$. Hence, although

the energy dissipation is due to diffusion with the rate $1/\tau_{\text{diff}}$ the dissipation rate of the energy is independent of the micro-physics acting at the scale l_{diss} . This allows to describe the dynamics of the turbulent MHD system by only the global quantities V , V_A and L .

In analogy to the kinetic Reynolds number it is useful to define a magnetic Reynolds number which compares the strength of the two terms on the right hand side of equation (6.2),

$$R_m = \frac{V L}{\eta} \quad . \quad (6.8)$$

The magnetic Prandtl number measures the efficiency of kinetic diffusion compared to magnetic diffusion,

$$P_m = \frac{\nu}{\eta} \quad . \quad (6.9)$$

Usually, in the early universe the Prandtl number is very large and one can neglect magnetic diffusion in turbulent MHD. Then one can see from equation (6.2) that the dynamics for the magnetic field is ruled by the eddy turnover time scale,

$$\frac{dv_A}{dt} \approx \frac{v_A}{\tau_l} \quad . \quad (6.10)$$

It is already clear from equation (6.1) that the time scale (6.6) which determines the dynamics of the magnetic field is not constant but depends also on the magnetic field v_A itself. This reflects the nonlinear interaction of the fluid motions and the magnetic field.

6.2. Turbulence

In the turbulent regime ($R_e \gg 1$) the small scale dissipation force has no direct influence on the global dynamics of the MHD system. Hence, due to the absence of a constant (or nearly constant) time scale in a turbulent plasma the evolution equation (6.10) does *not* obey an exponential decay. From the incompressible Euler equation (6.1) it is expected that due to back reactions of the fluid motion to the magnetic field and vice versa the system dynamically establish an equilibrium between kinetic and magnetic energy. By using numerical simulations, I could confirm this hypothesis at least for magnetic fields without helicity (cf. fig. 7.1). The time needed to reach the equilibrium state from an initial configuration is

$$\tau_{\text{eq}} = \min\left(\frac{L}{V}, \frac{L}{V_A}\right) \quad . \quad (6.11)$$

After the time when the equilibrium stage is established the fluid velocity “follows” the magnetic field, i.e. $v \sim v_A$. Then, for the energy dissipation one obtains

$$\frac{dE}{dt} \approx \frac{E^{3/2}}{L} \quad , \quad (6.12)$$

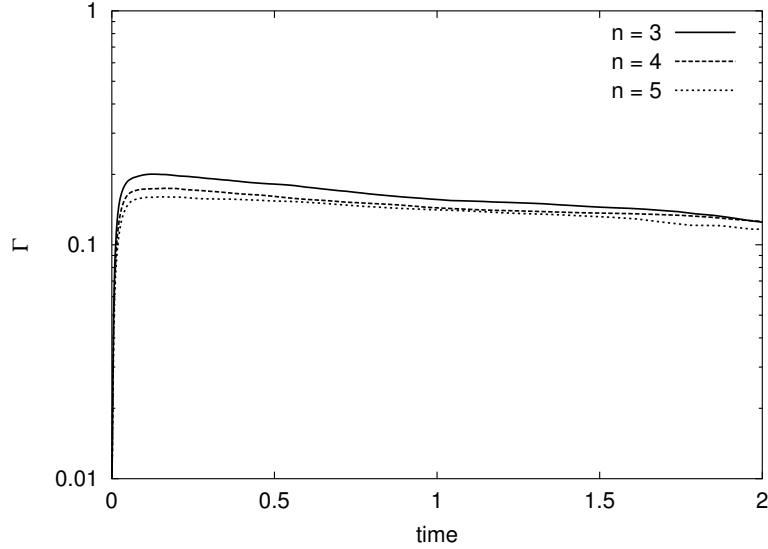


Figure 6.1.: Time evolution of $\Gamma = E_{\text{kin}}/E_{\text{mag}}$ for maximal helical magnetic fields with different spectral indices n in the turbulent regime. The initial kinetic energy was set to $10^{-4} E_{\text{mag}}$. The ratio Γ is nearly constant in time, although, equipartition of kinetic and magnetic energy is not established for helical magnetic fields. For these simulations the spectral cut-off was $k_c \approx 32$, i.e. one time step ($t = 1$) corresponds to $N \approx k_c \approx 32$ initial eddy turnovers at the integral scale.

where $E = V_A^2/2 \approx V^2/2$ (cf. also [26]). For most cases the solution of the simplified energy dissipation equation (6.12) is a power law dependence of the energy on time, i.e. $E \propto t^{-p}$ with a certain damping exponent p . Also the coherence length L could in principle be an arbitrary function of time, in particular $L \propto t^q$. But, dimensional arguments constrain the exponents p and q to $p/2 + q = 1$. This is due to the fact that the only available quantities in the considered MHD system are the velocities $V_A \sim V$ and the integral length scale L (the kinetic viscosity ν is not relevant for the dynamics during turbulence). Note, that this is different from a configuration with a constant magnetic field \mathbf{B}_0 , where $\mathbf{k} \cdot \mathbf{B}_0/\sqrt{4\pi\rho_0}$ and νk^2 are independent constant frequencies which determine the evolution of individual modes of the magnetic field.

6.3. Dynamics of helical magnetic fields

Although, the numerical simulations do not show equipartition of the kinetic and magnetic energy in the case when the magnetic field has maximal helicity, the ratio of the kinetic and magnetic energy is almost constant (cf. figure 6.1),

$$\Gamma \equiv \frac{E_{\text{kin}}}{E_{\text{mag}}} \approx \text{const.} \quad (6.13)$$

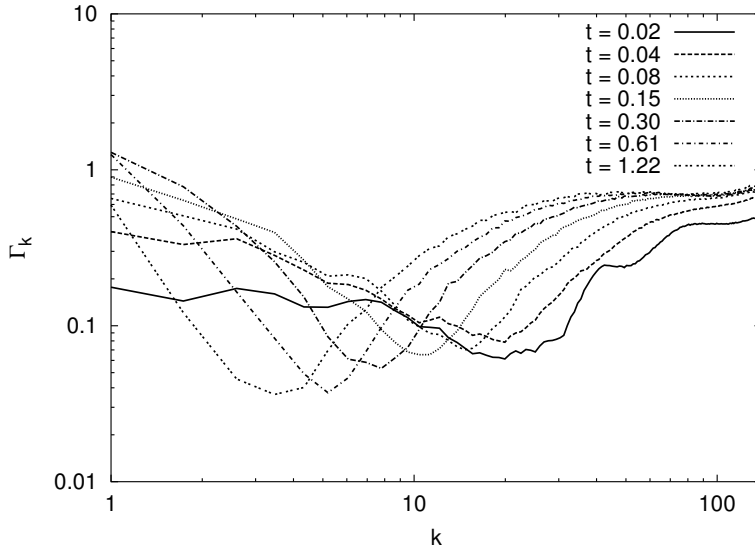


Figure 6.2.: The evolution of the ratio of the kinetic and magnetic energy spectrum $\Gamma_k = E_k^{\text{kin}}/E_k^{\text{mag}}$ for a maximal helical magnetic field in the turbulent regime. In this case equipartition ($\Gamma_k \approx 1$) is only established on very small scales. At the integral scale the kinetic energy is always much smaller than the magnetic energy.

The derivation of the time dependence of the energy (6.12) implies only the proportionality of the fluid velocity V and the Alfvén velocity V_A and is thus also valid in the case when Γ is constant. But, the reason why Γ is not of order unity is yet unclear and it has to be determined by numerical simulations so far (see also [92]). The authors of [93] claim, by using numerical simulations, that Γ is a time dependent function, which varies as $\Gamma \propto t^{-0.5}$. The simulations, I performed, do not show this behavior, but give a nearly constant Γ (see figure 6.1).

From the figure 6.2 it can be seen that the fluid energy “follows” the magnetic energy in k -space but the former is always located at smaller k (larger scales). This effect comes from the conserved magnetic helicity which tends to increase the coherence length of the magnetic field (see also figure 7.6. The velocity fluctuations are dynamically excited by the Lorentz force. This may lead to a delayed enhancement of the kinetic energy at increasingly large scale.

As already mentioned in section 4.2 for a maximal helical magnetic field, there is a dynamical relation between the energy of the magnetic field and the coherence length L . The conservation of the magnetic helicity in a medium with infinite conductivity forces the coherence length to grow while the magnetic energy is dissipated via interaction with the fluid by the relation [26]

$$L \propto E^{-1} \quad . \quad (6.14)$$

For a helical field this relation can be used to solve equation (6.12).

7. Damping of magnetic fields

In this chapter, I deduce damping laws for the magnetic fields in the different damping regimes (turbulence, diffusion and free streaming) within the framework used in the previous chapter. That means effects coming from the expansion of the universe (which can be separated by using properly rescaled variables) are neglected and a (nearly) incompressible fluid is considered. Furthermore, it is assumed that the magnetic fields and the fluid velocity fluctuations are isotropic. Hence, it is not necessary to take into account the vector character of the magnetic field and the fluid velocity.

The general results derived in this chapter can then be adopted to the evolution of magnetic fields in the early universe, which will be done in the next chapter.

In a MHD system with a homogeneous background magnetic field \mathbf{B}_0 and an Alfvén velocity $\mathbf{v}_A = \mathbf{B}_0/\sqrt{4\pi\rho_0}$, which was studied in detail by [22] and [23], one can define a characteristic time scale $\tau_k = (\mathbf{k} \cdot \mathbf{v}_A)^{-1}$ which determines the evolution of each mode \mathbf{b}_k . Then, for Alfvén waves these modes are damped oscillations with a frequency $(\mathbf{k} \cdot \mathbf{v}_A)$ and a damping rate which depends on the dissipation term in the Euler equation (cf. also chapter 5). In a MHD system without a homogeneous background magnetic field one finds that the evolution time scale of the magnetic field is the time scale of an eddy turnover on the integral scale L ,

$$\tau_{\text{dyn}} = \tau_{\text{eddy}} = \frac{L}{V} \quad . \quad (7.1)$$

This time scale evolves during the course of evolution itself leading to different damping laws compared to those of the linear regime with a homogeneous background magnetic field. In the following sections, I argue that magnetic fields are damped by power laws rather than exponential laws found in the linear analysis of the evolution of magnetic fields. The power law decay of the energy is well known from the studies of freely decaying (M)HD systems (see e.g. [26, 94]).

7.1. Damping in the turbulent regime

By assuming initially small velocity fluctuations, i.e. $v \lesssim v_A$, it can be seen from equation (6.1) that for individual modes* $b_l = \langle k^3 |b_k|^2 \rangle^{1/2}$ the onset of damping

*For Fourier conventions see appendix A.2.

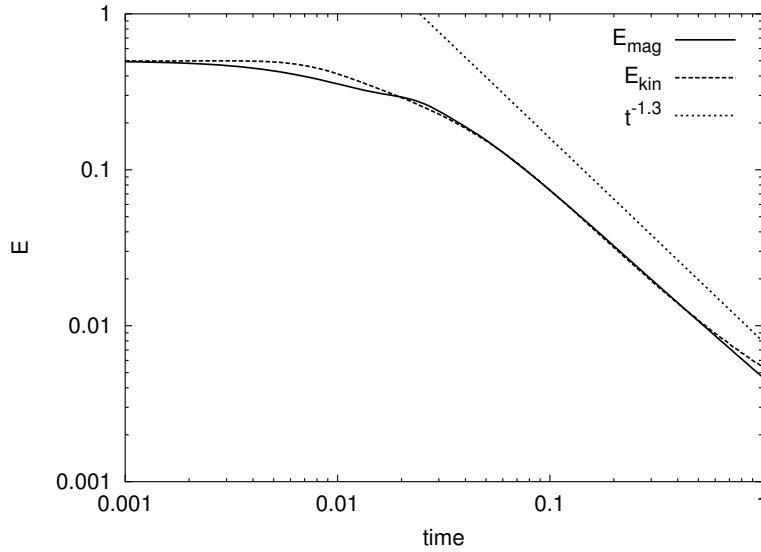


Figure 7.1.: Comparison of the time evolution of the magnetic (solid line) and the kinetic (dashed line) energy in the turbulent regime ($R_e \gg 1$) for a magnetic field without initial helicity. For comparison, also the theoretical damping law, $E \propto t^{-1.3}$, is shown (dotted line). Here, the simulation was performed on a mesh with 128^3 grid points and the magnetic field was excited up to $k_c \approx 16$ with a spectral index $n \approx 4$.

occurs after the time

$$\tau_l^A = \frac{l}{v_l^A} \quad , \quad (7.2)$$

when one can expect equipartition of kinetic and magnetic energy at this scale. Assuming a steep enough spectrum of the magnetic energy, i.e. with a spectral index $n \gtrsim 1$, the entire system can be described by inspecting the energies at the integral scale L . Then, the onset of dynamical evolution takes place after the time

$$\tau_L^A = \frac{L}{V_A} \quad . \quad (7.3)$$

when equipartition of total kinetic and magnetic energy has been established.

In the turbulent regime, where $R_e \gg 1$, the dissipation of energy is assumed to occur on a much smaller length scale than the integral scale and the dissipation time scale τ_{diss} has no influence on the damping of the large scale energy modes, because

$$R_e = \frac{\tau_{\text{diss}}}{\tau_L} \gg 1 \quad . \quad (7.4)$$

The only remaining time scale, which determines the system in the turbulent regime is the eddy turnover time τ_L . Due to the established equipartition of kinetic and magnetic energy after the time τ_L^A the fluid velocity V reaches the value of the

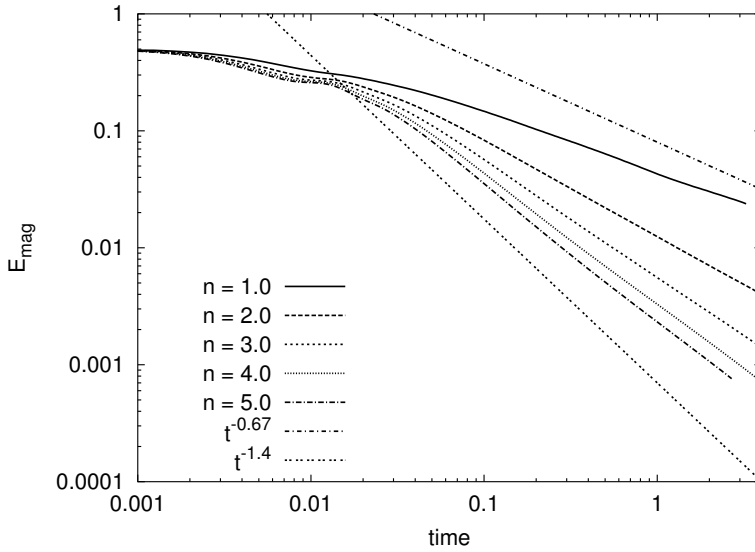


Figure 7.2.: The evolution of the magnetic energy in the turbulent regime for different initial energy spectra n , where $E_k = (8\pi)^{-1} k^3 |b_k|^2 \propto k^n$ with a cut-off $k_c \approx 32$. Here, the initial magnetic field is non-helical. In this case, the damping law depends on the spectral index (cf. equation (7.7)). For comparison, the theoretical predicted damping laws for $n = 1$ ($E \propto t^{-0.67}$) and for $n = 5$ ($E \propto t^{-1.4}$) are shown.

Alfvén velocity V_A and the damping time scale becomes τ_L^A . As already mentioned in the previous chapter, this yields the asymptotic damping law of the (magnetic) energy

$$\frac{\dot{E}}{E} = \frac{1}{\tau_L^A} = \frac{E^{1/2}}{L} \quad . \quad (7.5)$$

In the freely decaying turbulence, where there is no injection of energy at the integral scale L as in driven turbulence, one can not expect that the latter will stay constant with time. In contrast to the case of driven turbulence the system in the freely decaying case cannot maintain a perfect steady-state configuration. But, due to slow energy dissipation at the integral scale L by diffusion compared to the energy transfer from the integral scale to next neighboring scales the system will reach a quasi-steady-state alignment.

The time dependence of the integral scale L is not only seen in numerical simulations (see e.g. [95] and the figures 7.3 of this work) but can be deduced from the following arguments. First, consider an isotropic magnetic energy spectrum $E_k \propto k^n \sim l^{-n}$ with the spectral index n . Then, due to the increasing damping rate in k -space modes with larger wavenumber $k \sim 1/l$ decay more rapidly than modes with smaller wavenumber. At a certain time t only modes at the length scale $L(t)$ survived while modes with $l < L$ are already damped and the magnetic field B at scales larger than $L(t)$ is nearly the same as the initial one. This is called *selective*

7. Damping of magnetic fields

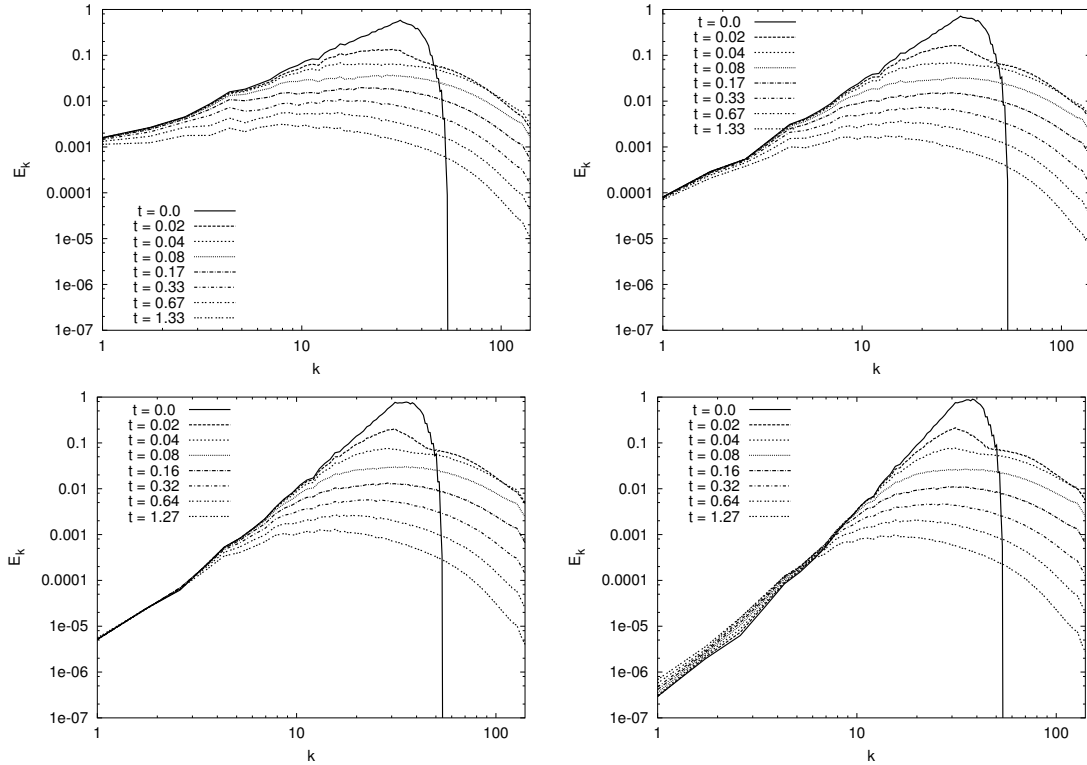


Figure 7.3.: Evolution of magnetic energy spectra in the turbulent regime for a magnetic field with no initial helicity. The initial energy spectra from top left to right bottom panel are $n \approx 2, 3, 4, 5$, respectively.

decay in k -space as not all but only selective modes are affected at a certain time [29]. Starting with an initially blue power spectrum the selective decay mechanism causes the modes with more power at larger wavenumber to cross the weaker modes at smaller wavenumber after some time (cf. fig. (7.4)). Therefore, the integral length scale $L(t)$ grows with time by “following” the slope of the initial spectrum. Assuming such a isotropic power law spectrum for the large scale tail,

$$E_k \propto k^n \propto l^{-n} \quad l \geq L \quad (7.6)$$

one can solve equation (7.5) yielding the asymptotic result:

$$E \propto t^{-2n/(2+n)} \quad \text{for } t > \tau_L^A(t_0) \quad , \quad (7.7)$$

where t_0 is the initial time. Then the integral scale L “follows” the slope of the spectrum with time,

$$L \propto t^{2/(2+n)} \quad . \quad (7.8)$$

For instance, a spectral index of $n = 3$ (which corresponds to an average of randomly magnetized spherical “bubbles” with typical size L [66]) the energy follows the law

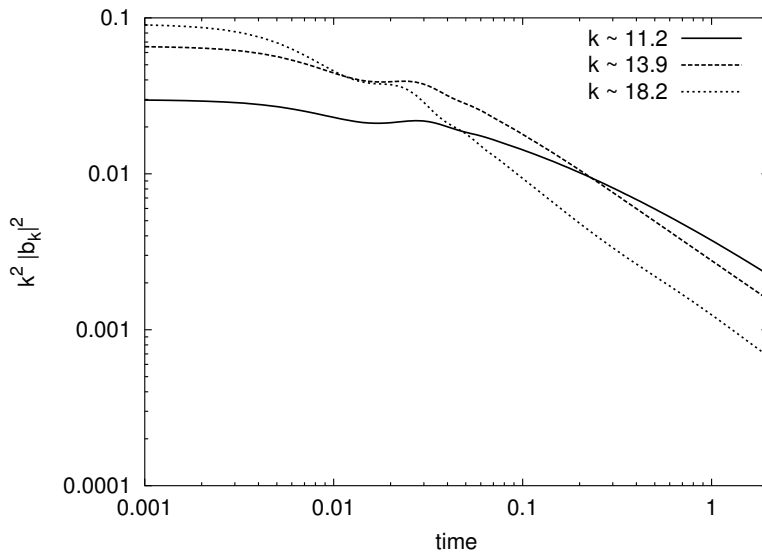


Figure 7.4.: Time evolution of different modes of the magnetic field $\hat{\mathbf{B}}_{\mathbf{k}}$. The modes with larger wavenumber k are damped faster than those with smaller wavenumber.

$E \propto t^{-6/5}$ which is Saffman’s law known from fluid dynamics [96, 94]. Note, that for very steep spectra, i.e. $n \rightarrow \infty$ (representing a δ function) the energy damping becomes $E \propto t^{-2}$ while the integral scale – as it must be – stays constant. Numerical simulations, which I performed for this work confirmed the general trend, that steeper spectra lead to faster dissipation of magnetic energy (cf. figure 7.2). But these simulations show also small deviations from the theoretically predicted damping laws for particular spectral indices n . Generally, the magnetic energy is dissipated more slowly in the numerical simulations than expected by the above considerations. This is due to finite resolution effects of the simulation box, which limits the Reynolds numbers to rather moderate values ($R_e \sim 100 - 1000$).

Second, a magnetic field with a non-vanishing helicity gives rise to a dynamical increase of the integral scale in a medium with a high Prandtl number (very large conductivity). This dynamical increase of the coherence length, which is due to the conservation of the helicity in such a medium, is very much different from the selective decay mechanism described above. Because of the energy dissipation at small scales the global conservation of the helicity affects not only modes on scales smaller than the integral scale but also the long range tail of the spectrum: the spectrum evolves self-similarly and is “shifted” towards larger scales (cf. figure 7.6). Therefore, the damping law is nearly independent of the spectral index n (dependence on the spectral index becomes only important for $n \lesssim 1$) when the magnetic field has a non-vanishing helicity. In chapter 4, I have shown that the helicity of a maximal helical field can be written as

$$\mathcal{H} \approx L E_{\text{mag}} \quad . \quad (7.9)$$

7. Damping of magnetic fields

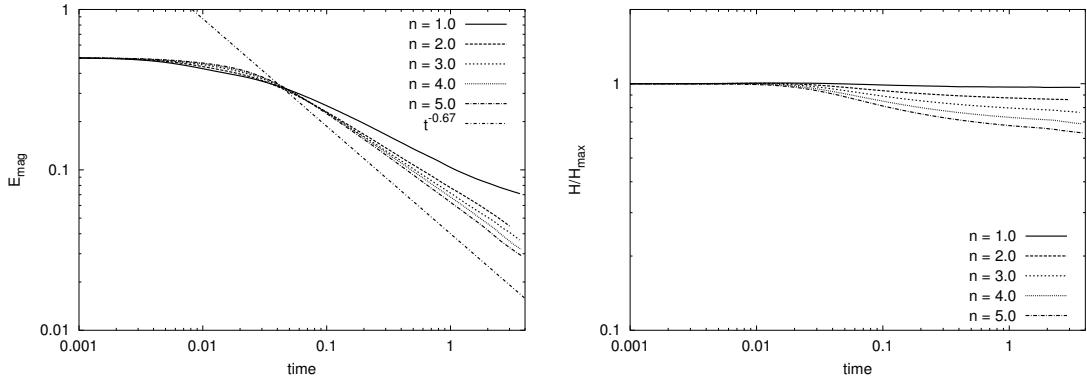


Figure 7.5.: *Left panel:* The Evolution of the magnetic energy in the turbulent regime for different initial energy spectra n , where $E_k = (8\pi)^{-1} k^3 |b_k|^2 \propto k^n$. Here, the initial magnetic field is maximal helical. For comparison, also the theoretical damping law, $E \propto t^{-0.67}$, is shown. In contrast to non-helical case, the damping law for a helical magnetic field is nearly independent of the spectral index n for $n < 1$. The n dependence of the damping laws (see section 7.1) may be due to numerical dissipation of helicity (*right panel*).

If the helicity is conserved, this implies that the energy and the integral scale are inversely proportional, i.e.

$$E \propto L^{-1} \quad . \quad (7.10)$$

Using the relation (7.10) to solve equation (7.5) one gets the asymptotic result for the energy damping

$$E \propto t^{-2/3} \quad (\text{for maximal helical fields}) \quad (7.11)$$

and the increase of the integral scale

$$L \propto t^{2/3} \quad (\text{for maximal helical fields}) \quad . \quad (7.12)$$

The plots of figure 7.5 show the compiled results of the numerical simulations, where the damping of the magnetic energy for maximal helical fields in the turbulent regime are presented. These results agree almost with the above damping law for maximal helical magnetic fields. Deviations from the theoretical predictions (in this case the damping laws should be independent of the spectral index n) may be due to numerical dissipation of helicity.

The results of this section can be summarized by the following generalized damping laws for the individual modes

$$b_l(t) = b_l(t_0) \left(1 + \frac{t}{\tau_l^A(t_0)} \right)^{-p} \quad , \quad (7.13)$$

and the total magnetic energy

$$E(t) = E(t_0) \left(1 + \frac{t}{\tau_L^A(t_0)} \right)^{-p} \quad . \quad (7.14)$$

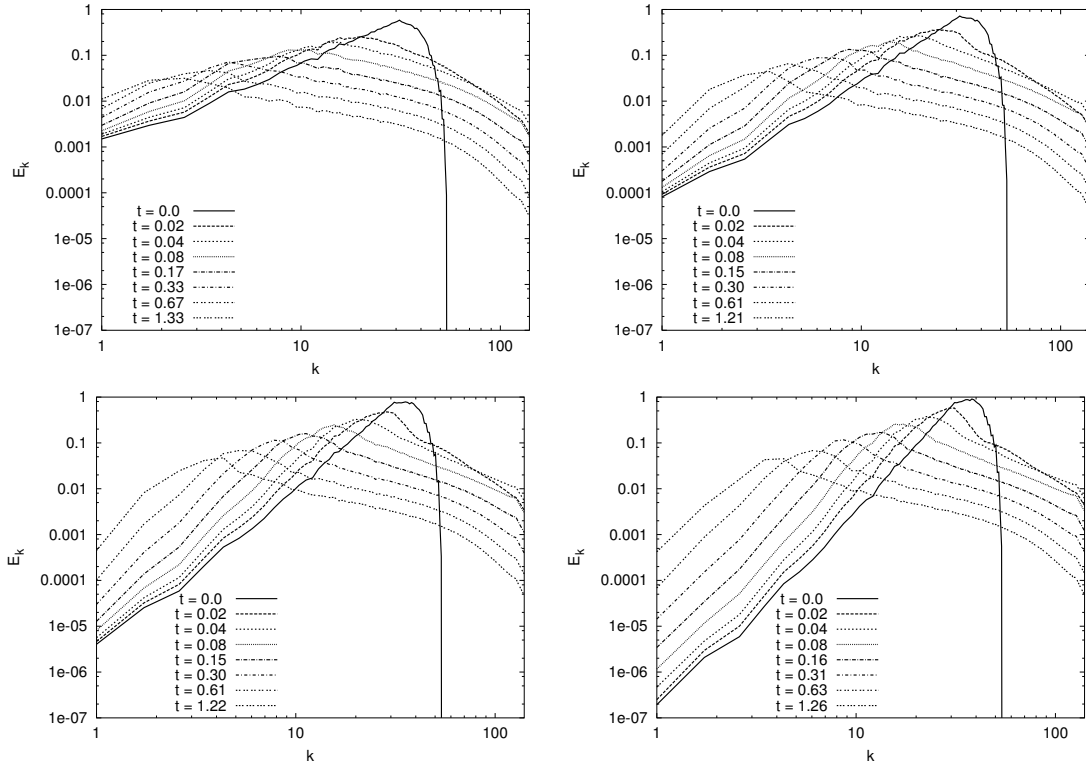


Figure 7.6.: Evolution of magnetic energy spectra in the turbulent regime for magnetic fields with initially maximal helicity. The initial energy spectra from top left to right bottom panel are $n \approx 2, 3, 4, 5$, respectively.

The damping index p depends on the initial configuration of the magnetic fields. For magnetic fields without helicity and a power law spectrum with the spectral index n the damping index is

$$p = \frac{2n}{2+n} \quad (\text{non-helical field}) \quad . \quad (7.15)$$

Whereas, for a maximal helical field with spectral slope $n > 1$ the damping index is independent of n and becomes

$$p = \frac{2}{3} \quad (\text{maximal helical field}) \quad . \quad (7.16)$$

The shift of the integral scale L in the turbulent regime can be summarized by the power law

$$L(t) = L(t_0) \left(1 + \frac{t}{\tau_L^A(t_0)} \right)^q \quad , \quad (7.17)$$

where the power law index q is

$$q = \frac{2}{2+n} \quad (\text{non-helical field}) \quad (7.18)$$

and

$$q = \frac{2}{3} \quad (\text{maximal helical field}) \quad . \quad (7.19)$$

7.2. Viscous damping

In the viscous regime, i.e. $R_e \ll 1$ dissipation becomes important not only at small scales but already at the integral scale L and the fluid motions are much smaller than during turbulence. On the other hand, the strength of the fluid velocity on the integral scale determines the damping rate of the magnetic energy. Therefore, the inhibited fluid motions in a strongly viscous medium lead also to a weaker damping of the magnetic field. The large damping time scale in the viscous regime can even be larger than the Hubble time during the considered epoch, as will be shown in the next chapter.

As the Reynolds number is a measure of the relative importance of the nonlinear interaction of the fluid motions and the dissipation force in the Euler equation (6.1), the latter can be written in the form

$$\frac{\partial v}{\partial t} + \frac{v^2}{l} + \frac{v_A^2}{l} \approx \frac{v^2}{l} / R_e \quad . \quad (7.20)$$

Then, in the viscous regime the fluid self interaction term, v^2/l can be neglected compared to the dissipation term, $v^2/l/R_e$. As in the turbulent regime, one can expect that the two “driving” terms in the reduced Euler equation will dynamically attain an equilibrium state, i.e.

$$v_A^2 \sim v^2 / R_e \quad . \quad (7.21)$$

Already from equation (7.21) it can be seen that equipartition of the kinetic energy ($v^2/2$) with the magnetic energy ($v_A^2/2$) will not be maintained. The magnetic energy will always be larger than the kinetic energy by a factor of R_e^{-1} . Because the Reynolds number is also a function of the fluid velocity, the ratio of the two energies varies also with time. This is also the case for constant kinetic viscosity or drag parameter, respectively.

From the equilibrium equation (7.21) one can estimate the damping time for the magnetic energy in the viscous regime,

$$\tau_{\text{visc.damp}} = \frac{l}{v} = \frac{l}{v_A R_e^{1/2}} \quad . \quad (7.22)$$

Therefore, the viscous damping rate is reduced by a factor of $R_e^{-1/2}$ compared to the turbulent damping leading to slower decrease of magnetic energy with time. Using the asymptotic damping law $\dot{E}/E = \tau_{\text{dyn}}$ one obtains the damping equation for viscous damping:

$$\frac{\dot{E}}{E} \approx \frac{1}{\tau_{\text{visc.damp}}} \approx \frac{V_A R_e^{1/2}}{L} \quad . \quad (7.23)$$

To solve equation (7.23) one must know the explicit form of the Reynolds number (which is in fact a time and velocity dependent function). To be more specific, I use the definitions (6.3) for the Reynolds number in the kinetic diffusion and the free streaming regime, respectively. In terms of the Alfvén velocity they are:

$$R_e = \begin{cases} \left(\frac{V_A L}{\nu} \right)^2 & : \quad \text{kinetic diffusion ("optically thick")} \\ \left(\frac{V_A}{\alpha L} \right)^2 & : \quad \text{drag ("optically thin")} \end{cases} \quad (7.24)$$

In the viscous regime the Reynolds numbers (7.24) are the ratios of the dissipation time scales and the Alfvén time *squared*, because, $V_A^2 \propto V$ in this case. Inserting the Reynolds numbers (7.24) into equation (7.22) the damping time scales become:

$$\tau_{\text{visc.damp}} = \begin{cases} \frac{\nu}{V_A^2} & : \quad \text{kinetic diffusion ("optically thick")} \\ \frac{\alpha L^2}{V_A^2} & : \quad \text{drag ("optically thin")} \end{cases} \quad (7.25)$$

These damping time scales are well known from the studies of MHD modes in the linear regime [22]. The authors of [22] analyzed the damping of magnetic field modes by assuming a large scale homogeneous background magnetic field. In the so called *overdamped* regime they found solutions of the dispersion relations for Alfvén waves having the same form as those found here (cf. also chapter 5). Because the damping of magnetic fields is due to the back reaction of the fluid motions and happens on the time scale of an eddy turnover $\tau = L/V$ the damping becomes less efficient for increasing strength of the dissipation parameters ν and α .

The solution of the damping equation (7.23) in the viscous regime is again (as in the nonlinear turbulent regime) a power law of time, rather than an exponential damping as found in the linear regime. This is due to the fact, that the damping rate $\tau_{\text{visc.damp}}^{-1}$ itself is a function of the (time dependent) magnetic energy. This has the consequence that $\dot{E}/E = t^{-1}$ and the asymptotic damping time (for $t > \tau_{\text{visc.damp}}(t_0)$) is equal to the evolution time itself, i.e.

$$\tau_{\text{visc.damp}} = t \quad . \quad (7.26)$$

This equation is of particular interest in the expanding universe, where the cosmic time t is given by the Hubble time $t_H = H^{-1}$. In principle, it is possible to use equation (7.26) to compute the magnetic energy and the integral scale for each epoch in the early universe.

Assuming constant dissipation coefficients ν and α the solutions of the equation (7.26) one obtains the damping laws in the two different viscous damping regimes

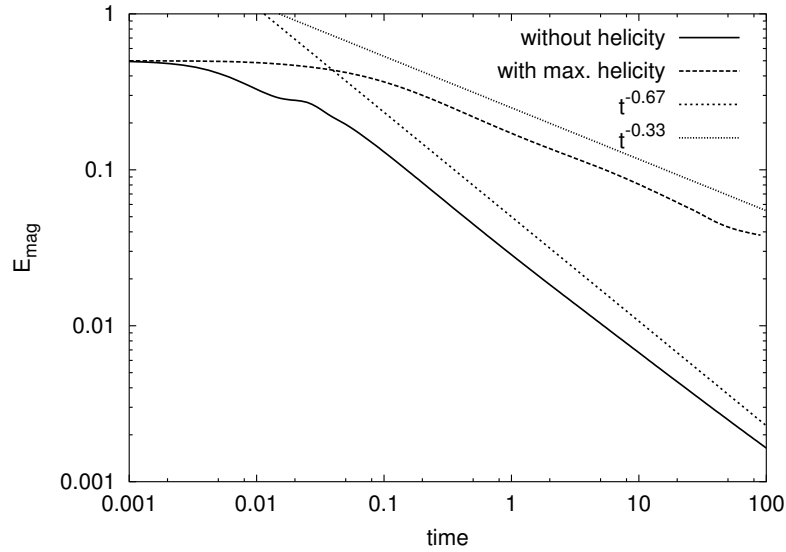


Figure 7.7.: Evolution of the magnetic energy without (solid) and with maximal (dashed) initial helicity in the viscous free streaming regime ($R_e < 1$). The simulations were performed on a mesh with 128^3 grid points, the cut-off was $k_c \approx 16$ and the spectral index $n \approx 4$. For comparison, also the theoretical expected damping laws are shown, i.e. $E_{\text{mag}} \propto t^{-0.67}$ (without helicity) and $E_{\text{mag}} \propto t^{-0.33}$ (with max. helicity).

for non-helical magnetic fields:

$$E_{\text{mag}}(t) = \begin{cases} E_{\text{mag}}(t_0) \left(1 + \frac{t}{\nu/V_A^2(t_0)}\right)^{-1} & : \quad \text{“optically thick”} \\ E_{\text{mag}}(t_0) \left(1 + \frac{t}{\alpha(\tau_L^A(t_0))^2}\right)^{-\frac{n}{2+n}} & : \quad \text{“optically thin”} \end{cases} \quad (7.27)$$

where an isotropic power law was used with the spectral index n for the magnetic energy spectrum.

Using the relation (7.6) one finds that the integral scale changes with time according to

$$L(t) = \begin{cases} L(t_0) \left(1 + \frac{t}{\nu/V_A^2(t_0)}\right)^{\frac{1}{n}} & : \quad \text{“optically thick”} \\ L(t_0) \left(1 + \frac{t}{\alpha(\tau_L^A(t_0))^2}\right)^{\frac{1}{2+n}} & : \quad \text{“optically thin”} \end{cases} \quad (7.28)$$

The damping laws for maximal helical magnetic fields can be obtained from the formulas (7.27) and (7.28) by using a “virtual” special index of $n = 1$. Note, that

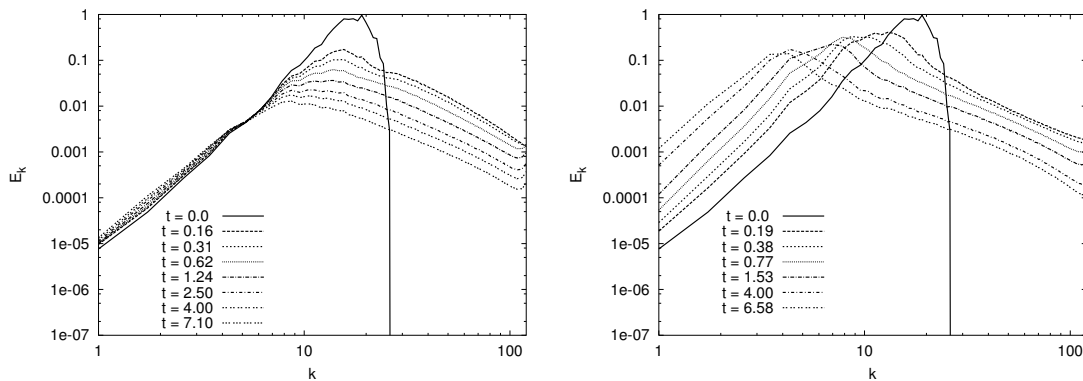


Figure 7.8.: The evolution of the magnetic energy spectra in the viscous free streaming regime ($R_e < 1$). *Left panel:* magnetic field without initial helicity; *right panel:* magnetic field with maximal helicity. The simulations were performed on a mesh with 256^3 grid points, and the cut-off was $k_c \approx 16$.

this gives the right damping laws for the *rms* values but does not describe the time evolution of the energy spectra. The time evolution of the energy spectra in the viscous free streaming regime for a non-helical and a maximal helical magnetic field is shown in figure 7.8.

In the viscous diffusion regime with a constant diffusion coefficient ν the damping should be independent of spectra and helicity of the magnetic field. Comparing the damping laws in the viscous free streaming regime and in the turbulent regime one can clearly see that the viscous damping is less efficient due to the inhibited fluid motions. The time dependence of the magnetic energy in the viscous free streaming regime resulting from numerical simulations is shown in figure 7.7.

8. Evolution of primordial magnetic fields

In the previous chapter, I considered the damping of magnetic energy due to dissipation of the induced velocity fluctuations into heat. This dynamical damping of magnetic fields is found to be a power law of time, i.e.

$$E_{\text{mag}} \propto t^{-p} \quad , \quad (8.1)$$

where p is the damping index. Because of the conformal invariance (or nearly conformal invariance in the matter dominated universe) the results found in the previous chapter can be directly assigned to the situation in the early universe. A convenient way to separate the adiabatic damping from the dynamical damping is to introduce the dimensionless magnetic energy density:

$$r \equiv \frac{\rho_{\text{mag}}}{s^{4/3}} \quad , \quad (8.2)$$

because ρ_{mag} is diluted by the expansion of the universe in the same way as $s^{4/3}$. Here,

$$s = \frac{2\pi^2}{45} g_S T^3 \quad (8.3)$$

is the entropy of relativistic particles. The ratio r is related to the quantity $r_{\text{rad}} \equiv \rho_{\text{mag}}/\rho_{\text{rad}}$ by:

$$r_{\text{rad}} = \frac{4}{3} \left(\frac{2\pi^2}{45} \right)^{1/3} \frac{g_S^{4/3}}{g_*} r \quad . \quad (8.4)$$

The latter is often used to express the magnetic field strength at the present epoch.

As discussed in the previous chapters the dynamics of the MHD system depends on the Alfvén velocity

$$V_A \equiv \frac{B}{\sqrt{4\pi (\rho_{\text{fluid}} + p_{\text{fluid}})}} \approx \sqrt{\frac{2\rho_{\text{mag}}}{\rho_{\text{fluid}} + p_{\text{fluid}}}} \quad , \quad (8.5)$$

where ρ_{fluid} and p_{fluid} are the energy density and pressure which contribute to the fluid, respectively. In the radiation dominated universe where $\rho_{\text{fluid}} \sim \rho_{\text{rad}}$, the Alfvén velocity (8.5) can be related to the ratio r .

The damping index p is *not* an universal parameter, but a function of several parameters such as initial helicity and spectra. It also depends on the cosmological epoch, differing, for example, between the diffusion and the free streaming regimes. In this chapter the results found in the previous chapters are now applied to cosmological magnetic fields in the expanding universe. Assuming that these fields, after once having been created in the early universe, (e.g. during a phase transition), evolve according to the description of a magnetized plasma, one can follow the fate of the energy and coherence length of the magnetic fields.

Depending on the global scale L and the mean free path l_{mfp} of the particles causing the damping, the magnetic field undergoes different damping regimes. In the turbulent diffusion regime the mean free path l_{mfp} is much smaller than the global scale L and the magnetized fluid possesses very large kinetic and magnetic Reynolds numbers. At the stage where the Reynolds number R_e becomes of order unity turbulence ceases and the kinetic and magnetic energy evolve in the viscous diffusion regime. It will be shown in section 8.3, that the comoving coherence lengths L^c and the Alfvén velocity V_A will not change during this regime. In the case where the mean free path of neutrinos or photons is much larger than the scale L , the MHD modes are dissipated in the free streaming regime. For a strong drag force the fluid becomes viscous in the free streaming regime.

Another aspect of the dynamics of magnetic field evolution comes from the different scaling properties of the comoving quantities under consideration. In the radiation dominated epoch the conformal time \hat{t} is proportional to the scale factor a and therefore inversely proportional to the temperature T of the universe. In contrast, in the matter dominated epoch the conformal time depends only logarithmically on the scale factor. Therefore, this epoch is dynamically much less important than the radiation dominated stage.

In the previous chapter, it was shown that the magnetic energy ρ_{mag} and the integral scale L do not evolve independently from each other. They are linked either by the energy spectrum, or by the conservation of magnetic helicity. To proceed with the description of the evolution of cosmic magnetic fields it is useful to make the following definitions. The magnetic energy density can be written as:

$$\begin{aligned} \rho_{\text{mag}}(T) &= \left(\frac{a(T)}{a(T_g)} \right)^{-4} \frac{1}{8\pi} \int_0^{k^I(T)} d \ln k B_{g_c}^2 \left(\frac{k}{k_g} \right)^n \\ &= \frac{B_{g_c}^2}{8\pi n} \left(\frac{L^c(T)}{L_g^c} \right)^{-n} \left(\frac{a(T)}{a_0} \right)^{-4}, \end{aligned} \quad (8.6)$$

where

$$B_{g_c} = B(T_g) \left(\frac{a_0}{a_g} \right)^{-4} \quad (8.7)$$

is the magnetic field strength at the epoch of magnetogenesis rescaled to the present epoch. Generally, the subscript g refers to quantities at the epoch of magnetogenesis

and the superscript c denotes comoving lengths referring to the present epoch. The magnetic field B_g is evaluated at the integral scale $L_g^c = 2\pi/k^I(T_g)$. The scale factor in terms of the temperature T is given by:

$$a(T) = \left(\frac{g_S(T)}{g_{S_0}} \right)^{-1/3} \left(\frac{T}{T_0} \right)^{-1}, \quad (8.8)$$

where the subscript 0 denotes the values evaluated today, i.e. $a_0 = 1$ at $T_0 \approx 2.7$ K. In the above equation g_S is the number of degrees of freedom of all relativistic particles contributing to the total entropy (see e.g. [55]):

$$g_S(T) = \sum_{i=\text{bosons}} g_i \left(\frac{T_i}{T} \right)^3 + \frac{7}{8} \sum_{i=\text{fermions}} g_i \left(\frac{T_i}{T} \right)^3. \quad (8.9)$$

Here, T_i is the temperature of the species i .

Using the relation (8.6) the ratio (8.2) becomes:

$$r(T) = r_g \left(\frac{L^c(T)}{L_g^c} \right)^{-n}, \quad (8.10)$$

where

$$r_g \equiv \frac{\rho_{\text{mag}}(T_g)}{s^{4/3}(T_g)} = \frac{B_g^2}{8\pi^3 n} \left(\frac{45}{2\pi^2} \right)^{4/3} \left(\frac{1}{g_{S_g}^{1/3} T_g} \right)^4 \quad (8.11)$$

is the relative magnetic energy density at the epoch of magnetogenesis at the temperature T_g . Note, that r_g can also be written in terms of quantities referring to the present epoch:

$$r_g = \frac{B_{g_c}^2}{8\pi^3 n} \left(\frac{45}{2\pi^2} \right)^{4/3} \left(\frac{1}{g_{S_0}^{1/3} T_0} \right)^4. \quad (8.12)$$

To compute the Alfvén velocity it is useful to define the fluid density and pressure in terms of the radiation energy density:

$$\rho_{\text{fl}} + p_{\text{fl}} \equiv \frac{4}{3} \frac{g_{\text{fl}}}{g_*} \rho_{\text{rad}}, \quad (8.13)$$

where g_{fl} accounts for the degrees of freedom of those particles coupled to the fluid. With this definition the Alfvén velocity at the integral scale becomes:

$$V_A = \sqrt{2} \left(\frac{2\pi^2}{45} \right)^{1/6} \frac{g_S^{2/3}}{g_{\text{fl}}^{1/2}} (n r)^{1/2} \quad (8.14)$$

$$= \sqrt{2} \left(\frac{2\pi^2}{45} \right)^{1/6} \frac{g_S^{2/3}}{g_{\text{fl}}^{1/2}} (n r_g)^{1/2} \left(\frac{L^c}{L_g^c} \right)^{-n/2} \quad (8.15)$$

8.1. Viscosities and conductivity in the early universe

To be able to discriminate between the different damping regimes we need to know the mean free path of the particles causing the dissipation of kinetic and magnetic energy into heat. In the very early universe before the electroweak phase transition, i.e. $T \sim m_W$, where m_W is the mass of the W boson, a typical mean free path is given by [55]

$$l_{\text{mfp}} \sim \frac{1}{g^4 T} \quad \text{for } T \gg 100 \text{ GeV} \quad (8.16)$$

because all – yet known particles – are relativistic at temperatures above $T \sim 100 \text{ GeV}$. For instance the gauge coupling constants g for neutrinos and photons are respectively, $g \approx 0.397$ and $g^2 \approx \alpha$, where $\alpha \approx 1/137$ is the fine structure constant.

For temperatures below the electroweak breaking scale until the neutrino decoupling at $T \sim 1 \text{ MeV}$ neutrinos are the most efficient transporters of momentum and heat due to their long mean free path [22]

$$l_\nu \simeq \frac{1}{G_F^2 T^2 (n_l + n_q)} \simeq \frac{7\pi^2}{6 \zeta(3)} \frac{1}{g_l + g_q} \frac{1}{G_F^2 T^5} \quad (8.17)$$

$$\simeq 5.68 \times 10^{-5} \left(\frac{T}{\text{GeV}} \right)^{-5} \left(\frac{g_l + g_q}{46} \right)^{-1} \text{ cm} \quad , \quad (8.18)$$

where $n_l = \frac{6}{7\pi^2} g_l \zeta(3) T^3$ and $n_q = \frac{6}{7\pi^2} g_q \zeta(3) T^3$ are the number densities of relativistic leptons and quarks*, respectively, and $G_F = 1.1663 \times 10^{-5} \text{ GeV}^{-2}$ is Fermi's constant. Here the statistical weights of the relativistic leptons are $g_l = 10$ (e^\pm , three neutrinos and anti-neutrinos) and g_q are the number of degrees of freedom for relativistic quarks $g_q = 36$ (for three light quarks). Below the temperature of the QCD phase transition ($T \sim 100 \text{ MeV}$) the quark degrees of freedom vanish, i.e. $g_q = 0$. After the electroweak phase transition the mean free path of neutrinos increases rapidly ($l_\nu \propto T^{-5}$) and will quickly overcome the coherence length of possibly existing magnetic fields. Although neutrinos interact weakly with the plasma of the early universe, consisting of relativistic leptons and quarks (the typical cross section is $G_F^2 T^2 \sim 5.3 \times 10^{-44} \text{ cm}^2 (T/\text{MeV})^2$), they may be able to efficiently damp velocity fluctuations until they freeze out entirely from the evolution of the universe.

The comoving mean free path of photons, l_γ/a , starts to increase after the temperature of the universe drops below the mass of the electron, $m_e = 0.511 \text{ MeV}$ when the electrons and the positrons become nonrelativistic. After the temperature drops below the e^+e^- annihilation temperature $T_{\text{annih}} \sim 20 \text{ keV}$ the photon mean free path is given by [22]

$$l_\gamma \simeq \frac{1}{\sigma_T n_e} \simeq 7.27 \times 10^{10} \left(\frac{T}{\text{keV}} \right)^{-3} \left(\frac{\Omega_B h^2}{0.0245} \right)^{-1} X_e^{-1} \text{ cm} \quad , \quad (8.19)$$

*For consistency the fermionic degrees of freedom include a factor 7/8

where $\sigma_T = 8\pi \alpha^2/3 m_e^2 = 6.6524 \times 10^{-25} \text{ cm}^2$ is the Thomson cross section, Ω_B is the baryon density, h is the Hubble constant measured in $100 \text{ km sec}^{-1} \text{ Mpc}^{-1}$, and n_e is the number density of electrons. The latter can be expressed by the number density of baryons n_B , i.e.

$$n_e = X_e n_B = X_e \frac{\rho_0}{m_p} \Omega_B \left(\frac{a}{a_0} \right)^{-3} \quad (8.20)$$

with the number of free electrons per baryon X_e . The present critical density ρ_0 is given by (see e.g. [55]):

$$\rho_0 \equiv \frac{3}{8\pi} M_{\text{Pl}}^2 H_0^2 \simeq 1.879 h^2 \times 10^{-29} \text{ g cm}^{-3} \quad (8.21)$$

The temperature dependence of the ionization fraction X_e can be computed by solving the Saha equation in thermal equilibrium [55]:

$$\frac{1 - X_e}{X_e^2} = \frac{4\sqrt{2}\zeta(3)}{\sqrt{\pi}} \eta \left(\frac{T}{m_e} \right)^{3/2} \exp\left(\frac{B}{T}\right) \quad , \quad (8.22)$$

where $\eta = 6.49 \times 10^{-10} (\Omega_B h^2/0.0245)$ is the baryon-to-photon ratio, $B = 13.6 \text{ eV}$ is the binding energy of hydrogen, and $\zeta(3) \approx 1.202$ is the Riemann zeta function of 3. The equation (8.22) is valid only until the reaction $e + p \leftrightarrow H + \gamma$ maintains an equilibrium state. After freeze-out of this reaction at $T \sim 0.26 \text{ eV}$ a residual ionization fraction of $X_e^\infty \simeq 2.7 \times 10^{-5} (\Omega_0^{1/2}/\Omega_B h)$ remains (see e.g. [55]).

Before the completion of the e^+e^- annihilation also pairs of electrons and positrons interact with the background photons and must also be taken into account to compute the photon mean free path. The latter is found to be [86]:

$$l_\gamma \simeq \frac{1}{\sigma_T (n_{\text{pair}}^2 + n_e^2)^{1/2}} \quad . \quad (8.23)$$

The number density of electron-positron pairs is given by [86]:

$$n_{\text{pair}} \approx \left(\frac{2 m_e T}{\pi} \right)^{3/2} \exp\left(-\frac{m_e}{T}\right) \left(1 + \frac{15}{8} \frac{T}{m_e} \right) \quad . \quad (8.24)$$

The expression (8.23) for the photon mean free path including e^+e^- pairs approaches the equation (8.19) for $n_{\text{pair}} \ll n_e$, i.e. after the e^+e^- annihilation. In figure 8.1, the temperature dependence of the number densities n_e and n_{pair} is shown. The latter drops very quickly and becomes much smaller than n_e below $T \sim 20 \text{ keV}$.

For a plasma comprised of relativistic particles, the mean free path is related to the effective shear viscosity by (cf. equation (3.62))

$$\nu_{\text{eff}} \equiv \frac{\nu}{\rho + p} = \frac{1}{5} l_{\text{mfp}} \quad . \quad (8.25)$$

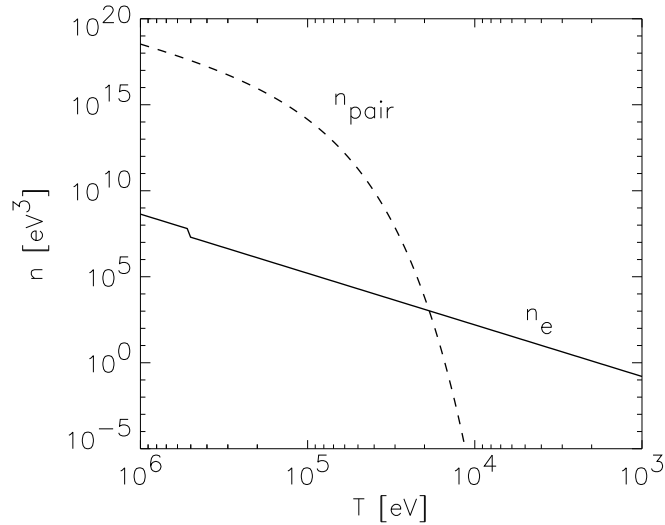


Figure 8.1.: The temperature dependence of the number densities of electron-positron pairs n_{pair} and free electrons n_e are shown. Below ~ 20 keV the total number density $(n_{\text{pair}}^2 + n_e^2)^{1/2}$ is dominated by free electrons.

Again, the “comoving” effective viscosity ν_{eff}/a , which I use in the conformally rescaled MHD equations, is increasing with decreasing temperature. This may change the dynamics of the MHD system. An initially turbulent stage will come into a viscous diffusion regime while the kinetic viscosity is increasing.

In the high temperature regime ($1 \text{ MeV} \lesssim T \lesssim m_W$) the electrical conductivity σ is given by [21]

$$0.76 T \lesssim \sigma \lesssim 6.7 T \quad , \quad (8.26)$$

where the larger value refers to the upper temperature bound.

At temperatures below the electron mass the conductivity becomes [82]

$$\sigma = \frac{\alpha n_e \tau_c}{m_e} \simeq \frac{m_e}{\alpha \ln \Lambda} \left(\frac{2 T}{\pi m_e} \right)^{3/2} \quad , \quad (8.27)$$

where τ_c is the mean time between two collisions, $\Lambda = \frac{1}{6\pi^{1/2}} \frac{1}{\alpha^{1/2}} \left(\frac{m^3}{n_e} \right)^{1/2} \left(\frac{T}{m_e} \right)$, and α is the fine structure constant.

The finite conductivity acts as a diffusion term in the induction equation (3.75)

$$\frac{\partial \tilde{\mathbf{B}}}{\partial \tilde{t}} = \nabla \times (\tilde{\mathbf{v}} \times \tilde{\mathbf{B}}) + \frac{1}{4\pi \tilde{\sigma}} \nabla^2 \tilde{\mathbf{B}} \quad , \quad (8.28)$$

with the rescaling

$$\tilde{\sigma} \equiv a \sigma \quad . \quad (8.29)$$

Note, that $\tilde{\sigma}$ is constant in the high temperature regime, whereas it is increasing with $\propto a^{1/2}$ for temperatures below m_e . But, as one can see from the equations (8.25) and (8.26), the magnetic Prandtl number P_m , which gives the relative importance of the kinetic and magnetic diffusion, is very large in the early universe,

$$P_m = 4\pi \nu_{\text{eff}} \sigma \simeq 2.9 \times 10^8 \left(\frac{\text{keV}}{T} \right)^{3/2} \left(\frac{\Omega_B h^2}{0.0245} \right)^{-1} X_e^{-1} \quad \text{for} \quad T < m_e \quad . \quad (8.30)$$

This allows one to neglect the dissipation of magnetic field energy due to finite conductivity. In the early universe, the indirect dissipation of magnetic fields via back reactions of the fluid motions is much more effective than the direct dissipation via a non-vanishing resistivity.

8.2. The turbulent regime

Turbulent motions start to develop when the nonlinear terms in the MHD equations become dominant compared to the dissipation terms such as the kinetic diffusion or drag force. The turbulent regime is quantified by a large Reynolds number,

$$R_e = \frac{V L}{\nu_{\text{eff}}} \sim V \frac{L}{l_{\text{mfp}}} \gg 1 \quad . \quad (8.31)$$

Assuming a magnetic energy density of one percent of the energy density in radiation, the typical Reynolds number can be as large as $R_e \sim V M_{\text{pl}}/T \sim \mathcal{O}(10^{15})$ at the electroweak scale. Due to strong increase of the comoving mean free path (cf. equations (8.17) and (8.19)) the Reynolds number is decreasing with time. For most cases this leads to the shut-down of the turbulent stage at a certain temperature T_{EoT} . The latter depends on the initial properties of the magnetic fields and is estimated in paragraph 8.2.3.

At least for non-helical magnetic fields one expects equipartition of kinetic and magnetic energy (cf. chapter 6) from which one can estimate the large scale fluid velocity,

$$V \approx V_A \quad . \quad (8.32)$$

In the case of a helical magnetic field the kinetic energy is found to be slightly smaller than the magnetic energy which leads to the relation

$$V \approx \sqrt{\Gamma} V_A \quad , \quad (8.33)$$

where Γ is almost constant and of the order of $\mathcal{O}(10^{-1})$ (see figure 6.1).

8.2.1. Dissipation time scale in the turbulent regime

From the general considerations in chapter 6 one knows that the energy dissipation rate is equal to the frequency of an eddy turnover

$$\tau^{-1} = \frac{V}{L} \quad (8.34)$$

Hence, it is clear that dynamical processes of the MHD system are only relevant at scales smaller than $V H^{-1}$ (V refers to the averaged velocity at the scale L), i.e.

$$L < L_{\max} = V H^{-1} \quad \text{for dynamical coupled MHD.} \quad (8.35)$$

Otherwise, the dynamics of the MHD system is decoupled from the evolution of the universe. Those patches with constant comoving integral scale L^c and Alfvén velocity V_A which are initially smaller than $V_A H^{-1}$ will remain coupled, because the Hubble time increases as $H^{-1} \propto a^2$. Note, that the time needed to establish MHD turbulence after magnetogenesis is at least one eddy turnover time which, again, must not be larger than the Hubble time at that epoch.

Let us assume that the considered magnetic fields were generated during the radiation dominated epoch at high temperatures and with large Reynolds numbers. Then, because the system can not establish turbulence on scales larger than $\sim V H^{-1}$, the comoving coherence length at magnetogenesis L_g^c can be estimated through the relation:

$$\frac{L}{V_A} = f H^{-1} \quad , \quad (8.36)$$

where I introduced the numerical parameter f which should be of order unity. The Hubble time during radiation domination is given by [55]:

$$H^{-1} = \sqrt{\frac{90}{8\pi^3}} \frac{1}{\sqrt{g_*}} \frac{M_{\text{Pl}}}{T^2} \quad , \quad (8.37)$$

where $M_{\text{Pl}} \approx 1.22 \times 10^{19}$ GeV is the Planck mass. Using the definition for the Alfvén velocity (8.15) and the equations (8.36) and (8.37) L_g^c becomes:

$$\begin{aligned} L_g^c &= f \left(\frac{2025}{4\pi^7} \right)^{1/6} \frac{g_{S_g}}{g_{\text{flg}}^{1/2} g_{*g}^{1/2}} g_{S_0}^{-1/3} (n r_g)^{1/2} \frac{M_{\text{Pl}}}{T_g} T_0^{-1} \\ &\simeq 2.2 \times 10^{-4} f \sqrt{n} \left(\frac{r_g}{0.01} \right)^{1/2} \left(\frac{T_g}{100 \text{ GeV}} \right)^{-1} \text{ pc} \quad , \end{aligned} \quad (8.38)$$

where in the second line of equation (8.38), I assumed $g_{\text{flg}} = g_{S_g} = g_{*g} = 86.25$ (bosons: 8 gluons and the photon; fermions: 5 light quarks, μ , τ , e and 3 ν 's) and $g_{S_0} = 3.91$.

8.2.2. Damping in the turbulent regime

To describe the damping of magnetic fields in the turbulent regime I parameterize the asymptotic evolution (after one eddy turnover) of the comoving coherence length and dimensionless magnetic energy density by power laws,

$$L^c \propto \tilde{t}^q \quad , \quad (8.39)$$

$$r \propto \tilde{t}^{-p} \quad . \quad (8.40)$$

As discussed in chapter 7, the damping indices q and p cannot be chosen independently from each other. From dimensional arguments they are constrained by:

$$p/2 + q = 1 \quad . \quad (8.41)$$

The damping exponent p in the turbulent regime is found to be

$$0.5 \lesssim p \lesssim 1.2 \quad , \quad (8.42)$$

depending on the structure of the initial magnetic fields. For non-helical magnetic fields the damping index has the following dependence on the spectral index n of the magnetic energy (cf. section 7.1):

$$p = \frac{2n}{2+n} \quad . \quad (8.43)$$

Assuming maximal helical magnetic fields one expects a damping index of $p = 2/3$. My numerical simulations show a slightly smaller damping index of $p \simeq 0.55$. This may be due to the fact that the fluid velocity V at the integral scale is smaller than the Alfvén velocity V_A . This in turn leads to a smaller dissipation rate (see figures 7.5, 6.1 and 6.2).

Combining the results of the above discussion and the fact that the conformal time \tilde{t} in the radiation dominated universe is proportional to the scale factor a , i.e.

$$\tilde{t} \propto a \propto g_S^{-1/3} T^{-1} \quad , \quad (8.44)$$

one obtains again the damping equation (8.36) for the turbulent regime.

The solution of the equation (8.36) in terms of the comoving coherence length and the magnetic energy is:

$$L^c = L_g^c \left[\left(\frac{g_{\text{flg}}}{g_{\text{fl}}} \right)^{1/2} \left(\frac{g_S}{g_{Sg}} \right) \left(\frac{g_{*g}}{g_*} \right)^{1/2} \right]^{\frac{2}{2+n}} \left(\frac{T}{T_g} \right)^{-\frac{2}{2+n}} \quad (8.45)$$

$$= f (n r_g)^{1/2} G_1 \frac{M_{\text{Pl}}}{T_g T_0} \left(\frac{T}{T_g} \right)^{-\frac{2}{2+n}} \quad (8.46)$$

$$r = r_g \left[\left(\frac{g_{\text{flg}}}{g_{\text{fl}}} \right)^{1/2} \left(\frac{g_S}{g_{Sg}} \right) \left(\frac{g_{*g}}{g_*} \right)^{1/2} \right]^{-\frac{2n}{2+n}} \left(\frac{T}{T_g} \right)^{\frac{2n}{2+n}} \quad , \quad (8.47)$$

where

$$G_1 \equiv \left(\frac{2025}{4\pi^7} \right)^{1/6} \frac{g_{Sg}}{g_{\text{flg}}^{1/2} g_{*g}^{1/2}} g_{S_0}^{-1/3} \left[\left(\frac{g_{\text{flg}}}{g_{\text{fl}}} \right)^{1/2} \left(\frac{g_S}{g_{Sg}} \right) \left(\frac{g_{*g}}{g_*} \right)^{1/2} \right]^{\frac{2}{2+n}} . \quad (8.48)$$

For example, using a spectral index of $n = 3$ and assuming that the MHD system evolves while it is turbulent, the coherence length and the magnetic energy becomes:

$$L^c \simeq 5.6 \times 10^2 L_g^c \left(\frac{T_g}{100 \text{ GeV}} \right)^{2/5} \left(\frac{T}{20 \text{ keV}} \right)^{-2/5} \quad (8.49)$$

$$\simeq 1.2 \times 10^{-1} f \left(\frac{r_g}{0.01} \right)^{1/2} \left(\frac{T_g}{100 \text{ GeV}} \right)^{-3/5} \left(\frac{T}{20 \text{ keV}} \right)^{-2/5} \text{ pc} , \quad (8.50)$$

$$r \simeq 5.6 \times 10^{-11} \left(\frac{r_g}{0.01} \right) \left(\frac{T_g}{20 \text{ keV}} \right)^{-6/5} \left(\frac{T}{20 \text{ keV}} \right)^{6/5} , \quad (8.51)$$

where $g_{\text{fl}} = 2$, $g_S = 3.91$, and $g_* = 3.36$ were used.

8.2.3. End of turbulence by diffusive viscosity

I mentioned already in section 8.1 that the effective diffusion parameter ν_{eff} is an increasing function of time. This implies that the kinetic viscosity can become strong enough to shut down the turbulent motions of the fluid. Turbulent motions cease at the time the kinetic Reynolds number becomes smaller than unity. As the resistivity is always much smaller than the shear viscosity it is sufficient to consider only the kinetic Reynolds number during turbulence:

$$R_e = \frac{V_A L}{\nu_{\text{eff}}} = \frac{5 V_A L}{l_{\text{mfp}}} . \quad (8.52)$$

Neutrino diffusion

After the electroweak phase transition at temperature $T \sim 100 \text{ GeV}$ neutrinos give the most contribution to the viscosity until they freeze-out at temperature $T \sim \text{MeV}$. Using the Alfvén velocity (8.15), the evolution of the coherence length (8.46), and the neutrino mean free path (8.17), one obtains the Reynolds number for neutrino diffusion:

$$R_e = f n r_g G_{\nu 1} \frac{M_{\text{Pl}} T_g^3}{G_{\text{F}}^{-2}} \left(\frac{T}{T_g} \right)^{-\frac{2-n}{2+n}} \left(\frac{T}{T_g} \right)^4 , \quad (8.53)$$

with

$$G_{\nu 1} \equiv \frac{90}{7\pi^3} \left(\frac{20\pi}{81} \right)^{\frac{1}{6}} \zeta(3) \frac{g_{Sg}}{g_{\text{flg}}^{1/2} g_{*g}^{1/2}} g_S^{1/3} \frac{g_l + g_q}{g_{\text{fl}}^{1/2}} \left[\left(\frac{g_{\text{flg}}}{g_{\text{fl}}} \right)^{\frac{1}{2}} \left(\frac{g_S}{g_{Sg}} \right) \left(\frac{g_{*g}}{g_*} \right)^{\frac{1}{2}} \right]^{\frac{2-n}{2+n}} . \quad (8.54)$$

Using a spectral index of $n = 3$ the Reynolds number (8.53) becomes:

$$R_e \sim 10^{-8} \left(\frac{r_g}{0.01} \right) \left(\frac{T_g}{100 \text{ GeV}} \right)^{-\frac{6}{5}} \left(\frac{T}{\text{MeV}} \right)^{\frac{21}{5}} \quad (8.55)$$

Using the Reynolds number for neutrino viscosity (8.53) one can estimate at which temperature turbulence ceases, i.e. $R_e \sim 1$,

$$T_{\text{EoT}} = \left[\frac{1}{f n r_g G_{\nu 1}} \frac{G_{\text{F}}^{-2}}{M_{\text{Pl}} T_g^3} \right]^{\frac{2+n}{6+5n}} T_g \quad , \quad (8.56)$$

and with $n = 3$

$$T_{\text{EoT}} \sim 10^2 \left(\frac{r_g}{0.01} \right)^{-\frac{5}{21}} \left(\frac{T_g}{100 \text{ GeV}} \right)^{\frac{2}{7}} \text{ MeV} \quad , \quad (8.57)$$

To solve the equation $R_e = 1$ in order to find T_{EoT} , I used a simple numerical scheme. The results for different parameters are summarized in the figures (8.2) and (8.3).

The comoving coherence length and the magnetic field at the end of turbulence by neutrino diffusion can be computed by inserting the result (8.56) in equations (8.46) and (8.47) resulting in:

$$L^c(T_{\text{EoT}}) = f^{\frac{8+5n}{6+5n}} G_0 (n r_g)^{\frac{10+5n}{12+10n}} G_{\nu 1}^{\frac{2}{6+5n}} \left(\frac{M_{\text{Pl}} T_g^3}{G_{\text{F}}^{-2}} \right)^{\frac{2}{6+5n}} \frac{M_{\text{Pl}}}{T_g T_0} \quad , \quad (8.58)$$

$$r(T_{\text{EoT}}) = r_g \left[\left(\frac{g_{\text{flg}}}{g_{\text{fl}}} \right)^{1/2} \left(\frac{g_S}{g_{Sg}} \right) \left(\frac{g_{*g}}{g_*} \right)^{1/2} \right]^{-\frac{2n}{2+n}} \left(\frac{1}{f n r_g G_{\nu 1}} \right)^{\frac{2n}{6+5n}} \left(\frac{G_{\text{F}}^{-2}}{M_{\text{Pl}} T_g} \right)^{\frac{2n}{6+5n}} \quad . \quad (8.59)$$

Photon diffusion

The comoving photon mean free path and therefore the effective viscosity caused by the interactions of e^\pm with photons starts to increase at the time when the electrons and positrons become nonrelativistic. The Reynolds number (8.52) by photon diffusion in the turbulent regime is:

$$R_e = f n r_g G_{\gamma 1} \frac{M_{\text{Pl}} \sigma_T \tilde{n}}{T_g T} \left(\frac{T}{T_g} \right)^{-\frac{2-n}{2+n}} \quad (8.60)$$

with

$$G_{\gamma 1} \equiv \frac{15}{\pi} \left(\frac{20 \pi}{81} \right)^{\frac{1}{6}} \frac{g_{Sg}}{g_{\text{flg}}^{1/2} g_{*g}^{1/2}} g_S^{1/3} g_{\text{fl}}^{-1/2} \left[\left(\frac{g_{\text{flg}}}{g_{\text{fl}}} \right)^{\frac{1}{2}} \left(\frac{g_S}{g_{Sg}} \right) \left(\frac{g_{*g}}{g_*} \right)^{\frac{1}{2}} \right]^{\frac{2-n}{2+n}} \quad , \quad (8.61)$$

8. Evolution of primordial magnetic fields

where $\tilde{n} = \sqrt{n_{\text{pair}}^2 + n_e^2}$. After the e^+e^- annihilation at $T \sim 20$ keV the number density of electrons and positrons is given mainly by free electrons and the Reynolds number becomes (see equation (8.23) and figure 8.1):

$$R_e = f n r_g G_{\gamma 2} \frac{M_{\text{Pl}} T_g \sigma_T \rho_0}{m_p T_0^3} \Omega_B X_e \left(\frac{T}{T_g} \right)^{-\frac{2-n}{2+n}} \left(\frac{T}{T_g} \right)^2 \quad (8.62)$$

with

$$G_{\gamma 2} \equiv \frac{15}{\pi} \left(\frac{20 \pi}{81} \right)^{\frac{1}{6}} \frac{g_{Sg}}{g_{\text{flg}}^{1/2} g_{*g}^{1/2}} \frac{g_S^{4/3}}{g_{S0}} g_{\text{fl}}^{-1/2} \left[\left(\frac{g_{\text{flg}}}{g_{\text{fl}}} \right)^{\frac{1}{2}} \left(\frac{g_S}{g_{Sg}} \right) \left(\frac{g_{*g}}{g_*} \right)^{\frac{1}{2}} \right]^{\frac{2-n}{2+n}} \quad (8.63)$$

For $n = 3$ the Reynolds number (8.62) becomes:

$$R_e \sim 10^{-5} \left(\frac{r_g}{0.01} \right) \left(\frac{\Omega_B h^2}{0.0245} \right) \left(\frac{T_g}{100 \text{ GeV}} \right)^{4/5} \left(\frac{T}{\text{keV}} \right)^{11/5} \quad (8.64)$$

For the derivation of the above equation it was assumed that the MHD system is in a turbulent stage after T_{annih} .

The temperature at end of turbulence T_{EoT} caused by photon diffusion can be computed for temperatures below T_{annih} :

$$T_{\text{EoT}} = \left[\frac{1}{f n r_g G_{\gamma 2}} \frac{m_p T_0^3}{M_{\text{Pl}} T_g \sigma_T \rho_0} \Omega_B^{-1} X_e^{-1} \right]^{\frac{2+n}{2+3n}} T_g \quad (8.65)$$

For $n = 3$ this temperature is approximately:

$$T_{\text{EoT}} \sim 10^2 \left(\frac{r_g}{0.01} \right)^{-\frac{5}{11}} \left(\frac{\Omega_B h^2}{0.0245} \right)^{-\frac{5}{11}} \left(\frac{T_g}{100 \text{ GeV}} \right)^{-\frac{4}{11}} \text{ keV} \quad (8.66)$$

For higher temperatures one has to take into account the electron-positron pairs to compute the photon viscosity. Because of the exponential factor in the number density of n_{pair} (see equation (8.24)) the equation (8.60) can not be inverted analytically in order to find the temperature T_{EoT} . The temperature T_{EoT} can be read off the figures 8.2 and 8.3 where the evolution of coherence length for different models of magnetogenesis are shown.

8.3. The viscous diffusion regime

After the turbulence is shut down by the increasing kinetic viscosity, i.e. when

$$R_e < 1 \quad , \quad (8.67)$$

the MHD system will reach a state where an increase of the magnetic coherence length, or integral scale, is temporarily halted.

The following arguments show that magnetic energy is not dissipated (and therefore, the comoving coherence length is not growing) during the viscous diffusion regime in the early universe. In section 7.2, I showed that the damping time scale in the viscous diffusion regime is given by:

$$\tau_{\text{visc.diff}} = \frac{\nu_{\text{eff}}}{V_A^2} = \frac{1}{20} \left(\frac{45}{2\pi^2} \right)^{1/3} \frac{g_{\text{fl}}}{g_S^{4/3}} \frac{l_{\text{mfp}}}{nr} \quad . \quad (8.68)$$

Using this fact and the relation at onset of viscous diffusion ($R_e = 1$)

$$\frac{V_A L}{\nu_{\text{eff}}} = 1 \quad , \quad (8.69)$$

the dissipation time scale (8.68) at the beginning of viscous diffusion (end of turbulence, respectively) becomes:

$$\tau_{\text{visc.diff}} = \frac{L}{V_A} = f H^{-1} \quad \text{at} \quad T = T_{\text{EoT}} \quad . \quad (8.70)$$

From equation (8.68) it is also obvious that the dissipation time scale $\tau_{\text{visc.diff}}$ is increasing faster than the Hubble time H^{-1} due the rapidly growing mean free path l_{mfp} . During radiation domination one finds for neutrinos

$$\frac{l_\nu}{H^{-1}} \propto T^{-3} \quad (8.71)$$

and for photons

$$\frac{l_\gamma}{H^{-1}} \propto T^{-1} \quad . \quad (8.72)$$

The increasing dissipation time scale (compared to the Hubble time) prevents further dissipation of magnetic energy during the viscous diffusion regime (either by neutrino diffusion or photon diffusion). Also the comoving coherence length L^c is not growing during this epoch. This epoch lasts until the background radiation particles enter the free streaming regime.

8.4. The free streaming regime

Before the background radiation particles decouple from the evolution of the universe (“freeze-out”) the mean free path l_{mfp} of those particles will first exceed the coherence length $L < H^{-1}$ of the magnetic field. Then the background radiation particles are free streaming over the entire system, i.e.

$$l_{\text{mfp}} > L \quad . \quad (8.73)$$

In this case of a “optically thin” medium the interaction of the fluid particles and the background radiation is described by the drag force parameterized with the drag coefficient α . In contrast to the diffusion regime where the viscosity gets stronger with time, in the free streaming regime the drag force gets weaker with time due to the dilution of fluid particles. This implies also, that the damping time scale is decreasing while the temperature of the universe drops leading to the situation where a highly viscous fluid may start to move again. In this case the magnetic energy again will be dissipated.

The dissipation of kinetic energy occurs on time scales comparable to the drag time α^{-1} . Therefore, the Reynolds number in the free streaming regime is given by (cf. chapter 6):

$$R_e = \frac{V}{\alpha L} \quad . \quad (8.74)$$

As the drag coefficient α is a decreasing function of time (see equations (8.83) and (8.96)) the Reynolds number (8.74) in the free streaming regime is increasing with time. This has the consequence, that at the beginning of radiation free streaming the comoving coherence length is halted, while it starts to increase when the damping time scale drops below the Hubble time. This is in contrast to the diffusion regime where the Reynolds number and the damping time scale are decreasing.

From the discussion in the previous section it can be seen that the comoving coherence length is not growing after the end of turbulence in the diffusion regime. Therefore, it is useful to calculate the proper integral scale after the end of turbulence to get an estimate for the beginning of free streaming. Using the evolution equation for the comoving integral scale (8.45) in the turbulent regime, one obtains the proper length scale $L = a L^c$ at the end of turbulence ($T = T_{\text{EoT}}$):

$$L = f (n r_g)^{1/2} G_1 \left(\frac{g_{S_0}}{g_S} \right)^{1/3} \left(\frac{T_{\text{EoT}}}{T_g} \right)^{-\frac{2}{2+n}} \frac{M_{\text{Pl}}}{T_g T} \quad . \quad (8.75)$$

8.4.1. Neutrino free streaming

Neutrinos are the particles which decouple first from the fluid and have the longest mean free path in the early universe due to their weak interaction. Neutrinos start to free stream at the temperature T_{SoF} where

$$l_\nu(T_{\text{SoF}}) = L(T_{\text{SoF}}) \quad , \quad (8.76)$$

i.e. at:

$$\begin{aligned} T_{\text{SoF}} = & (f G_1)^{-1/4} (n r_g)^{-1/8} \left(\frac{7\pi^2}{6\zeta(3)} \right)^{1/4} \left(\frac{1}{g_l + g_q} \right)^{1/4} \left(\frac{g_S}{g_{S_0}} \right)^{1/12} \\ & \times \left(\frac{T_g}{M_{\text{Pl}}} \right)^{1/4} \left(\frac{T_{\text{EoT}}}{T_g} \right)^{\frac{1}{4+2n}} G_{\text{F}}^{-1/2} \quad . \quad (8.77) \end{aligned}$$

Here, the temperature T_{EoT} at the end of turbulence is given from equation (8.56). The beginning of neutrino free streaming can be read off the figures 8.2 and 8.3, where the neutrino mean free path and the comoving coherence length are shown.

After neutrinos start to free stream over the main fluid fluctuations they are also decoupled from the fluid itself. Therefore, they do not contribute to the energy density and pressure of the fluid. In this case the fluid is comprised of all relativistic particles except the neutrinos, i.e.

$$\rho_{\text{fluid}} = \rho_{\text{rad}} - \rho_{\nu} \quad , \quad (8.78)$$

where

$$\rho_{\nu} = g_{\nu} \frac{\pi^2}{30} T^4 \quad (8.79)$$

is the neutrino energy density before neutrino freeze-out at $T \sim 1$ MeV, and $g_{\nu} = 5.25$ is the number of degrees of freedom for 3 light neutrinos. Using the definition for the fluid density and pressure (8.13) the degrees of freedom of those relativistic particles contributing to the fluid becomes:

$$g_{\text{fl}} = g_* - g_{\nu} \quad (8.80)$$

The drag coefficient α_{ν} and the heat exchange coefficient β_{ν} are nearly the same in the high temperature regime where neutrinos are free streaming. By averaging the energy transfer in each scatter over the distribution of background and fluid particles, they are [86, 22]

$$\beta_{\nu} = \sigma_{\text{w}} n_{\text{w}} \frac{\rho_{\nu}}{\rho_{\text{rad}}} = \frac{g_{\nu}}{g_* l_{\nu}} \quad (8.81)$$

and

$$\alpha_{\nu} \simeq \beta_{\nu} \quad , \quad (8.82)$$

where σ_{w} is the neutrino cross section with another weakly interacting particles, n_{w} is the number density of the weakly interacting particles. Together with the neutrino mean free path (8.17) the drag coefficient (8.82) is given by:

$$\alpha_{\nu} = \frac{6 \zeta(3)}{7\pi^2} \frac{g_{\nu} (g_l + g_q)}{g_*} G_{\text{F}}^2 T^5 \quad (8.83)$$

Comparing the drag coefficient α_{ν} with the Hubble rate gives

$$\frac{\alpha_{\nu}}{H} = \frac{9 \zeta(3)}{7\pi^3} \left(\frac{5}{\pi}\right)^{1/2} \frac{g_{\nu} (g_l + g_q)}{g_*^{3/2}} \frac{M_{\text{Pl}} G_{\text{F}}^{-2}}{T^5} \quad (8.84)$$

$$\simeq 5.4 \times 10^{-2} \left(\frac{T}{\text{MeV}}\right)^3 \left(\frac{g_{\nu}}{5.25}\right) \left(\frac{g_*}{10.75}\right)^{-3/2} \left(\frac{g_l}{3.5}\right) \quad . \quad (8.85)$$

The drag force by neutrino free streaming becomes ineffective if $\alpha_\nu/H < 1$ which coincides essentially with the freeze-out of neutrinos, i.e. when $l_\nu \simeq l_H$. Then, the temperature at which dragging by neutrinos becomes ineffective is:

$$T \simeq 2.6 \left(\frac{g_\nu}{5.25} \right)^{-1/3} \left(\frac{g_*}{10.75} \right)^{1/2} \left(\frac{g_l}{3.5} \right)^{-1/3} \text{ MeV} \quad . \quad (8.86)$$

8.4.2. Photon free streaming

The comoving photon mean free path starts to increase when the electrons and positrons become nonrelativistic at temperature around $T \sim m_e$. Because the comoving coherence length L^c stays constant during the viscous photon diffusion regime the temperature T_{SoF} at which photons start to free stream can be estimated from the equation

$$l_\gamma(T_{\text{SoF}}) = L(T_{\text{SoF}}) \quad , \quad (8.87)$$

where the proper integral scale is given by equation (8.75). After the e^+e^- annihilation the mean free path of photons is given by $l_\gamma \simeq 1/(\sigma_T n_e) \propto T^{-3}$ and the temperature T_{SoF} is:

$$T_{\text{SoF}} \simeq (f G_1)^{-1/2} (n r_g)^{-1/4} \left(\frac{g_S}{g_{S_0}} \right)^{2/3} \left(\frac{M_{\text{Pl}}}{T_g} \right)^{1/2} \left(\frac{T_{\text{EoT}}}{T_g} \right)^{\frac{1}{2+n}} \left(\frac{T_0^3}{\sigma_T n_{B_0} X_e} \right)^{1/2} , \quad (8.88)$$

where

$$n_{B_0} \equiv \frac{\rho_0}{m_p} \Omega_B \quad (8.89)$$

is the number density of baryons today (note, that before cosmological recombination $n_e = n_B$). For the equation (8.88) it was assumed that the MHD system is turbulent until photon diffusion shuts down turbulence at T_{EoT} (see equation (8.65)).

Before, the completion of e^+e^- annihilation one has to solve the equation (8.87) numerically to obtain the temperature T_{SoF} .

In the photon free streaming regime the fluid consists of nonrelativistic protons and electrons and the main contribution to the thermal energy density is due to these particles [22],

$$\rho_{\text{thermal}} = \frac{3}{2} (n_p + n_e) T = 3 n_B T \quad , \quad (8.90)$$

where n_B is the number density of baryons, and n_p and n_e are the number densities of protons and electrons, respectively. I assumed also a fully ionized plasma with $n_p = n_e$. As the radiation background particles are decoupled from the fluid they can not support any restoring pressure force and the pressure is given by the thermal pressure of the fluid particles, e.g.

$$p_B = (n_p + n_e) T = 2 n_B T \quad . \quad (8.91)$$

Because, the adiabatic sound velocity in the nonrelativistic fluid [22]

$$c_s = \sqrt{\left(\frac{\partial p}{\partial \rho_B}\right)_S} = \sqrt{2 \frac{5}{3} \frac{T}{m_p}} \quad (8.92)$$

is small, the pressure contribution to the Alfvén velocity can be neglected and it becomes:

$$V_A = \sqrt{\frac{2 \rho_{\text{mag}}}{\rho_B}} = \sqrt{2} \left(\frac{2 \pi^2}{45}\right)^{1/6} \frac{g_S^{2/3}}{g_*^{1/2}} (n r)^{1/2} R_B^{-1/2} \quad , \quad (8.93)$$

where

$$R_B \equiv \frac{3}{4} \frac{\rho_B}{\rho_{\text{rad}}} \quad (8.94)$$

gives the relative importance of the baryonic density to the radiation density. Comparing the expression (8.93) with the definition (8.13) one finds that

$$g_{\text{fl}} = g_* R_B \quad . \quad (8.95)$$

The drag coefficient and heat exchange coefficient are given by [97, 98]:

$$\alpha_\gamma \simeq \frac{4}{3} \frac{1}{l_\gamma} \frac{\rho_\gamma}{\rho_B} = \frac{1}{l_\gamma} \frac{2}{g_*} R_B^{-1} = \frac{4}{3} \frac{\sigma_T \rho_\gamma}{m_p} X_e \quad , \quad (8.96)$$

and

$$\beta_\gamma \simeq \frac{8}{3} \frac{X_e}{1 + X_e} \frac{\sigma_T \rho_\gamma}{m_p} \quad , \quad (8.97)$$

where $\Delta T = T_e - T_\gamma$, and T_e and T_γ are the temperatures of electrons and photons, respectively.

Here, the ratio of the dissipation rate and the Hubble rate during the radiation dominated universe is

$$\frac{\alpha_\gamma}{H} \simeq 4.8 \times 10^3 \left(\frac{T}{\text{eV}}\right)^2 \left(\frac{g_*}{3.36}\right)^{-1/2} X_e \quad , \quad (8.98)$$

where it is assumed that the only relativistic particles are photons and neutrinos. From equation (8.98) it can be seen that, the dissipation by photon dragging is efficient at least until photon freeze-out at $T \approx 0.26 \text{ eV}$ [55], when the universe starts to recombine.

8.5. Damping in the Viscous free streaming regime

The turbulent stage ceases and the system enters the viscous regime when the drag force becomes sufficiently strong. Again, this condition is given by:

$$R_e = \frac{V}{\alpha L} \leq 1 \quad . \quad (8.99)$$

8. Evolution of primordial magnetic fields

As discussed in section 7.2, in the viscous free streaming regime the fluid velocity and the Alfvén velocity are related by

$$V = \frac{V_A^2}{\alpha L} \quad , \quad (8.100)$$

because, the nonlinear fluid interaction (cf. equation (3.79)) becomes negligible when $R_e < 1$. Then, the Reynolds number in terms of the Alfvén velocity is given by:

$$R_e = \left(\frac{V_A}{\alpha L} \right)^2 \quad . \quad (8.101)$$

Damping of magnetic energy occurs on time scales equal to the eddy turnover of the fluid motions L/V which becomes in the strong viscous regime:

$$\tau_{\text{visc.free}} = \frac{\alpha L^2}{V_A^2} \quad . \quad (8.102)$$

As the drag coefficients α decrease with time (see equations (8.83) and (8.96)) the damping time (8.102) decreases with increasing time. This may lead to the effect that the damping at the beginning of neutrino/photon free streaming is very inefficient (i.e. $\tau_{\text{visc.free}} > t_H$), whereas, it becomes efficient at a later stage.

In analogy to the turbulent regime the damping equation in the viscous free streaming regime is:

$$\tau_{\text{visc.free}} = f H^{-1} \quad . \quad (8.103)$$

The following simple arguments show that a MHD system once entering the viscous free streaming regime will never come to a turbulent stage until the free streaming particles decouple from the cosmological evolution, i.e. $l_{\text{mfp}} > H^{-1}$. The condition for turbulence is that the Reynolds number (8.101) becomes much larger than unity. Using the damping equation (8.103) during viscous free streaming the Reynolds number can be estimated:

$$R_e \approx \left(\frac{H}{\alpha} \right) \quad . \quad (8.104)$$

But, the condition for efficient damping by the drag force is $\alpha > H$ which in turn results in a Reynolds number smaller than unity.

Using the Alfvén velocity (8.15) and the initial integral scale (8.38) the dissipation time scale (8.102) can be written as:

$$\tau_{\text{visc.free}} = f^2 \frac{90}{8 \pi^3} \frac{g_{\text{fl}}}{g_{\text{flg}} g_{*g}} \left(\frac{g_{Sg}}{g_S} \right)^2 \left(\frac{M_{\text{Pl}}}{T_g} \right)^2 \left(\frac{L^c}{L_g^c} \right)^{2+n} \frac{\alpha}{T^2} \quad . \quad (8.105)$$

8.5.1. Viscous neutrino free streaming

While the neutrinos are free streaming the damping time (8.102) is

$$\tau_{\text{visc.free}} = f^2 \frac{270 \zeta(3)}{28 \pi^5} \frac{g_{\text{fl}} g_\nu (g_l + g_q)}{g_{\text{flg}} g_* g_{*g}} \left(\frac{g_{Sg}}{g_S} \right)^2 \left(\frac{M_{\text{Pl}}}{T_g} \right)^2 \left(\frac{L^c}{L_g^c} \right)^{2+n} G_{\text{F}}^2 T^3 \quad (8.106)$$

Solving the damping equation (8.103) one can compute the evolution of the co-moving coherence length in the viscous neutrino free streaming regime:

$$L^c = L_g^c \left(\frac{f^{-1} G_{\nu 2}}{G_{\text{F}} M_{\text{Pl}} T_g} \right)^{\frac{1}{2+n}} \left(\frac{T}{T_g} \right)^{-\frac{5}{2+n}} \quad (8.107)$$

where

$$G_{\nu 2} \equiv \frac{49 \pi^7}{405 \zeta(3)} \frac{g_{\text{flg}} g_{*g}}{g_{Sg}^2} g_{\text{fl}}^{-1} \frac{g_S g_*^{1/2}}{g_\nu (g_l + g_q)} \quad (8.108)$$

Together with the definition (8.10) the ratio r evolves as:

$$r = r_g \left(\frac{f^{-1} G_{\nu 2}}{G_{\text{F}} M_{\text{Pl}} T_g} \right)^{-\frac{n}{2+n}} \left(\frac{T}{T_g} \right)^{\frac{5n}{2+n}} \quad (8.109)$$

After the decoupling of neutrinos the drag force is inefficient and the fluid becomes turbulent again.

8.5.2. Viscous photon free streaming

When the photons are free streaming over the fluid they do not contribute to the fluid density and the Alfvén velocity is given by the equation (8.93). Then the damping time (8.105) becomes:

$$\tau_{\text{visc.free}} = f^2 \frac{90}{4\pi^3} \frac{1}{g_{\text{flg}} g_{*g}} \left(\frac{g_{Sg}}{g_S} \right)^2 \left(\frac{M_{\text{Pl}}}{T_g} \right)^2 \left(\frac{L^c}{L_g^c} \right)^{2+n} \frac{\sigma_T n_{B_0} X_e T}{T_0^3} \quad (8.110)$$

The evolution of the comoving coherence length is then given by:

$$L^c = L_g^c \left(G_{\gamma 3} \frac{T_0}{M_{\text{Pl}}} \frac{T_0}{\sigma_T n_{B_0} X_e} \frac{T_0}{T_g} \right)^{\frac{1}{2+n}} \left(\frac{T}{T_g} \right)^{-\frac{3}{2+n}}, \quad (8.111)$$

with

$$G_{\gamma 3} \equiv f^{-1} \frac{\pi^3}{45} \frac{g_{\text{flg}} g_{*g}}{g_{Sg}^2} g_*^{-1/2} g_S^2, \quad (8.112)$$

where radiation domination was assumed for the above expressions. And the magnetic energy is given by:

$$r = r_g \left(G_{\gamma 3} \frac{T_0}{M_{\text{Pl}}} \frac{T_0}{\sigma_T n_{B_0}} \frac{T_0}{X_e T_g} \right)^{-\frac{n}{2+n}} \left(\frac{T}{T_g} \right)^{\frac{3n}{2+n}} \quad (8.113)$$

While the photon mean free path l_γ is smaller than H^{-1} the Reynolds number in the viscous free streaming regime is given by (cf. equations (8.103), (8.101), and (8.96)):

$$R_e = \left(\frac{l_\gamma}{f H^{-1}} \right)^2 \frac{R_B^2}{4 g_*} \quad (8.114)$$

At the beginning of the recombination process in the early universe at $T_{\text{rec}} \simeq 0.31$ eV, the ionization fraction X_e drops very fast from ~ 1 to $\sim 10^{-5}$ until completion of recombination at $T \simeq 0.26$ eV (see e.g. [55]). Therefore, the mean free path of photons increases very rapidly during this epoch and overcomes the Hubble length H^{-1} by a large factor. At the same time the baryonic matter density becomes important, namely:

$$R_B \simeq 3.3 \times 10^{-1} \left(\frac{\Omega_B h^2}{0.0245} \right) \frac{0.3 \text{ eV}}{T} \quad (8.115)$$

Hence, the MHD system becomes turbulent again after recombination.

8.6. Evolution after recombination

Due to the decoupling of photons after recombination, the magnetized fluid becomes turbulent. Then, the evolution of the magnetic field is again given by the damping equation (8.36). During cosmological recombination the universe is already matter dominated and the Hubble parameter is given by [55]:

$$H = \sqrt{\frac{8\pi}{3} \frac{\rho_{\text{matt}}}{M_{\text{pl}}^2}} \propto a^{-3/2} \quad (8.116)$$

As the fluid comprises only nonrelativistic pressure-less baryon and electrons, the Alfvén velocity is (cf. equation (8.93)):

$$V_A \approx \sqrt{\frac{r}{R_B}} \propto a^{-1/2} \quad (8.117)$$

Using the comoving quantities L^c and r in the matter dominated era, the general damping equation in the turbulent regimes, i.e. $L/V_A \approx t$ (cf. section 7.1), becomes:

$$\frac{L^c}{r^{1/2}} \approx t_H R_B^{-1/2} a^{-1} \propto a^0 \quad (8.118)$$

As the r.h.s. of equation (8.118) is constant in time the ratio of the l.h.s. is also not changing in time. Thus, one can infer that the comoving coherence L^c and magnetic energy r remains constant in the matter dominated universe. Apart from equation (8.118) this fact can also be made plausible by inspecting the ratio L/V_A , which is the damping time during turbulence. In the era of matter domination the scaling is $L/V_A \propto a^{3/2}$ which in turn is the same scaling as for the Hubble time t_H , resulting in a constant ratio of the two. Any further dynamical damping, proceeds therefore only through logarithmic growth of the integral scale L^c . In the radiation dominated universe the damping time scales as $L/V_A \propto a$ and the Hubble time scales as $t_H \propto a^2$. This allows additional processing apart from the adiabatic dilution of the magnetic fields and stretching of the coherence length due to the expansion of the universe.

Using the damping equation in the turbulent regime (8.36) and the Hubble parameter in the matter dominated universe (8.116), one obtains the following evolution equation for the comoving coherence length after recombination,

$$L^c = L_g^c \left[\frac{\sqrt{g_{\text{flg}} g_{*g}}}{g_{Sg}} \frac{\Omega_\gamma}{\sqrt{3} \Omega_B \Omega_0} g_{S_0} \ln(a/a_{\text{rec}}) \right]^{\frac{2}{2+n}} \left(\frac{T_g}{T_0} \right)^{\frac{2}{2+n}} \quad (8.119)$$

$$= f (n r_g)^{1/2} G_2 \frac{M_{\text{Pl}}}{T_g} \left(\frac{T_g}{T_0} \right)^{\frac{2}{2+n}} T_0^{-1} \quad (8.120)$$

with

$$G_2 = \left(\frac{2025}{4 \pi^7} \right)^{1/6} \frac{g_{Sg}}{g_{\text{flg}}^{1/2} g_{*g}^{1/2}} g_{S_0}^{-1/3} \left[\frac{\sqrt{g_{\text{flg}} g_{*g}}}{g_{Sg}} \frac{\Omega_\gamma}{\sqrt{3} \Omega_B \Omega_0} g_{S_0} \ln(a/a_{\text{rec}}) \right]^{\frac{2}{2+n}}. \quad (8.121)$$

Here, Ω_γ is the fractional contribution of photons to the critical density at the present epoch and $a_{\text{rec}} \approx 1/1100$ is the scale factor at recombination. The logarithmic correction in the above equation is due to the functional form of the conformal time: $\tilde{t} = H_0^{-1} \ln(a/a_0)$. Then, the relative magnetic energy is

$$r = r_g \left[\frac{\sqrt{g_{\text{flg}} g_{*g}}}{g_{Sg}} \frac{\Omega_\gamma}{\sqrt{3} \Omega_B \Omega_0} g_{S_0} \ln(a/a_{\text{rec}}) \right]^{-\frac{2n}{2+n}} \left(\frac{T_g}{T_0} \right)^{-\frac{2n}{2+n}}. \quad (8.122)$$

8.7. Damping scales

The mean free path l_{mfp} of radiation particles (neutrinos or photons) is a rapidly increasing function of time, i.e. l_{mfp}/l_H is increasing and the wavelengths of all sub-horizon modes are increasing slower than the Hubble length l_H . From the previous section it can be seen that, the comoving coherence lengths L^c of magnetic fields

8. Evolution of primordial magnetic fields

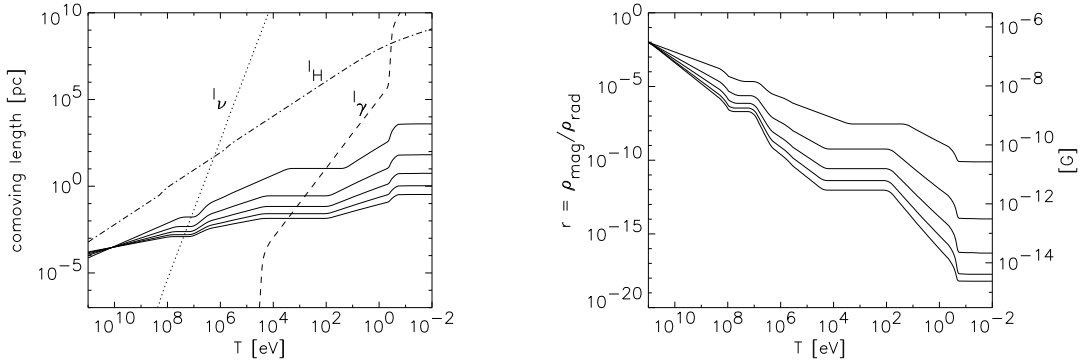


Figure 8.2.: *Left panel:* Evolution of coherence length for different spectral indices n and maximal helical magnetic field (solid lines from top to bottom: max. helical, $n = 2$, $n = 3$, $n = 4$, $n = 5$). *Right panel:* The appropriate magnetic energy r in units of the radiation energy density. A model of magnetogenesis during the electroweak phase transition was assumed.

are not increasing anymore (apart from small logarithmic corrections) after recombination. Hence, it is sufficient to compute the damping scale (coherence length) at the time of recombination. During this epoch, primordial magnetic fields suffer damping in the viscous free streaming regime of photons. Using the damping equation in the viscous free streaming regime (8.102), the photon drag (8.96), and the definition of the Alfvén velocity (8.93), then one obtains for the largest scale which suffers damping in the early universe,

$$L_{\text{damp}} = (n r_{\text{rad}})^{1/2} g_*^{1/2} (l_\gamma t_H)^{1/2} . \quad (8.123)$$

Note, that $d_\gamma \sim (l_\gamma t_H)^{1/2}$ is roughly the diffusion length of photons. In chapter 7 it was already pointed out that, the damping time scales derived in this work coincide with the damping time scales computed in [22]. Hence, it is not surprising that the damping scales coincide as well. In contrast to the Silk damping [24] of density perturbations, the damping scale for magnetic fields depends on the strength of the fields itself. From equation (8.123) it can be seen that initially smaller magnetic fields lead to smaller damping scales.

8.8. Examples

In section, I present some examples to illustrate the general formalism developed in this chapter to calculate the evolution of the energy density and the coherence length of primordial magnetic fields. For these examples it was assumed that the magnetic fields were generated during electroweak phase transition (i.e. at $T \sim 100$ GeV) and QCD phase transition (i.e. at $T \sim 100$ MeV), respectively. Furthermore, the initial

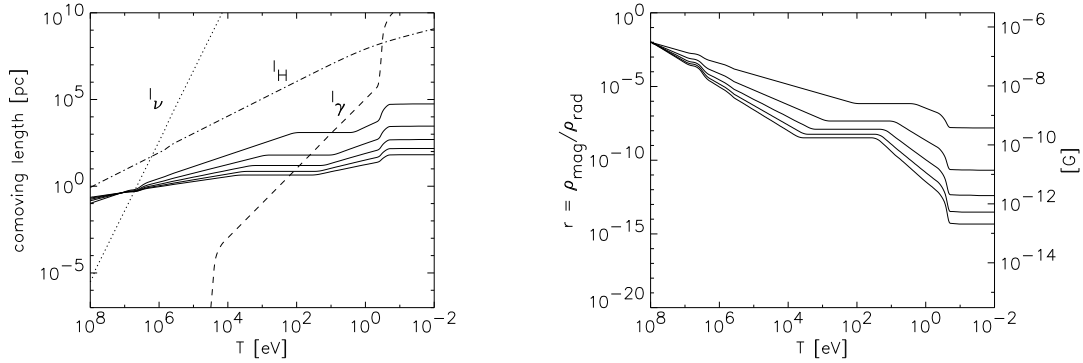


Figure 8.3.: Similar figures than 8.2. Here, a model of magnetogenesis during the QCD phase transition was assumed.

magnetic energy density was set to one percent of the energy density of radiation, i.e. $r_{\text{rad}}(T_g) = 0.01$. The results of these examples are summarized in the figures 8.2 and 8.3 and the table 8.8. These examples show the magnetic energy density in terms of the energy density of radiation, the magnetic field strength, and the coherence length of the magnetic fields scaled to the present epoch, respectively.

configuration	T_g [GeV]	r_{rad}	B_0 [G]	L^c [pc]
max. helical	100	7.5×10^{-11}	2.6×10^{-11}	4.0×10^3
$n = 2$	100	1.0×10^{-14}	3.1×10^{-13}	65.4
$n = 3$	100	5.0×10^{-17}	2.1×10^{-14}	5.5
$n = 4$	100	1.4×10^{-18}	3.5×10^{-15}	1.1
$n = 5$	100	1.2×10^{-19}	1.0×10^{-15}	0.3
max. helical	0.1	1.5×10^{-8}	3.7×10^{-10}	5.7×10^4
$n = 2$	0.1	2.1×10^{-11}	1.4×10^{-11}	2.9×10^3
$n = 3$	0.1	4.0×10^{-13}	1.9×10^{-12}	4.9×10^2
$n = 4$	0.1	2.7×10^{-14}	5.0×10^{-13}	1.5×10^2
$n = 5$	0.1	4.2×10^{-15}	1.9×10^{-13}	66.8

Table 8.1.: Final values of the magnetic field strength and the coherence length at the present epoch for different magnetic field configurations: maximal helical magnetic fields and non-helical fields with energy spectra $E_k \propto k^n$.

9. Summary and conclusions

In this work, I studied the evolution of potentially existing primordial magnetic fields in the early universe starting from the time shortly after their generation until the onset of structure formation. The focus of this work is to trace the fate of such magnetic fields and to calculate their energy density and coherence length of these magnetic fields at the present epoch, where these depend on several initial conditions such as the temperature of the universe at magnetogenesis, the magnetic field spectra, and the amount of magnetic helicity. With this information in hand, one can, for example, predict present-day values of magnetic energy and coherence length for certain models of magnetogenesis. Such a comprehensive prediction, which properly takes into account the dynamics of the magnetic fields, has so far not yet been accomplished in the literature. For this purpose, the fully nonlinear MHD equations were solved numerically using the three dimensional MHD solver ZEUS3D which was adapted to investigate the evolution of stochastic, primordial magnetic fields. Results of these numerical simulations were then employed to derive analytic expressions for the temperature dependence of the global quantities such as the total magnetic energy density and the magnetic field coherence length.

It has been shown that magnetic fields are not only diminished by the adiabatic expansion of the universe, but also suffer substantial dynamical damping due to their interactions with the fluid. In the case of solely adiabatic dilution, the ratio of the magnetic and radiation energy densities would remain (nearly) constant. The dynamical dissipation of magnetic energy is an indirect process via excitations of velocity perturbations in the fluid. This is due to the large electrical conductivity (small resistivity) in the early universe which prevents magnetic fields from direct dissipation by Ohmic resistance. Indicators of this situation are the large Prandtl numbers in the early universe. The time scale for dynamical magnetic energy dissipation is governed by the eddy turnover time of fluid eddies at the integral scale (resp. coherence length).

In the early universe, one can distinguish different damping regimes. In the turbulent regime, indicated by a large Reynolds number, one expects equipartition of kinetic and magnetic energy. The energy dissipation occurs through successive cascading of energy from larger to smaller scales (direct cascade), where it is finally dissipated into heat at a very small dissipation scale l_{diss} . The time scale of energy loss in the turbulent regime is independent of the underlying micro-physics which

causes the energy dissipation into heat. In fact, the damping time is only a function of the magnetic field properties at the integral scale.

While the mean free paths of the radiation background particles (i.e. neutrinos and photons) are smaller than the coherence length of the magnetic field, the energy dissipation is due to diffusion processes. In the viscous diffusion regime, where the Reynolds numbers are smaller than unity, fluid motions are strongly suppressed and existing velocity fluctuations are damped very quickly. This is also due to the fact that the effective viscosities, caused by neutrino or photon interactions with the magnetized fluid, are increasing while the universe is cooling down. Moreover, this implies that magnetic fields are not able to excite further velocity fluctuations. The small fluid velocity implies a long dissipation time scale for the magnetic energy dissipation, which in fact is larger than the Hubble time. This prevents further damping of magnetic fields in the viscous diffusion regime.

In the expanding universe the mean free paths of neutrinos and photons are increasing faster than the coherence length of the magnetic field. In the cases where the mean free paths exceed the coherence length, neutrinos and photons are free streaming over the fluid fluctuations. In contrast to the diffusion regime, where the dissipation time scale increases with decreasing temperature, in the free streaming regime the dissipation time scale decreases with decreasing temperature. The damping time scale, which is usually much larger than the Hubble time at the beginning of the free streaming era, will eventually become smaller than the Hubble time. Thus, after the background radiation particles start to free stream over the fluid fluctuations, magnetic energy dissipation at first inefficient but may become operative after a while. It should be stressed that in this case effective magnetic energy dissipation takes place even in the case of fluid flows with Reynolds numbers substantially smaller than unity. The epoch of viscous free streaming lasts until neutrinos or photons freeze out entirely from the evolution of the universe. Afterwards, the fluid will become turbulent again because its interaction rate with the background radiation is then small.

At the time of photon freeze-out (around the time of cosmological recombination) the universe is already matter dominated. Due to the change of the equation of state from the radiation to the matter dominated era, the dependence of the Hubble time and eddy turnover time on the scale factor a changes. In fact, now both times depend in the same way on the scale factor a . This prevents (apart from logarithmic corrections) any further dynamical damping of the magnetic energy after photon decoupling.

Apart from the different damping regimes, I could also demonstrate that the evolution of the cosmic magnetic fields depends on its internal structure. The slope of the magnetic field spectra, characterized by the spectral index n , determines the final damping law of the magnetic energy density. Steeper spectra result in a faster dissipation of the magnetic energy. If the initial fields possess non-vanishing helicity the dissipation occurs more slowly because the conservation of the helicity impedes

rapid damping. Furthermore, in this case energy is not only transferred to smaller length scales, where it is dissipated, but also to larger scales (*inverse cascade*) which leads to the dynamical increase of the coherence length.

In this work, I also applied the general findings of the evolution of primordial magnetic fields to specific models of magnetogenesis. For the considered models it was assumed that the magnetic fields were generated by a causal process (e.g. a phase transition) during a stage of small kinetic viscosity. For instance, models of magnetogenesis around the electroweak phase transition ($T \sim 100 \text{ GeV}$) with initially one percent of the total energy density in magnetic fields and a spectral index $n = 3$, as emergent in models of randomly spherical magnetic “bubbles”, result in a coherence length of $L \sim 5 \text{ pc}$ and a magnetic field strength of $B \sim 2 \times 10^{-14} \text{ G}$ at the present epoch. The same model with initially maximal helical magnetic fields gives a coherence length of $L \sim 4 \text{ kpc}$ and a field strength of $B \sim 2.6 \times 10^{-11} \text{ G}$. When the magnetic fields were generated during the QCD phase transition ($T \sim 100 \text{ MeV}$) the coherence length and the magnetic field strength would be for a maximal helical field (for a non-helical field with $n = 3$) $L \sim 57 \text{ kpc}$ ($L \sim 0.5 \text{ kpc}$) and $B \sim 3.7 \times 10^{-10} \text{ G}$ ($B \sim 1.9 \times 10^{-12} \text{ G}$), respectively. Especially in the case of helical magnetic fields one could explain the observed field strength of the order of μG in galaxy clusters, where primordial magnetic fields of the order of $B \sim 10^{-11} \text{ G}$ are enhanced by adiabatic compression and shear flows during the gravitational collapse of primordial gas clouds.

Although, the primordial magnetic fields suffer a substantial damping during the evolution of the early universe, for a wide class of magnetogenesis models the magnetic field strength will be sufficient to seed a galactic dynamo where field strengths of $B \sim 10^{-20} \text{ G}$ could be strong enough.

9. Summary and conclusions

A. Appendix

A.1. Notations for the FRW universe

In this work greek indices take the values 0, 1, 2, 3 and Einstein's summation convention is assumed.

The symmetrization operator is defined by

$$X^{(\mu_1\mu_2\dots\mu_n)} \equiv \frac{1}{n!} (X^{\mu_1\mu_2\dots\mu_n} + \text{sum over all permutations}) \quad (\text{A.1})$$

and the anti-symmetrization operator by

$$X^{[\mu_1\mu_2\dots\mu_n]} \equiv \frac{1}{n!} (X^{\mu_1\mu_2\dots\mu_n} + \text{sum over all permutations with index } \pm 1) . \quad (\text{A.2})$$

Here, the total antisymmetric Levi-Civita tensor has the entry

$$\epsilon^{0123} = +1 \quad . \quad (\text{A.3})$$

The matrix $\Lambda^\mu{}_\nu = \partial x^\mu / \partial x'^\nu$ which transforms tensors from Minkowski space with the metric

$$g'_{\mu\nu} = \text{diag}(1, -1, -1, -1) \quad (\text{A.4})$$

to the FRW metric

$$g_{\mu\nu} = \text{diag}(1, -a^2, -a^2, -a^2) \quad (\text{A.5})$$

is given by

$$\Lambda^\mu{}_\nu = \text{diag}(1, 1/a, 1/a, 1/a) \quad . \quad (\text{A.6})$$

The non-vanishing Christoffel symbols $\Gamma^\alpha_{\beta\gamma}$ of second kind for the metric (A.5) are

$$\begin{aligned} \Gamma_{01}^1 &= \Gamma_{02}^2 = \Gamma_{03}^3 = H \\ \Gamma_{10}^1 &= \Gamma_{20}^2 = \Gamma_{30}^3 = H \\ \Gamma_{11}^0 &= \Gamma_{22}^0 = \Gamma_{33}^0 = a \dot{a} \end{aligned} \quad (\text{A.7})$$

and the covariant derivatives are given by [79]

$$X_{;\mu} = X_{,\mu} \equiv \frac{\partial X}{\partial x^\mu} \quad , \quad (\text{A.8})$$

$$X^\mu{}_{;\nu} \equiv \frac{\partial X^\mu}{\partial x^\nu} + \Gamma^\mu_{\lambda\nu} X^\lambda \quad , \quad (\text{A.9})$$

$$X^{\mu\nu}{}_{;\lambda} \equiv \frac{\partial X^{\mu\nu}}{\partial x^\lambda} + \Gamma^\mu_{\gamma\lambda} X^{\gamma\nu} + \Gamma^\nu_{\gamma\lambda} X^{\mu\gamma} \quad , \quad (\text{A.10})$$

where X , X^μ and $X^{\mu\nu}$ are a scalar, a 4-vector, and a contravariant tensor of rank two, respectively.

The electromagnetic field-strength tensor is explicitly given by

$$F^{\mu\nu} = \begin{pmatrix} 0 & E_x/a & E_y/a & E_z/a \\ -E_x/a & 0 & B_z/a^2 & -B_y/a^2 \\ -E_y/a & -B_z/a^2 & 0 & B_x/a^2 \\ -E_z/a & B_y/a^2 & -B_x/a^2 & 0 \end{pmatrix}. \quad (\text{A.11})$$

The covariant derivative of any 4-vector $b^\mu = (b_0, b_x, b_y, b_z) \equiv (b_0, \mathbf{b})$ in the coordinate system with the metric (A.5) reads

$$b^\mu{}_{;\nu} = \begin{pmatrix} \partial_t b_0 & \partial_x b_0 + a\dot{a} b_x & \partial_y b_0 + a\dot{a} b_y & \partial_z b_0 + a\dot{a} b_z \\ \partial_t b_x + H b_x & \partial_x b_x + H b_0 & \partial_y b_x & \partial_z b_x \\ \partial_t b_y + H b_y & \partial_x b_y & \partial_y b_y + H b_0 & \partial_z b_y \\ \partial_t b_z + H b_z & \partial_x b_z & \partial_y b_z & \partial_z b_z + H b_0 \end{pmatrix} \quad (\text{A.12})$$

The generalized convective derivative

$$\dot{b}^\mu \equiv b^\mu{}_{;\nu} u^\nu \quad (\text{A.13})$$

with the 4-velocity $u^\mu \equiv (u_0, \mathbf{u})$ is explicitly given by:

$$\dot{b}^\mu = \begin{pmatrix} (u_0 \partial_t + \mathbf{u} \cdot \nabla) b_0 & + & a\dot{a} \mathbf{u} \cdot \mathbf{b} \\ (u_0 \partial_t + \mathbf{u} \cdot \nabla) \mathbf{b} & + & H (u_0 \mathbf{b} + \mathbf{u} b_0) \end{pmatrix}. \quad (\text{A.14})$$

The covariant divergence is

$$b^\mu{}_{;\mu} = \partial_t b_0 + \nabla \cdot \mathbf{b} + 3 H b_0 \quad (\text{A.15})$$

General relations to compute the total energy-momentum tensor $T^{\mu\nu} = T_{\text{fluid}}^{\mu\nu} + T_{\text{em}}^{\mu\nu}$ and its derivatives:

$$P^{\mu\nu} \equiv g^{\mu\nu} - u^\mu u^\nu \quad (\text{A.16})$$

$$\sigma^{\mu\nu} \equiv \frac{1}{2} \left(P^\nu{}_\lambda u^{\mu;\lambda} + P^\mu{}_\lambda u^{\nu;\lambda} \right) - \frac{\Theta}{3} P^{\mu\nu} \quad (\text{A.17})$$

$$\omega^{\mu\nu} \equiv \frac{1}{2} \left(P^\nu{}_\lambda u^{\mu;\lambda} - P^\mu{}_\lambda u^{\nu;\lambda} \right) \quad (\text{A.18})$$

$$\Theta \equiv u^\mu{}_{;\mu} \quad (\text{A.19})$$

$$q^\mu \equiv P^\mu{}_\nu (T^{\nu}{}_{;\nu} + T \dot{u}^\nu) \quad (\text{A.20})$$

$$u^\mu{}_{;\nu} = \sigma^\mu{}_\nu + \omega^\mu{}_\nu + \frac{\Theta}{3} P^\mu{}_\nu + \dot{u}^\mu u_\nu \quad (\text{A.21})$$

$$\dot{u}_\nu E^\nu + u_\nu \dot{E}^\nu = 0 \quad (\text{A.22})$$

$$\dot{u}_\nu B^\nu + u_\nu \dot{B}^\nu = 0 \quad (\text{A.23})$$

$$\omega^{\mu\nu} = \epsilon^{\mu\nu\lambda\gamma} u_\lambda \omega_\gamma \quad (\text{A.24})$$

$$\epsilon^{\mu\nu\lambda\gamma} u_{\mu;\nu} = \epsilon^{\mu\nu\lambda\gamma} (\omega_{\mu\nu} + \dot{u}_\mu u_\nu) \quad (\text{A.25})$$

$$\epsilon^{\mu\nu\lambda\gamma} u_{\mu;\nu} u_\lambda = \epsilon^{\mu\nu\lambda\gamma} \omega_{\mu\nu} u_\lambda = 2 \omega^\gamma \quad (\text{A.26})$$

In the small velocity approximation the 4-velocity in the FRW universe can be written as

$$u^\mu \approx (1, \mathbf{v}/a) \quad , \quad (\text{A.27})$$

where $|\mathbf{v}| \ll 1$. The components of the electric and magnetic field are given by

$$E^\mu = \Lambda^\mu{}_\nu E'^\nu = (0, \mathbf{E}/a) \quad , \quad (\text{A.28})$$

$$B^\mu = \Lambda^\mu{}_\nu B'^\nu = (0, \mathbf{B}/a) \quad . \quad (\text{A.29})$$

From these the following relations result (where only terms to the highest order in $|\mathbf{v}|$ and H are kept):

$$P^{\mu\nu} \approx \begin{pmatrix} 0 & -v_x/a & -v_y/a & -v_z/a \\ -v_x/a & -1/a^2 & 0 & 0 \\ -v_y/a & 0 & -1/a^2 & 0 \\ -v_z/a & 0 & 0 & -1/a^2 \end{pmatrix} \quad , \quad (\text{A.30})$$

$$u^\mu{}_{;\nu} \approx \frac{1}{a} \begin{pmatrix} 0 & a^2 H v_x & a^2 H v_y & a^2 H v_z \\ \partial_t v_x & a H + \partial_x v_x & \partial_y v_x & \partial_z v_x \\ \partial_t v_y & \partial_x v_y & a H + \partial_y v_y & \partial_z v_y \\ \partial_t v_z & \partial_x v_z & \partial_y v_z & a H + \partial_z v_z \end{pmatrix} \quad , \quad (\text{A.31})$$

$$u^\mu{}_{;\mu} = \Theta \approx 3H + \frac{1}{a} (\nabla \cdot \mathbf{v}) \quad , \quad (\text{A.32})$$

$$P^\mu{}_\nu p^\nu \approx \begin{pmatrix} -a^{-1} (\mathbf{v} \cdot \nabla) p \\ -a^{-1} \mathbf{v} \partial_t p - a^{-2} \nabla p \end{pmatrix} \quad (\text{A.33})$$

$$P^\mu{}_\nu \dot{u}^\nu \approx \frac{1}{a} \left(\frac{\partial}{\partial t} + \frac{1}{a} (\mathbf{v} \cdot \nabla) + H \right) \mathbf{v} \quad , \quad (\text{A.34})$$

$$P^\mu{}_\nu q^\nu = \mathbf{q} \approx \frac{1}{a^2} \left(\mathbf{v} \frac{\partial T}{\partial t} - \nabla T \right) + \frac{1}{a} T \left(\frac{\partial}{\partial t} + \frac{1}{a} (\mathbf{v} \cdot \nabla) + H \right) \mathbf{v} \quad , \quad (\text{A.35})$$

$$P^\mu{}_\nu E^\nu{}_{;\mu} = \frac{1}{a} \nabla \cdot \mathbf{E} \quad , \quad (\text{A.36})$$

$$P^\mu{}_\nu \dot{E}^\nu \approx \frac{1}{a} \left(\frac{\partial}{\partial t} + \frac{1}{a} (\mathbf{v} \cdot \nabla) \right) \mathbf{E} \quad , \quad (\text{A.37})$$

$$\left(\sigma^{\mu\nu} + \omega^{\mu\nu} - \frac{2}{3} \Theta P^{\mu\nu} \right) E_\nu \approx \frac{1}{a^2} (\mathbf{E} \cdot \nabla) \mathbf{v} - \frac{1}{a^2} \mathbf{E} (\nabla \cdot \mathbf{v}) - \frac{1}{a} 2H \mathbf{E} \quad , \quad (\text{A.38})$$

$$P^\mu{}_\nu \epsilon^{\mu\lambda\gamma\sigma} (u_\lambda E_{\gamma;\sigma} - E_\lambda u_{\gamma;\sigma}) \approx \frac{1}{a^2} \nabla \times \mathbf{E} + \frac{1}{a} \left(\frac{\partial}{\partial t} + 2H \right) (\mathbf{v} \times \mathbf{E}) \quad , \quad (\text{A.39})$$

$$\begin{aligned}
u_\mu (\Theta P^{\mu\nu})_{;\nu} &= -\Theta^2 \\
&\approx -\frac{1}{a^2} (\nabla \cdot \mathbf{v})^2 - \frac{6}{a} H (\nabla \cdot \mathbf{v}) - 9H^2 \quad , \quad (\text{A.40})
\end{aligned}$$

$$\begin{aligned}
P^\mu_\gamma (\Theta P^{\gamma\nu})_{;\nu} &= -P^\mu_\nu (\Theta \dot{u}^\nu - \Theta^{,\nu}) \\
&\approx -\frac{1}{a} \left(3H + \frac{1}{a} (\nabla \cdot \mathbf{v}) \right) \left(\frac{\partial}{\partial t} + \frac{1}{a} (\mathbf{v} \cdot \nabla) + H \right) \mathbf{v} \\
&\quad - \frac{1}{a^3} \nabla (\nabla \cdot \mathbf{v}) \quad , \quad (\text{A.41})
\end{aligned}$$

$$\begin{aligned}
u_{\mu;\nu} u^{\mu;\nu} + u_{\mu;\nu} u^{\nu;\mu} &\approx - \left| \frac{\partial \mathbf{v}}{\partial t} \right|^2 + 2H \frac{\partial \mathbf{v}}{\partial t} \cdot \mathbf{v} - \frac{1}{a^2} \mathbf{v} \cdot (\nabla^2 \mathbf{v}) \\
&\quad - \frac{1}{a^2} |\nabla \times \mathbf{v}|^2 + 4 \frac{H}{a} (\nabla \cdot \mathbf{v}) + 6H^2 \quad , \quad (\text{A.42})
\end{aligned}$$

$$\begin{aligned}
2 u_\mu \sigma^{\mu\nu}_{;\nu} &= (\dot{u}_\mu \dot{u}^\mu - u_{\mu;\nu} u^{\mu;\nu} - u_{\mu;\nu} u^{\nu;\mu}) + \frac{2}{3} \Theta^2 \\
&\approx -2 \frac{\partial \mathbf{v}}{\partial t} \left(2H + \frac{1}{a} (\mathbf{v} \cdot \nabla) \right) \mathbf{v} + \frac{1}{a^2} \mathbf{v} \cdot (\nabla^2 \mathbf{v}) \\
&\quad + \frac{1}{a^2} |\nabla \times \mathbf{v}|^2 + \frac{2}{3} \frac{(\nabla \cdot \mathbf{v})^2}{a^2} \quad , \quad (\text{A.43})
\end{aligned}$$

$$\begin{aligned}
2 P^\mu_\lambda \sigma^{\lambda\nu}_{;\nu} &= P^\mu_\gamma \left(u^{\gamma;\nu}_{;\nu} - \ddot{u}^\gamma - \frac{1}{3} \Theta \dot{u}^\gamma - \frac{1}{3} \Theta^{,\gamma} - u^{\gamma;\nu} \dot{u}^\nu - u^{\gamma\nu} \dot{u}^\nu_{;\nu} \right) \\
&\approx -\frac{1}{a^3} \left(\nabla^2 \mathbf{v} + \frac{1}{3} \nabla (\nabla \cdot \mathbf{v}) \right) \quad , \quad (\text{A.44})
\end{aligned}$$

$$\begin{aligned}
2 u_\mu \left(u^{(\mu} q^{\nu)} \right)_{;\nu} &= q^\mu_{;\mu} + u_\mu \dot{q}^\mu + \Theta u_\mu q^\mu \\
&\approx \nabla \cdot \mathbf{q} - a \mathbf{v} \left(\frac{\partial}{\partial t} + \frac{1}{a} (\mathbf{v} \cdot \nabla) + 3H \right) \mathbf{q} \quad , \quad (\text{A.45})
\end{aligned}$$

$$\begin{aligned}
2 P^\mu_\lambda \left(u^{(\lambda} q^{\nu)} \right)_{;\nu} &= u^\mu_{;\nu} q^\nu + P^\mu_\nu (\Theta q^\nu + \dot{q}^\nu) \\
&\approx \left(\frac{\partial}{\partial t} + 5H + \frac{1}{a} (\mathbf{v} \cdot \nabla) \right) \mathbf{q} + \frac{1}{a} (\mathbf{q} \cdot \nabla) \mathbf{v} \\
&\quad + \frac{1}{a} \mathbf{q} (\nabla \cdot \mathbf{v}) \quad . \quad (\text{A.46})
\end{aligned}$$

A.2. Conventions for Fourier transformations

In this work I use the following conventions for Fourier transformations

$$\Phi(\mathbf{x}) = \frac{1}{(2\pi)^3} \int d^3k \hat{\Phi}_{\mathbf{k}} e^{-i\mathbf{k}\cdot\mathbf{x}} \quad (\text{A.47})$$

with

$$\hat{\Phi}_{\mathbf{k}} = \int d^3k \Phi(\mathbf{x}) e^{i\mathbf{k}\cdot\mathbf{x}} \quad . \quad (\text{A.48})$$

Quantities evaluated at a certain length scale $l = 2\pi/k$ and averaged over the solid angle $d\Omega$ are defined by

$$\Phi_l \equiv (2\pi)^{-3/2} \sqrt{k^3 \Phi_k^2} \quad (\text{A.49})$$

where

$$\Phi_k^2 = \langle \Phi_{\mathbf{k}}^2 \rangle \equiv \int d\Omega_k \Phi_{\mathbf{k}}^2 \quad , \quad (\text{A.50})$$

and $k = |\mathbf{k}|$.

In this work I use isotropic one dimensional magnetic energy spectra E_k defined by

$$E_k \equiv \frac{1}{2} \frac{k^3}{(2\pi)^3} \langle |\hat{\mathbf{B}}_{\mathbf{k}}|^2 \rangle = \frac{1}{2} \frac{k^3}{(2\pi)^3} \int d\Omega_k |\hat{\mathbf{B}}_{\mathbf{k}}|^2 \quad , \quad (\text{A.51})$$

which has the same dimension than the total energy

$$E = \frac{1}{2} \int d^3x \mathbf{B}^2(\mathbf{x}) = \frac{1}{2} \int d \ln k E_k \quad . \quad (\text{A.52})$$

The solid angle element in k -space is given by $d\Omega_k = d \cos \theta_k d\varphi_k$.

A.3. Numerical method

With the help of numerical simulations, I was able to study the evolution of a non-linear MHD system in different damping regimes. For this purpose, I used the MHD solver ZEUS3D* [32, 33, 34] developed at the National Center for Supercomputing Applications (NCSA). This code is a three dimensional ideal (non-resistive, non-viscous, adiabatic) magnetohydrodynamical (MHD) fluid equation solver for non-relativistic fluid velocities. It integrates the following coupled partial differential equations as a function of time and space:

$$\frac{\partial \rho}{\partial t} + \nabla \cdot (\mathbf{v} \rho) = 0 \quad (\text{A.53})$$

$$\frac{\partial \mathbf{v}}{\partial t} + (\mathbf{v} \cdot \nabla) \mathbf{v} = -\frac{1}{\rho} \nabla p - \frac{\mathbf{B} \times (\nabla \times \mathbf{B})}{\rho} - \nabla \Phi \quad (\text{A.54})$$

$$\frac{\partial e}{\partial t} + \nabla \cdot (\mathbf{v} e) = -p \nabla \cdot \mathbf{v} \quad (\text{A.55})$$

$$\frac{\partial \mathbf{B}}{\partial t} = \nabla \times (\mathbf{v} \times \mathbf{B}) \quad (\text{A.56})$$

$$\Delta \Phi = 4\pi \rho \quad , \quad (\text{A.57})$$

where ρ , \mathbf{v} , p , \mathbf{B} , Φ , and e are the matter density, fluid velocity, thermal pressure, magnetic field[†], gravitational potential, and internal energy, respectively.

*Informations and the code to download are available from the Laboratory for Computational Astrophysics (LCA) at http://zeus.ncsa.uiuc.edu/lca_intro_zeus3d.html.

[†]The magnetic field used by ZEUS3D differs by a factor $1/\sqrt{4\pi}$ from the convention I used within this work. Hence, the magnetic energy density using ZEUS3D units is just $\rho_{\text{mag}} = B^2/2$.

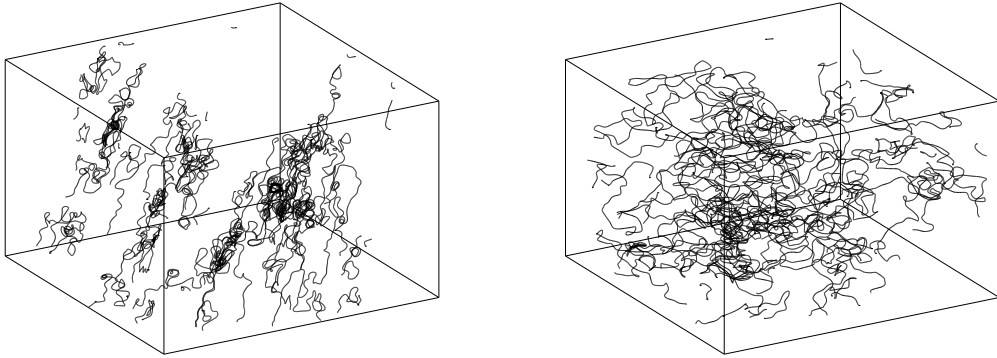


Figure A.1.: Magnetic field lines for a magnetic field in a simulation box with 256^3 grid points with the cut-off $k_c \approx 16$. The *left panel* shows a magnetic field with zero helicity and the *right panel* shows a magnetic field with maximal helicity. The non-helical field is much more clumpy than the helical one.

To close the above coupled set of differential equations the ZEUS3D code relates the thermal pressure p and the internal energy density e by an adiabatic equation of state for an ideal gas:

$$p = (\gamma - 1) e \quad , \quad (\text{A.58})$$

where γ is the adiabatic index. It is also possible to an isothermal equation of state, where the pressure p is related to the matter density ρ by the constant and uniform sound speed c_s :

$$c_s^2 = \frac{p}{\rho} \quad . \quad (\text{A.59})$$

In this case, which I used for the purpose of this work, the equation (A.55) does not need to be solved.

The MHD equations (A.53) through (A.57) are solved on a fully staggered Eulerian grid in real space, with the scalars (ρ , p and e) zone centered, the vector components (\mathbf{v} and \mathbf{B}) face centered, and the derived vector components ($\nabla \times \mathbf{B}$ and $\nabla \times (\mathbf{v} \times \mathbf{B})$) edge centered. All simulation runs were performed with periodic boundary conditions. This mimics an infinitely large volume, where the surface integrals of the MHD variables around the entire box vanish exactly.

Although, the code is strictly Newtonian and nonrelativistic it is sufficient to study the evolution of a magnetized fluid in the early universe, due to the conformal invariance of the MHD equations during the radiation dominated epoch and due to the approximately conformal invariance during the matter dominated epoch (cf. chapter 3). Furthermore, the considered velocity fluctuations are small compared to the speed of light (which is certainly the case in the early universe), for which it is sufficient to study the incompressible limit. Thus, the Newtonian treatment for nonrelativistic fluid velocities is adequate for the purpose of this work.

The code ZEUS3D had to be extended and adapted for several reasons. First of all, the simulations should start with the desired **initial conditions**[‡] for the magnetic field, the velocity fluctuations, and the matter density. For all simulations, I used a Gaussian random field for the initial fluctuations of the magnetic components with *zero mean*. To ensure a divergence-free magnetic field this is done by exciting modes of the vector potential $\hat{\mathbf{A}}_{\mathbf{k}}$ in k -space in the following way: The complex vector potential $\hat{\mathbf{A}}_{\mathbf{k}} = (\hat{A}_{\mathbf{k}}^1, \hat{A}_{\mathbf{k}}^2, \hat{A}_{\mathbf{k}}^3)$ is generated by

$$\hat{A}_{\mathbf{k}}^i = |\hat{A}_{\mathbf{k}}^i| e^{i\varphi_{\mathbf{k}}} \quad i \in [1, 2, 3] \quad , \quad (\text{A.60})$$

where the amplitudes $|\hat{A}_{\mathbf{k}}^i|$ are randomly selected using a Gaussian distribution, i.e.

$$P(|\hat{A}_{\mathbf{k}}^i|) = \frac{1}{\sqrt{2\pi} \sigma_{\mathbf{k}}} \exp\left\{-\frac{|\hat{A}_{\mathbf{k}}^i|^2}{2\sigma_{\mathbf{k}}^2}\right\} \quad , \quad (\text{A.61})$$

and the phases $\varphi_{\mathbf{k}}$ are randomly selected with a uniform distribution from the interval $[0, 2\pi]$. The amplitudes are also related to the variance $\sigma_{\mathbf{k}}$ by

$$|\hat{A}_{\mathbf{k}}^i|^2 \propto \sigma_{\mathbf{k}}^2 \propto k^n \quad , \quad (\text{A.62})$$

where I assumed an isotropic universe, i.e. $\hat{A}_{\mathbf{k}}^i = \hat{A}_k^i$. Furthermore, I did not excite all available modes in the grid, but used a cut-off k_c up to which modes were excited.

The initial magnetic field in real space $\mathbf{B}(\mathbf{x})$, which is used by the ZEUS3D code, can be easily computed from the vector potential (A.60) by first computing $\mathbf{A}(\mathbf{x})$ using a Fast Fourier Transformation (FFT) and second using the relation $\mathbf{B}(\mathbf{x}) = \nabla \times \mathbf{A}(\mathbf{x})$. I normalized the magnetic field using its *rms* value, i.e.

$$\left[\frac{1}{V} \int dx^3 \mathbf{B}^2(\mathbf{x})\right]^{\frac{1}{2}} = B_0 \quad , \quad (\text{A.63})$$

where V is the volume of the simulation box. Note, that the mean value of the magnetic field was zero, i.e. $V^{-1} \int dx^3 \mathbf{B} = 0$, for all simulations with a stochastic initial field. To excite helical magnetic fields, I use a proper coordinate system in k -space which is described in chapter 4. In figure A.1 magnetic field lines of an initial helical and non-helical magnetic field is shown.

The initial stochastic velocity field is generated in the same way as the initial magnetic field described above. In addition one can either generate the stochastic velocity field \mathbf{v} by using equation (A.61) directly, or one can generate a *divergence-free* velocity field by first exciting a vector potential \mathbf{A} and then computing $\mathbf{v} = \nabla \times \mathbf{A}$. The latter avoids strong density perturbations. For the study of the incompressible MHD evolution it is sufficient to use a homogeneous initial density field ρ .

I checked the correctness of these implementations of the initial conditions firstly by comparing the spectra of the magnetic and kinetic energy after exciting the modes

[‡]This was partially done in [87] for magnetic fields without a specific helicity.

at the Eulerian grid with the theoretically expected one (cf. equation (A.62)). And secondly, by inspecting the magnetic helicity. As the spectrum and the magnitude of the magnetic helicity is initially known (cf. chapter 4) it can be compared with the numerical values which one gets out of the simulation box. Additionally, I verified whether the mean value and the divergence of the magnetic field are really zero, at least up to numerical accuracy.

Furthermore, because the ZEUS3D code is an *ideal* MHD solver, dissipation terms had to be implemented to account for dissipation in the diffusion and free streaming regimes. This is realized by adding additional “source” terms on the r. h. s. of the Euler equation (A.54). In the diffusion regime the modified Euler equation becomes:

$$\frac{\partial \mathbf{v}}{\partial t} + (\mathbf{v} \cdot \nabla) \mathbf{v} = -\frac{1}{\rho} \nabla p - \frac{\mathbf{B} \times (\nabla \times \mathbf{B})}{\rho} + \nu \nabla^2 \mathbf{v} \quad (\text{A.64})$$

and in the free streaming regime it is:

$$\frac{\partial \mathbf{v}}{\partial t} + (\mathbf{v} \cdot \nabla) \mathbf{v} = -\frac{1}{\rho} \nabla p - \frac{\mathbf{B} \times (\nabla \times \mathbf{B})}{\rho} - \alpha \mathbf{v} \quad (\text{A.65})$$

Whereas the diffusion coefficient η and the Compton drag α may be time dependent but are homogeneous in space. I tested the correctness of the above modifications to the code in the linear regime (see chapter 5), where analytic solutions are known which in turn can be compared with the numerical results.

The simulations were performed on the vector supercomputers Cray J90 and NEC SX-5 where grids with maximal 512^3 grid points could be used. But, to get reasonable results within reasonable time scales (e.g. $\mathcal{O}(1)$ days) I used mainly resolutions with 128 and 256^3 grid points. Results of 128^3 simulations are shown in figures A.2 and A.3, where 2D slices of the magnetic field strength for different time steps are plotted.

Units

As already mentioned in chapter 6, an incompressible MHD system possesses only *two* independent dimensions (the constant density ρ is set to unity). In this work, one is associated with the velocity V and the other fundamental dimensional quantity is the length L . According to this convention the kinetic and magnetic energy density are given by

$$E_{\text{kin}} = \frac{1}{2} v^2 \quad , \quad (\text{A.66})$$

$$E_{\text{mag}} = \frac{1}{2} v_A^2 \quad , \quad (\text{A.67})$$

where v and v_A are the *rms* values of the fluid velocity and the Alfvén velocity, respectively.

The other important quantity in the MHD system is the evolution time t . Its dimension T is build up by the two fundamental ones, i.e. $T = L/V$. Because, the simulation box size L_{box} is fixed and set to unity,

$$L_{\text{box}} \equiv 1 \quad , \quad (\text{A.68})$$

the evolution time t depends on the velocities v and v_A . The interpretation of the time t shown in the figures of this work is the following. Because for all performed simulations the *rms* Alfvén velocity v_A was set to one, an Alfvén wave with the velocity v_A needs exactly the time $t = L_{\text{box}}/v_A = 1$ to cross the entire simulation box. But this is only the minor part of the interpretation. The more important one is the consideration of the time needed for one eddy turnover at the integral scale L_I . The latter is associated with cut-off wavelength k_c [§] by $L_I = 1/k_c$ (the cut-off is stated in the figure captions). Hence, the eddy turnover time is $t_{\text{eddy}} \approx v_A k_c$ and in one time unit there are

$$N_{\text{eddy}} \approx k_c \quad (\text{for } t = 1) \quad (\text{A.69})$$

turnovers at the integral scale.

[§]Except otherwise stated, the quoted wavelengths k in the figures of this work are given in fractions of the box size $L_{\text{box}} = 1$, i.e. without the factor 2π .

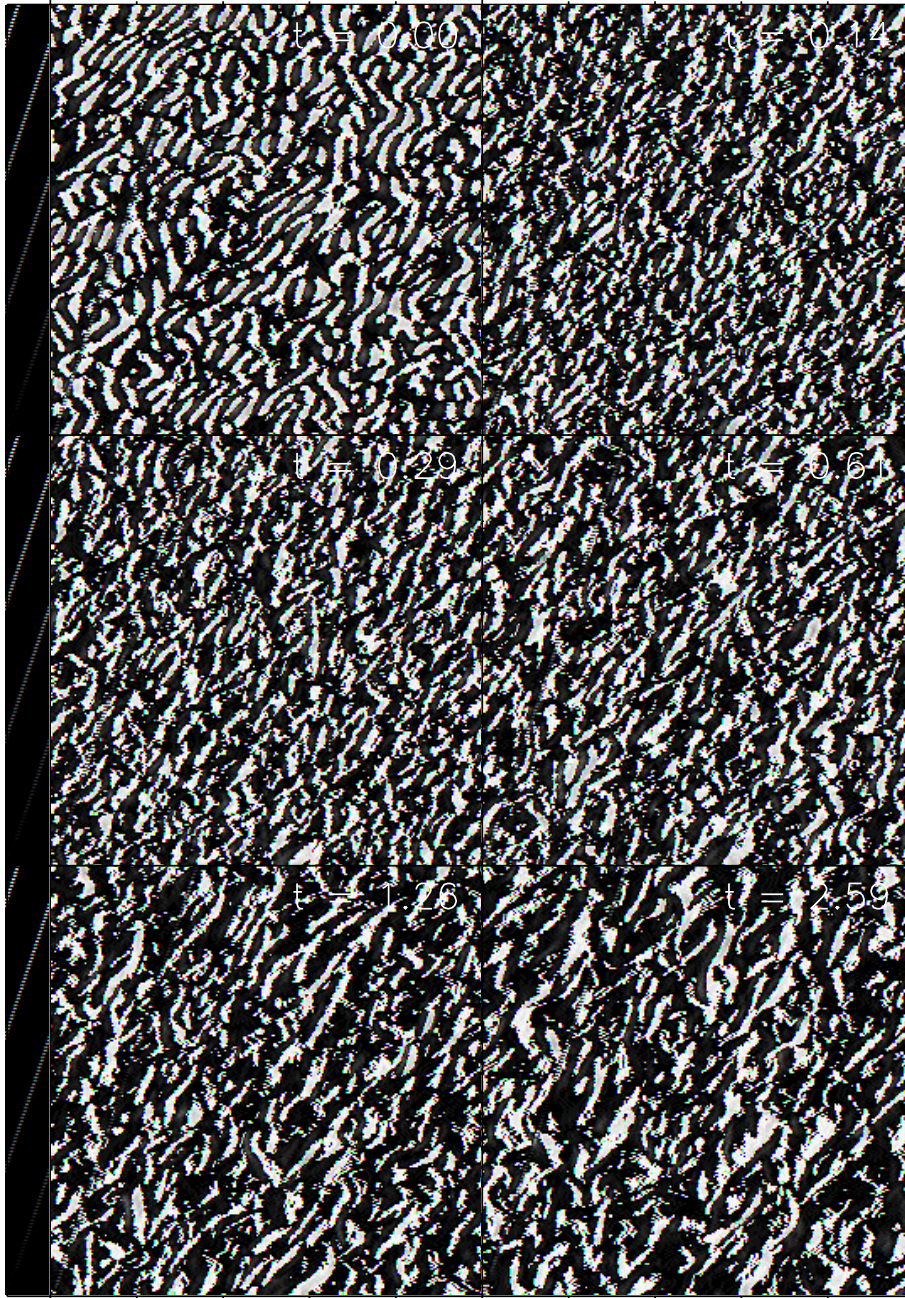


Figure A.2.: The panels show the magnitude of the magnetic field strength at different times t in the turbulent regime. Each panel is scaled to its own minimum (black) and maximum (white) value. Here, the images are 2D xy -slices of a simulation performed on a 128^3 grid. The initial magnetic field has zero helicity and a cut-off wavenumber $k_c \approx 16$.

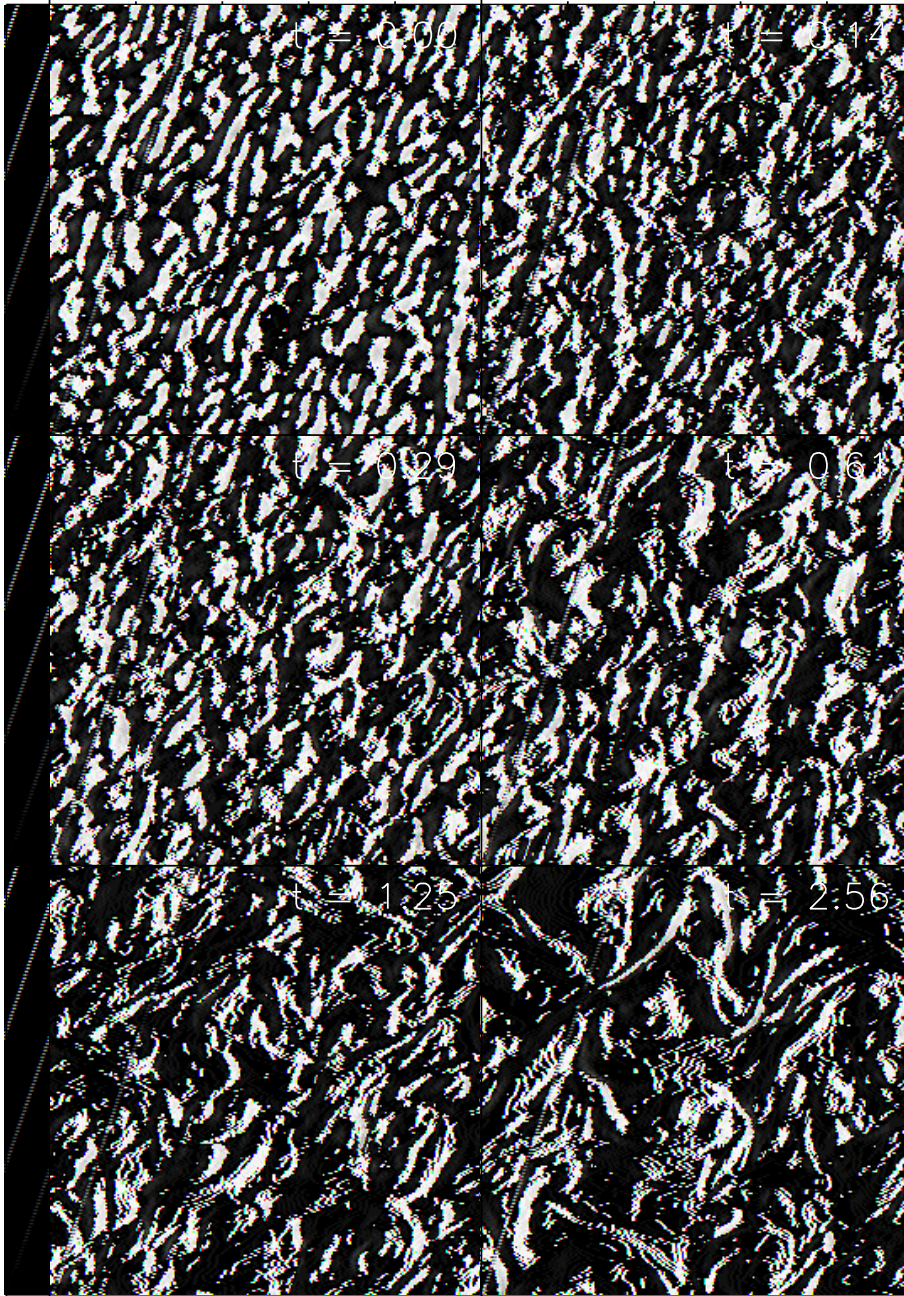


Figure A.3.: Similar to figure A.2, except that the initial magnetic field is maximal helical. Compared to the situation shown in figure A.2, much larger structures emerge in the same time if the magnetic fields have non-vanishing helicity. This indicates also a growing of the coherence length of the magnetic field.

Bibliography

- [1] R. Beck, A. Brandenburg, D. Moss, A. Shukurov and D. Sokoloff, *Ann. Rev. Astron. Astrophys.* **34** (1996) 155.
- [2] K. T. Kim, P. C. Tribble and P. P. Kronberg, *Astrophys. J.* **379** (1991) 80
- [3] A. C. Davis, M. Lilley and O. Törnkvist, *Phys. Rev. D* **60** (1999) 021301
- [4] Ya. B. Zeldovich, A. A. Ruzmaikin and D. D. Sokoloff, *Magnetic fields in astrophysics* Gordon and Breach, New York, (1983)
- [5] K. Subramanian, D. Narasimha and S. M. Chitre, *Mon. Not. Roy. Astron. Soc.* **271** (1994) L15
- [6] R. M. Kulsrud, R. Cen, J.P. Ostriker and D. Ryu, *Astrophys. J.* **480** (1997) 481
- [7] A. M. Howard and R. M. Kulsrud, *Astrophys. J.* **483** (1997) 648
- [8] L. M. Widrow, arXiv:astro-ph/0207240
- [9] R. Kulsrud, S. C. Cowley, A. V. Gruzinov and R. N. Sudan *Phys. Rept.* **283** (1997) 213
- [10] G. B. Taylor and C. Carilli *Annu. Rev. Astron. Astrophys.* **40** (2002) 319
- [11] P. P. Kronberg, *Rept. Prog. Phys.* **57** (1994) 325
- [12] S. Furlanetto and A. Loeb, *Astrophys. J.* **556** (2001) 619
- [13] P. P. Kronberg, Q. W. Dufton, H. Li and S. A. Colgate, *Astrophys. J.* **560** (2001) 178
- [14] S. A. Colgate and H. Li, *Astrophys. Space Sci.* **264** (199) 357
- [15] K. Dolag, M. Bartelmann and H. Lesch *Astron. Astrophys.* **348** (1999) 351
- [16] I. Wassermann, *Astrophys. J.* **224** (1978) 337
- [17] E. j. Kim, A. V. Olinto and R. Rosner, *Astrophys. J.* **468** (1996) 28

- [18] D. Grasso and H. R. Rubinstein, Phys. Rept. **348** (2001) 163
- [19] M. Giovannini, arXiv:hep-ph/0111220
- [20] G. Baym and H. Heiselberg, Phys. Rev. D **56** (1997) 5254
- [21] J. Ahonen and K. Enqvist, Phys. Lett. B **382** (1996) 40
- [22] K. Jedamzik, V. Katalinić and A .V. Olinto, Phys. Rev. D **57** (1998) 3264
- [23] K. Subramanian and J. D. Barrow, Phys. Rev. D **58** (1998) 083502
- [24] J. Silk, Astrophys. J. **151** (1968) 459
- [25] L. D. Landau and E.M. Lifschitz, Bd. VI *Hydrodynamik*, Akademie Verlag, Berlin (1991)
- [26] D. Biskamp, *Nonlinear Magnetohydrodynamics*, Cambridge University Press (1993)
- [27] J. M. Cornwall Phys. Rev. D **56** (1997) 6146
- [28] K. Enqvist, Int. J. Mod. Phys. D **7** (1998) 331
- [29] D. T. Son, Phys. Rev. D **59** (1999) 063008
- [30] G. B. Field and S. M. Carroll, Phys. Rev. D **62** (2000) 103008
- [31] G. Sigl, arXiv:astro-ph/0202424
- [32] J. Stone and M. Norman, Astrophys. J. Suppl. **80** (1992) 753
- [33] J. Stone and M. Norman, Astrophys. J. Suppl. **80** (1992) 791
- [34] D. A. Clarke, R. A. Fiedler and M. L. Norman, ZEUS3D User Manual, NCSA Technical report #015 (1994)
- [35] M. Giovannini, arXiv:hep-ph/0208152
- [36] J. C. Mather *et al.*, Astrophys. J. **420** (1994) 439
- [37] E. F. Bunn and M. J. White, Astrophys. J. **480** (1997) 6
- [38] K. S. Thorne, Astrophys. J. **148** (1967) 51
- [39] J. D. Barrow, P. G. Ferreira and J. Silk, Phys. Rev. Lett. **78** (1997) 3610
- [40] K. Jedamzik, V. Katalinić and A .V. Olinto, Phys. Rev. Lett. **85** (2000) 700

- [41] D. J. Fixsen, *et al.*, *Astrophys. J.* **473** (1996) 576
- [42] K. Subramanian and J.D. Barrow, *Phys. Rev. Lett.* **81** (1998) 3575
- [43] K. Subramanian and J. D. Barrow, arXiv:astro-ph/0205312
- [44] R. Durrer, T. Kahniashvili and A. Yates, *Phys. Rev. D* **58** (1998) 123004;
- [45] A. Kosowsky and A. Loeb, *Astrophys. J.* **469** (1996) 1
- [46] D. D. Harari, J. D. Hayward and M. Zaldarriaga, *Phys. Rev. D* **55** (1997) 1841
- [47] J. Adams, U. H. Danielsson, D. Grasso and H. Rubinstein, *Phys. Lett. B* **388** (1996) 253
- [48] P. Chen, *Phys. Rev. Lett.* **74** (1995) 634
- [49] R. Durrer, P. G. Ferreira and T. Kahniashvili, *Phys. Rev. D* **61** (2000) 043001
- [50] J. J. Matese and R. F. O'Connell, *Phys. Rev.* **180** (1969) 1289
- [51] R. .F. O'Connell and J. .J. Matese, *Bulletin of the American Astronomical Society* **1** (1969) 255
- [52] R. .F. O'Connell and J. .J. Matese, *Nature* **222** (1969) 649
- [53] J. .J. Matese and R. .F. O'Connell, *Astrophys. J.* **160** (1970) 451
- [54] G. S. Greenstein, *Nature* **223** (1969) 938
- [55] E. W. Kolb and M. S. Turner, *The early universe*, Addison-Wesley (1990)
- [56] G. S. Greenstein, *Astrophys. Space Sci.* **2** (1968) 155
- [57] B. I. Cheng, A. V. Olinto, D. N. Schramm and J. W. Truran, *Phys. Rev. D* **54** (1996) 4714 (This work was commented in the paper [99])
- [58] D. Grasso and H. R. Rubinstein, *Phys. Lett. B* **379** (1996) 73
- [59] P. J. Kernan, G. D. Starkman and T. Vachaspati, *Phys. Rev. D* **54** (1996) 7207
- [60] L. Biermann, *Z. Naturforsch.* **5a** (1950) 65
- [61] L. Biermann and A. Schlüter, *Phys. Rev.* **82** (1951) 863
- [62] A. D. Dolgov, arXiv:hep-ph/0110293
- [63] M. S. Turner and L. M. Widrow, *Phys. Rev. D* **37** (1988) 2743

- [64] M. Giovannini and M. E. Shaposhnikov, Phys. Rev. D **62** (2000) 103512
- [65] K. Dimopoulos, T. Prokopec, O. Törnkvist and A. C. Davis, Phys. Rev. D **65** (2002) 063505
- [66] C. J. Hogan, Phys. Rev. Lett. **51** (1983) 1488
- [67] T. Vachaspati, Phys. Lett. B **265** (1991) 258
- [68] K. Enqvist and P. Olesen, Phys. Lett. B **319** (1993) 178
- [69] G. Baym, D. Bodeker and L. D. McLerran, Phys. Rev. D **53** (1996) 662
- [70] G. Sigl, A. V. Olinto and K. Jedamzik, Phys. Rev. D **55** (1997) 4582
- [71] J. M. Quashnock, A. Loeb and D. N. Spergel, Astrophys. J. **344** (1989) L49
- [72] B. I. Cheng and A. V. Olinto, Phys. Rev. D **50** (1994) 2421
- [73] T. Vachaspati, Phys. Rev. Lett. **87** (2001) 251302
- [74] A. D. Dolgov and D. Grasso, Phys. Rev. Lett. **88** (2002) 011301
- [75] T. Vachaspati and A. Vilenkin, Phys. Rev. Lett. **67** (1991) 1057
- [76] E. R. Harrison, Mon. Not. Roy. Astron. Soc. **147** (1970) 279
- [77] M. J. Rees, Quart. J. Roy. Astron. Soc. **28** (1987) 197
- [78] G. F. R. Ellis, Cargèse Lectures in Physics, Vol. VI, Ed. E. Schatzman (1973) 1
- [79] S. Weinberg, *Gravitation and Cosmology*, John Wiley & Sons (1972)
- [80] C. W. Misner, K. S. Thorne and J. A. Wheeler, *Gravitation*, W. H. Freeman & Co. (1973)
- [81] C. G. Tsagas and J. D. Barrow, Class. Quant. Grav. **14** (1997) 2539
- [82] J. D. Jackson, *Classical Electrodynamics*, John Wiley & Sons, New York (1975)
- [83] C. Caprini and R. Durrer, Phys. Rev. D **65** (2002) 023517
- [84] S. Weinberg, Astrophys. J. **168** (1971) 175
- [85] R. M. Wald, *General relativity*, Chicago University Press (1984)
- [86] K. Jedamzik and G. M. Fuller, Astrophys. J. **423** (1994) 33

- [87] A. Kercek, K. Jedamzik, T. Abel and M.-M. Mac Low, not published
- [88] H. Martel and P. R. Shapiro, *Mon. Not. Roy. Astron. Soc.* **297** (1998) 467
- [89] R. Jackiw and S. Y. Pi, *Phys. Rev. D* **61** (2000) 105015
- [90] M. Christensson, M. Hindmarsh and A. Brandenburg, arXiv:astro-ph/0011321
- [91] M. Hindmarsh, M. Christensson and A. Brandenburg, arXiv:astro-ph/0201466
- [92] D. Biskamp and W.-C. Müller, *Phys. Plasmas* **7** (2000) 4889
- [93] D. Biskamp and W.-C. Müller, *Phys. Rev. Lett.* **83** (1999) 2195
- [94] M. Lesieur, *Turbulence in Fluids*, Kluwer, Dordrecht (1997)
- [95] M.-M. Mac Low, *Astrophys. J.* **524** (1999) 169
- [96] P. G. Saffman, *Phys. Fluids* **10** (1967) 1349
- [97] P. J. E. Peebles, *Astrophys. J.* **142** (1965) 1317
- [98] P. J. Peebles, *Principles Of Physical Cosmology*, Princeton, USA: Univ. Pr. (1993) 718 p
- [99] P. J. Kernan, G. D. Starkman and T. Vachaspati, *Phys. Rev. D* **56** (1997) 3766

Danksagung

Mein besonderer Dank gilt meinem Betreuer, Karsten Jedamzik, für die freundschaftliche und lehrreiche Zusammenarbeit am MPA und Umgebung, für die Bereitschaft und das Engagement mir bei der Erstellung dieser Arbeit hilfreich zur Seite zu stehen und auch für die aufschlußreichen Gespräche (oft auch nicht über Physik) bei und nach dem ein oder anderen Bierchen. Karsten hat auch wesentlich dazu beigetragen, daß ich hier am MPA eine äußerst angenehme Atmosphäre vorgefunden habe.

Gebührenden Dank gilt auch Andreas Kercek und Tom Abel, die als erste damit begonnen haben den ZEUS-code für die Untersuchung komischer Magnetfelder fit zu machen. Schade, daß sie ihr angefangenes Paper [87] nicht abgeschlossen haben. Andreas und Tom waren auch unter den ersten Kontakten die ich am Institut hatte, und konnten somit erheblich dazu beitragen, mein Weltbild des “Physikers” aufzubessern.

Danken möchte ich auch Simon White, der den offiziellen Teil der Betreuung übernommen hat und dafür, daß er die Zeit gefunden hat diese Arbeit vorab durchzusehen und mit seinen Anmerkungen inhaltlich und stilistisch aufzuwerten.

Meinen Dank möchte ich auch Harald Lesch aussprechen, der sich bereit erklärt hat das Zweitgutachten zu erstellen.

Ich muß mich auch bei den MPA-und-Nachbarinstituts-Kickern für die schweißtreibenden Stunden auf dem Fußballacker bedanken, obwohl ich mir ziemlich sicher bin, daß das regelmäßige Bearbeiten besagten Ackers nicht wirklich dazu beigetragen hat, meine Fußballkünste auf ein geldbringendes Niveau zu steigern.

Desweiteren danke ich Postdocs, an deren regelmäßigen Zusammenkünften ich auch als Predoc teilnehmen durfte.

Mein Dank gilt auch den Systembetreuern am MPA und am Garchinger Rechenzentrum für deren Einsatz, die Rechner Tag und Nacht am laufen zu halten.

Lebenslauf

Name: Robi Stefan **Banerjee**
Geburtstag: 21. Oktober 1967
Geburtsort: Nürnberg, BRD

Ausbildung

- Sept. 1983 – Juli 1985 : Mittlere Reife
an der Wirtschaftsschule Nunnenbeckstraße, Nürnberg
- Sept. 1985 – Juli 1988 : Ausbildung zum
Datenverarbeitungskaufmann
- Aug. 1988 – Aug. 1990 : Tätigkeit als Programmierer
- Sept. 1990 – Juli 1993 : Allgemeine Hochschulreife
am Nürnberg Kolleg
- Okt. 1993 – Sept. 1996 : Studium der Physik
an der Universität Hamburg,
Abschluß mit dem Vordiplom
- Okt. 1996 – Feb. 1999 : Studium der Physik
an der Friedrich-Alexander-Universität Erlangen-Nürnberg
Abschluß mit dem Diplom
Titel der Diplomarbeit: "Relativistische Berechnung der
Eta-Produktion in Proton-Proton-Kollisionen an der
Produktionsschwelle"
Betreuer: Prof. Dr. Manfred Dillig
- Juni 1999 – Okt. 2002 : Doktorand am Max-Planck-Institut für Astrophysik,
Garching